

Block Copolymer Self-assembly and Co-assembly

Shape Function and Application

Feng Li

Thesis committee

Thesis supervisors

Prof. dr. F.A.M. Leermakers

Personal chair at the Laboratory of Physical Chemistry and Colloid Science
Wageningen University

Prof. dr. E.J.R. Sudhölter

Professor of Nano-Organic Chemistry
Department of Chemical engineering DelftChemTech
Delft University of Technology

Thesis co-supervisors

Dr. A.T.M. Marcelis

Associate professor, Laboratory of Organic Chemistry
Wageningen University

Other members

Prof. dr. H. van Amerongen

Wageningen University

Prof. dr. J.H. Van Esch

Delft University of Technology

Prof. dr.ir. W.E. Hennink

Utrecht University

Prof. dr. R.J.M. Nolte

Radboud University Nijmegen

This research was conducted under the auspices of the Graduate School VLAG

Block Copolymer Self-assembly and Co-assembly

Shape Function and Application

Feng Li

Thesis

submitted in partial fulfilment of the requirements for the degree of doctor
at Wageningen University

by the authority of the Rector Magnificus

Prof. dr. M.J. Kropff,

in the presence of the

Thesis Committee appointed by the Doctorate Board

to be defended in public

on Friday 30 October 2009

at 11:00 AM in the Aula.

ISBN: 978-90-8585-473-9

To my family, Yuan & KuoKuo

This research was supported by NanoNed, a national nanotechnology program coordinated by the Dutch Ministry of Economic Affairs

CONTENTS

1	Introduction	1
I	Polymer self assembly	11
2	Stabilization of polymersome vesicles by an interpenetrating polymer network	13
3	Gentle immobilization of nonionic polymersomes on solid substrates	29
II	Polymer co-assembly	49
4	Small monodisperse unilamellar vesicles from binary copolymer mixtures	51
5	Field Theoretical Modeling of the Coexistence of Micelles and Vesicles	63
6	Formation of nanotapes by co-assembly of polypeptide and polythiophenes	99
7	Nanowires formed by the co-assembly of gelator and polythiophene	115
III	Applications	129
8	Pluronic polymersomes stabilized by core cross-linked polymer micelles	131
9	Triggered Templated Assembly of Protein Polymersomes	145
10	Mobility of fluorescently labeled polymer micelles in living cells	159
11	Fluorescent micelle thermometer with a potential use in biological cells	171
12	Summary and general discussion	183
	Samenvatting	189
	Acknowledgements	191
	List of Publications	195
	Curriculum Vitae	197

Chapter 1

Introduction

In nature, supramolecular nano- or micro-objects formed by the self-assembly of amphiphilic molecules or macromolecules are omnipresent (*e.g.* cells, liposomes, viral capsids, etc.) and come in a wide range of sizes, shapes and functions. The functions and shapes of these objects are often closely related to each other. One important parameter that controls the shape of the objects is the balance between the hydrophobic and hydrophilic moieties within the amphiphilic molecules. Typically those molecules with a relatively small hydrophilic part have the tendency to form vesicles (Chapter 2 and Chapter 3). While the hydrophobic parts of the molecules interact unfavorably with water, modest hydrophilic components in the molecules make the local lamellar configuration compatible with the aqueous solution. When, on the one hand, the protection by the hydrophilic groups of the molecule is not enough, *i.e.*, the hydrophobic forces overwhelm the hydrophilic ones, the vesicle structure can easily become unstable and an insoluble lamellar phase is formed. On the other hand, when the hydrophilic moieties are sufficiently large, the molecules may assemble into objects with a well-defined, strong curvature, such as small spherical micelles (Chapter 10 and Chapter 11). The lamellar phase and the spherical micelle are extreme forms of self-assembly. In practice, many alternative and intermediate forms of assembly are possible, like linear fibers (Chapter 6 and Chapter 7).

In biomedical applications there is a strong demand for robust targetable nano-sized containers. It is a challenge to develop a general strategy for the assembly of functional biomolecules into stable nanostructures with controlled size and shape.

Vesicles composed of lipids, so-called liposomes, are extremely fragile and have little stimuli responsiveness and chemical diversity.[1] Synthetic amphiphilic copolymers represent an attractive biomimetic class of compounds that become increasingly popular to produce nano- and micro-assemblies such as polymer vesicles, polymer micelles, nanofibers and nanotubes. The polymer approach to these assemblies opens up huge possibilities in chemical diversity and composition that may yield assemblies responding strongly to small triggers while remaining intact in a variety of environments. Although applications in drug delivery have driven much of this research, other opportunities exist for these polymer assemblies including their use as nanoreactors or sensors.

Stepping up in complexity, we recognize that spontaneous co-assembly of more than one type of molecule into nano-sized objects with fixed stoichiometry is a novel and versatile strategy to realize bottom-up nanotechnologies. Within co-assembled objects one can combine functionalities of its constituents in a controlled way. In this dissertation we explore several functional nano- and micro-objects, namely, polymer vesicles, polymer fibers and polymer micelles, which are generated by self assembly or co-assembly of block copolymers. Their applications in respective fields are also discussed.

1.1 Polymer vesicles

Polymer vesicles, commonly called polymersomes, are spherical hollow structures that have an aqueous compartment enclosed by a bilayer membrane made from amphiphilic block copolymers. Compared to liposomes, their low molecular weight analogues, polymersomes have many superior properties like higher toughness, better stability and tailorable membrane properties,[2-6] which make them attractive candidates for applications including encapsulation, drug delivery, nanoreactors and templates for micro- or nano-structured materials. Many potential applications require the ability to control the release of substances encapsulated in the interior aqueous compartment and/or in the hydrophobic core of the membrane. To achieve this goal, stimuli-responsive polymer vesicles were developed. Classical chemical stimuli such as pH changes, hydrolysis, oxidation or reduction reactions, have been used to trigger a change in the hydrophilic-hydrophobic balance of the amphiphilic copolymers. Among these polymer vesicles, protein polymersomes are an example of promising stimuli-responsive polymer vesicles.

Polypeptides are a special class of building blocks for vesicle-forming amphiphilic block copolymers because of their stimuli-responsiveness, secondary structure, functionality and biocompatibility. Nevertheless, there are only a limited number of examples of polymersomes made from polypeptide-containing block copolymers.[7, 8]

In this dissertation we elaborate on a temperature-responsive system. In this system, vesicles can assemble and disassemble upon modest temperature changes. More specifically, the polymer Pluronic L121 is used for this. L121 is a non-toxic commercially available product, which is able to form unilamellar vesicles. The low cost is rather exceptional for molecules that can form vesicles and this makes Pluronic polymers interesting molecules for future large scale applications. Interestingly, some members of the Pluronic family have been shown to have a potential for gene therapy and have been approved in medical applications. The bare L121 vesicle, however, is only marginally stable and, to the best of our knowledge, have not yet found any use in applications. Depending on the temperature, L121 vesicles normally aggregate and precipitate within a few hours after preparation. This thermal instability is attributed to the rather short hydrophilic polyethylene groups in the molecule. We developed and studied three ways to make the L121 vesicles more stable: *(I)* We introduced an interpenetrating polymer network (IPN) into the hydrophobic bilayer of the vesicle, which increased the vesicle stability from hours to months. *(II)* We introduced Pluronic P85 micelles, which were stabilized themselves by an IPN, into the vesicle. This improved the thermal stability of the vesicles to temperatures close to body temperature. *(III)* We used co-assembly of genetically expressed polypeptide block copolymers with the Pluronic L121 vesicle, similar to the assembly of membrane proteins in phospholipid membranes in biological systems. Using this approach it was also possible to integrate several other functional biomolecules into the protein polymersome.

For the sake of brevity, a schematic illustration of our three approaches is given in Figure 1.1. As can be seen from this Figure, in approach *I* the hydrophilic moieties are similar in length, while in approaches *II* and *III*, the longer hydrophilic moieties stretch out from the bilayer core of the vesicle. These longer hydrophilic moieties make the vesicle much more chemically and thermally stable. The properties of these vesicle systems are described in great detail in this dissertation.

We note that initially the peptide block copolymers, produced by yeast, were

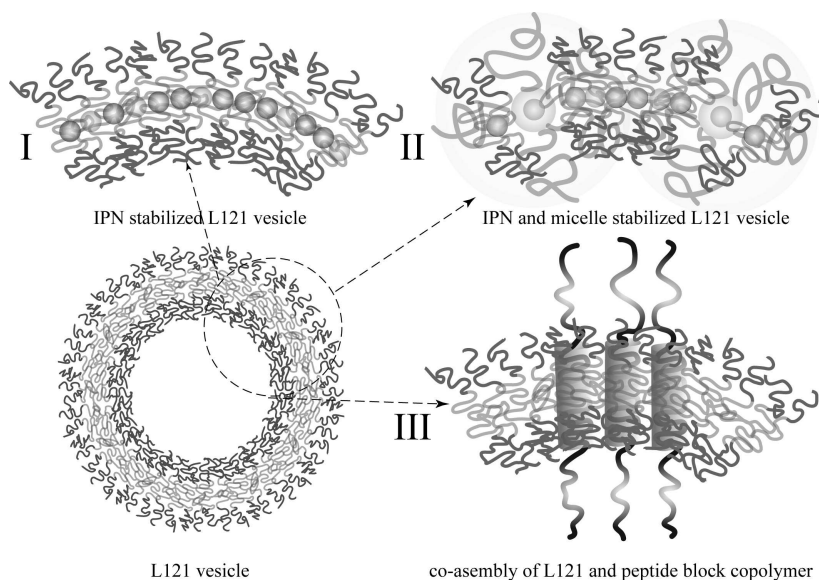


Figure 1.1: Illustration of three different approaches for vesicle stabilization used in this thesis. In increasing order of stability: (I) Vesicles stabilized by an interpenetrating PETA network, where the hydrophobic cross linker, PETA, associates and polymerizes in the hydrophobic core of the vesicle bilayer. (II) Double stabilized vesicles by Pluronic micelle and PETA interpenetrating network. The micelles associate with the bilayer of the vesicle. (III) Co-assembly of peptide block copolymers with the Pluronic matrix. The protein polymer is a pH-sensitive peptide block copolymer which associates to the vesicle bilayer when the charges are neutralized. This neutralization can be done with a pH change, but also by using biomolecules, such as proteins or DNA, with opposite charge. These biomolecules can therefore co-assemble with the protein-polymers inside the Pluronic matrix. Protected from the environment, these biomolecules can then be delivered to cells for medical applications.

investigated in aqueous solution and found to form pH-responsive fibers with a ribbon topology. In the presence of L121 vesicles they were found to strongly associate to the vesicles. In some systems we found the formation of fibers. This is briefly discussed in Chapter 6.

1.2 Polymer fibers

Peptide amphiphiles (PAs) can be considered as block copolymers. PAs usually consist of a hydrophilic peptide sequence to which a hydrophobic tail is attached - this may be a hydrocarbon chain or a sequence of hydrophobic amino acids. Fiber formation of peptide block copolymers has been studied thoroughly.[9, 10] They may potentially be used to fabricate biomaterials, such as scaffolds for biomineralization.[11, 12] In comparison to fibers that are build up from classical synthetic block copolymers, PAs fibers have an improved solubility, an enhanced stability against dilution, a reduced toxicity and immunogenicity.[13-15] A few examples of chemical synthetic triblock peptide copolymers have been studied to understand the basic rules of nanoscale self-assembly and ways of controlling the nanostructures.[16, 17] In addition to these chemicosynthetic peptide block copolymers, biosynthetic peptide block copolymers, biologically expressed from a designed DNA template, have been studied extensively. These block copolymers all have identical designed length and primary structure, while chemically synthesized polymers usually lack these features.[18, 19]

In this dissertation, we show how the co-assembly of peptides to a synthetic π -conjugated polymer can lead to a conductive nano-fiber when the peptide has an opposite charge compared to a π -conjugated polymer. The molecules interact with each other through electrostatic interactions and these are assisted by hydrophobic interactions (see Figure 1.2). Due to the association of the π -conjugated polymer along the length of the PA fiber a potentially conductive nano-fiber is formed. The same principle has also been applied to small fiber-forming organogelator molecules: the conjugated polymer also co-assembles with these molecules to form nano-fibers (Chapters 6 and 7).

The objects mentioned above, polymer vesicles and polymer fibers, usually have a diameter or length of 100 nm up to several micrometer. Much smaller objects, namely polymer micelles, are also discussed in Chapter 10.

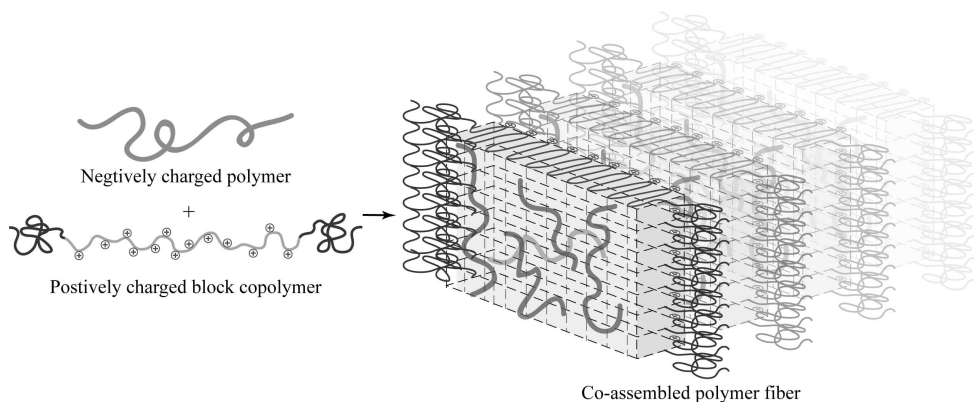


Figure 1.2: Schematic representation of peptide triblock copolymers that co-assemble with oppositely charged polymers leading to a nano-fiber with specified dimensions. The outer blocks of the block copolymer act as a protective layer against aggregation on the exterior of the nano-fibers.

1.3 Polymer micelles

Polymeric micelles are a major class of nanoscopic carriers, being studied for drug solubilization, controlled drug release and drug targeting in pharmaceutical research.[20-22] In addition to these polymer-drug conjugates, recent experiments have been carried out on polymeric micelles that carry biomolecules, like DNA, proteins and magnetic resonance imaging (MRI) active agents.[23-26] At this stage, much is already known about the physical properties of polymeric micelles that are the key for drug delivery systems. However, only few studies on the uptake and fate of these polymeric micelles inside cells.[27]

In this dissertation, we developed a Pluronic micelle that has a hydrophobic fluorescent probe covalently linked in the interpenetrating network of the micelle core, see Figure 1.3. The fluorescence of this micelle has a sharp temperature sensitivity, and the micelles can be spontaneously taken up by cells. Therefore it is suggested that these micelles can act as intracellular thermometers. The diffusive motion of these micelles within single cells has also been studied in Chapter 10 of this thesis.

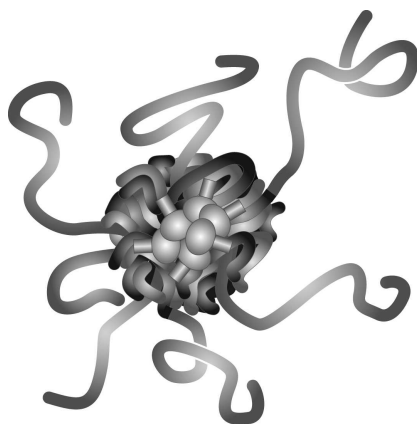


Figure 1.3: Schematic drawing of IPN-stabilized Pluronic micelles loaded with green fluorescent probes. The Pluronic polymers are not attached to the IPN, whereas the fluorescent probes are covalently linked to it.

1.4 Outline of the thesis

This thesis is divided into three parts. In **Part 1** we focus on polymer self-assembly. In Chapter 2 the stability and thermal sensitivity of a polymer vesicle composed of Pluronic molecules in aqueous solution is presented. In Chapter 3 the surface immobilization of such polymer vesicles is described. **Part 2** concentrates on polymer co-assembly. In Chapter 4 we present a study on the spontaneous formation of polymer vesicles from a mixture of block copolymers. A corresponding first-order explanation using a self consistent field model is discussed in Chapter 5. In Chapter 6 a study on the co-assembly of conductive nanowires from a conductive polymer and polypeptide block copolymers is presented. In Chapter 7 an investigation of the co-assembly of a conductive polymer with a small organic gelator leading to conductive nanowires is described. **Part 3** deals with the application of polymer self-assembly and co-assembly. In Chapter 8 the uptake of polymer vesicles by cells as studied by detecting the fluorescent micelles that are incorporated in the vesicles is presented. In Chapter 9 we describe the cellular uptake of protein polymer vesicles that have biomolecules encapsulated. In Chapter 10 the mobility of core-stabilized micelles in living cells is discussed. The fluorescence temperature sensitivity of the stabilized micelle is shown in Chapter 11. In chapter 12 a summary and general discussion of this dissertation is given.

Bibliography

- [1] D.E. Discher, A. Eisenberg, *Science*, **2002**, *297*, 967-973
- [2] B.M. Discher, Y.Y. Won, D. S. Ege, J.C.M. Lee, F.S. Bates, D.E. Discher and D.A. Hammer, *Science*, **1999**, *284*, 1143.
- [3] J.C.M. van Hest, D.A.P. Delnoye, M.W.P.L. Baars, M.H.P. Genderen and E.W. Meijer, *Science*, **1995**, *268*, 1592.
- [4] L. Zhang, K. Yu and A. Eisenberg, *Science*, **1996**, *272*, 1777.
- [5] J.J.L.M. Cornelissen, M. Fischer, N.A.J.M. Sommerdijk and R.J.M. Nolte, *Science*, **1998**, *280*, 1427.
- [6] T. Azzam and A. Eisenberg, *Angew. Chem. Int. Ed.*, **2006**, *45*, 7443.
- [7] E. Holowka, V.Z. Sun, D.T. Kamei, T.J. Deming, *Nature Materials*. **2007**, *6*, 52-57
- [8] J. Rodriguez-Hernandez, S. Lecommandoux, *J. Am. Chem. Soc.*, **2005**, *127*, 2026
- [9] H.M. Knig, A.F.M. Kilbinger, *Angew. Chem. Int. Ed.* **2007**, *46*, 8334-8340
- [10] I.W. Hamley, *Angew. Chem. Int. Ed.* **2007**, *46*, 8128-8147
- [11] J. D. Hartgerink, E. Beniash, S. I. Stupp, *Science* **2001**, *294*, 1684.
- [12] J. D. Hartgerink, E. Beniash, S. I. Stupp, *Proc. Natl. Acad. Sci. USA* **2002**, *99*, 5133.
- [13] G.W.M. Vandermeulen, C. Tziatzios, H.A. Klok, *Macromolecules* **2003**, *36*, 4107.

- [14] G.W.M. Vandermeulen, H.A. Klok, *Macromol. Biosci.* **2004**, *4*, 383.
- [15] I.W. Hamley, *Block Copolymers in Solution*, Wiley, Chichester, **2005**.
- [16] H. Dong, S.E. Paramonov, L. Aulisa, E.L. Bakota, H.D. Hartgerink, *J. Am. Chem. Soc.* **2007**, *129*, 12468-12472.
- [17] C.W.G. Fishwick, A.J. Beevers, L.M. Carrick, C.D. Whitehouse, A. Aggeli, N. Boden, *Nano Letters* **2003**, *3*, 1475-1479.
- [18] D.N. Woolfson, M.G. Ryadnov, *Current Opinion In Chemical Biology* **2006**, *10*, 559-567.
- [19] M.T. Krejchi, E.D. Atkins, A.J. Waddon, M.J. Fournier, T.L. Mason, D.A. Tirrell, *Science* **1994**, *265*, 1427-1432.
- [20] A. Klaukherd, C. Nagamani, S. Thayumanavan, *J. Am. Chem. Soc.* **2009**, *131*, 4830-4838.
- [21] N. Nasongkla, X.T. Shuai, H. Ai, B.D. Weinberg, J. Pink, D.A. Boothman, J.M. Gao, *Angew. Chem. Int. Ed.* **2004**, *43*, 6323 -6327.
- [22] D. Kim, E.S. Lee, K.T. Oh, Z.G. Gao, Y.H. Bae, *Small*, **2008**, *4*, 2043-2050.
- [23] S. Takae, K. Miyata, M. Oba, T. Ishii, N. Nishiyama, K. Itaka, Y. Yamasaki, H. Koyama, K. Kataoka, *J. Am. Chem. Soc.* **2008**, *130*, 6001-6009.
- [24] Y. Lee, T. Ishii, H. Cabral, H.J. Kim, J.H. Seo, N. Nishiyama, H. Oshima, K. Osada, K. Kataoka, *Angew. Chem. Int. Ed.* **2009**, *48*, 1-5.
- [25] N. Nasongkla, E. Bey, J. Ren, H. Ai, C. Khemtong, J.S. Guthi, S.F. Chin, A.D. Sherry, D.A. Boothman, J.M. Gao, *Nano Letters*, **2006**, *6*, 2427-2430.
- [26] J.M. Jamjic, M. Srinivas, D.K. Kadayakkara, E.T. Ahrens, *J. Am. Chem. Soc.* **2008**, *130*, 2832-2841.
- [27] R. Savic, L. Luo, A. Eisenberg, D. Maysinger, *Science* **2003**, *300*, 615 - 618.

Part I

Polymer self assembly

Chapter 2

Stabilization of polymersome vesicles by an interpenetrating polymer network

Vesicles from Pluronic L121(PEO₅-PPO₆₈-PEO₅) triblock copolymers were stabilized by an interpenetrating polymer network from pentaerythritol tetraacrylate (PETA) by UV or thermal initiator induced radical polymerization. Fluorescence labelling, AFM and electron microscopy studies are used to study the morphology of the particles and show that stable hollow vesicles are formed. The block copolymers are non-covalently trapped in the interpenetrating acrylate network. The stabilized vesicles retain their size for more than one month at room temperature. Upon cooling the vesicles reversibly loose block copolymer.

In slightly modified form published as: F. Li, T. Ketelaar, A.T.M. Marcelis, F.A.M. Leermakers, M.A. Cohen Stuart, E.J.R. Sudhölter. *Macromolecules* **2007**

2.1 Introduction

Polymersomes have been studied extensively in the past ten years. Many amphiphilic block copolymers, especially those with large hydrophobic and relatively small hydrophilic blocks can self-assemble into vesicles[1-18] at low concentrations. Recently, pH-sensitive polymersomes,[19, 20] biodegradable polymersomes,[21] and near-infrared (NIR)-emissive polymersomes[22] were made. Moreover, integral membrane proteins can be inserted in the shells[23] and viral DNA has been inserted into the polymer vesicles.[24] Vesicles from block copolymers often have a glassy hydrophobic block, which helps to keep them stable for quite long times. The block copolymers that have been used to prepare polymersomes are usually not commercially available. There are only a few exceptions; one of these are some Pluronics, poly(ethyleneoxide)-poly(propyleneoxide)-poly(ethyleneoxide) triblock copolymers. Pluronics are non-toxic and widely used in drug delivery systems and surface chemistry applications and may provide an exciting opportunity for gene therapies. These polymers are readily available and depending on the size and lengths of the blocks form micelles or vesicles in water. Pluronic L121 (PEO₅-PPO₆₈-PEO₅) for example, forms small vesicles, approximately 100 nm in size,[25, 26] which are, however, stable only for a few hours after preparation. They slowly revert to flat lamellar structures. The hydrophobic PPO part does not become glassy at low temperatures, which could contribute to the instability of the vesicles. Furthermore, these block copolymers are rather temperature sensitive[29-31]; at low temperatures they dissolve as unimers in water, while at higher temperatures they form aggregates. The poor stability limits their potential use in, e.g., novel polymer-based controlled-release systems.

In this work, we described a way to stabilize Pluronic L121 vesicles with a permanent interpenetrating network of polymerized pentaerythritol tetraacrylate (PETA), which prevents vesicles from reverting into more stable flat bilayers. Pentaerythritol tetraacrylate is a small hydrophobic molecule, which was used recently as a cross-linking agent for stabilizing Pluronic micelles.[30, 31] The polymerization of PETA took place mostly in the core of the micelles. A similar approach for stabilizing Pluronic L121 vesicles was used. The formation of the interpenetrating network in the vesicles was induced by either UV or thermal initiator induced free radical polymerization of PETA. The morphology of the resulting stabilized vesicles was studied by AFM, SEM, TEM and CLSM. Their

stability in time and as a function of temperature was studied by dynamic light scattering (DLS).

2.1.1 Materials

Poly(ethyleneoxide)-*b*-poly(propyleneoxide)-*b*-poly(ethyleneoxide) (PEO₅-PPO₆₈-PEO₅) (Pluronic L121) was obtained as a kind gift from BASF Corp. Pentaerythritol tetraacrylate (PETA), Nile red and carboxyfluorescein were purchased from Sigma. The thermal initiator 2,2'-azobis(4-methoxy-2,4-dimethyl valeronitrile) (V-70) was obtained from Wako. The extruder and the extrusion membranes were purchased from Avanti Polar Lipids.

2.1.2 Preparation of vesicles from PEO₅-PPO₆₈-PEO₅ copolymer

Pluronic L121 and PETA were intimately mixed by dissolving them in a few milliliters of dichloromethane, which was evaporated under a nitrogen stream and dried under vacuum overnight. An aqueous solution of the mixture containing 0.2 wt% copolymer and 0.006 wt% PETA was prepared and frozen in liquid nitrogen and subsequently thawed in a 25 °C water bath while stirring. This process was repeated five times. Then the mixture was extruded 25 times through a membrane with 100 nm diameter pores. Larger vesicles for fluorescent studies were made by extrusion through a membrane with 800 nm diameter pores. PETA-loaded vesicle solutions were put into a quartz cuvette, and photo-polymerization was performed with UV irradiation (Heraeus TQ150 UV lamp, 150 W) for 40 min. Alternatively, 5 μl of a stock solution of thermal radical initiator (V-70; 0.6 mg/ml) in ethanol, was added to 1 ml of freshly prepared vesicle solution, and the mixture was incubated at 25 °C for 40 min to produce vesicles stabilized by thermally induced polymerization of PETA. The latter method was used in combination with fluorescent probes to avoid photo-bleaching.

Hydrophobic Nile red containing vesicle solutions were prepared by adding 5 μl of a stock solution of Nile red (2 mg/ml) to 1 ml of a vesicle solution containing PETA before the extrusion step. After extrusion the polymer network was formed by thermally induced polymerization. Vesicles containing both Nile red and carboxyfluorescein were prepared by performing the same vesicle preparation and thermally induced polymerization reaction in a 20 mM carboxyfluorescein stock solution at pH 8. The carboxyfluorescein that was not trapped in the vesicles

was removed by size exclusion chromatography on a Sephadex G10 column with water as eluent.

2.1.3 Confocal laser scanning microscopy

The solutions with stabilized vesicles containing Nile red or Nile red and carboxy-fluorescein as fluorescent probe were deposited on a glass surface, covered with a slide, and then visualized directly using a confocal laser scanning microscopy (Zeiss LSM 510 Meta). Both samples were imaged one day after preparation.

2.1.4 Electron Microscopy

Samples for electron microscopy were dried on a copper grid overnight before doing the measurements. Transmission electron microscopy (TEM) measurements were performed on a TEM microscope (JEOL 1200 EX) operating at 120 kV. For scanning electron microscopy (SEM) the grid holder containing the dried vesicles was placed in a dedicated preparation chamber (Oxford Instruments CT 1500 HF, Eynsham, England), and sputter-coated with 5 nm platinum. The specimens were analyzed with a field emission scanning electron microscope (JEOL 6300 F, Tokyo, Japan) at room temperature, with SE detection at 2.5 - 5 kV. All images were recorded digitally (Orion, 6 E.L.I. sprl., Belgium) at a scan rate of 100 seconds (full frame) at a size of 2528 x 2030, 8 bit.

2.1.5 Atomic force microscopy

Tapping mode atomic force microscopy (AFM) experiments were carried out on a MFP-3D atomic force microscope from Asylum Research (Santa Barbara, CA). Height and phase imaging was done in AC mode in air using OMCL-AC240 silicon cantilevers (Olympus Corporation, Japan). One drop of the vesicle solution was deposited on a freshly cleaved mica surface at room temperature and dried overnight before measurements.

2.1.6 Dynamic light scattering

DLS was carried out on an ALV/DLS-5000 light-scattering apparatus (ALV, Langen, Germany), equipped with an argon ion laser (LEXEL, Palo Alto, CA) operating at a wavelength of 514.5 nm. All experiments were performed at a scattering

angle of 90° . Temperature was controlled by using a Haake C35 thermostat. The hydrodynamic radius was calculated from cumulant fits or a CONTIN multi-exponential fit. The relative intensity was obtained according to the intensity ratio of vesicles and the toluene.

2.2 Results and Discussion

2.2.1 Morphology study

L121 vesicles were prepared at 25°C in the L_1/L_α two-phase regime[25]. To avoid undesired aggregation, the freeze-thaw step and extrusion processes were strictly performed below 25°C . Pluronic L121 was well mixed with PETA during freeze-thaw cycling; no phase separation was observed within one hour after this process. The mixture was extruded and stabilized by either UV-induced or thermally induced free radical polymerization.

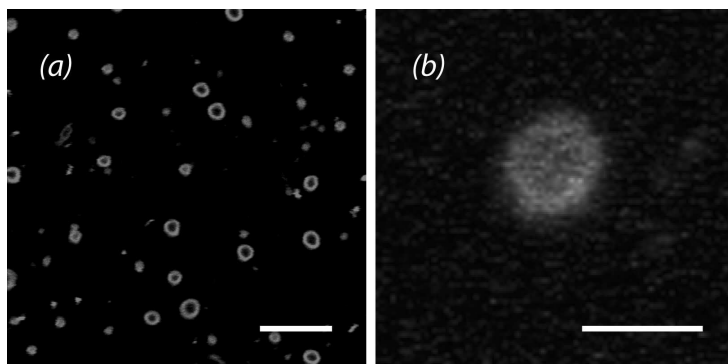


Figure 2.1: CLSM images of vesicles extruded through a 800 nm membrane (a) containing membrane encapsulated Nile red, scale bar $5\ \mu\text{m}$ (b) containing Nile red and aqueous entrapped carboxyfluorescein, scale bar $2\ \mu\text{m}$.

To prove that the particles are indeed hollow, fluorescent labeling experiments were done. For this purpose, larger vesicles were prepared, because they can be directly visualized by fluorescent microscopy. Both hydrophobic probe Nile red and water-soluble carboxyfluorescein were used.

Figure 2.1 shows the CLSM images of vesicles prepared by extrusion through an 800 nm membrane. The images show vesicles with a size of around $1\ \mu\text{m}$, which is comparable to the pore size of the membranes used for the preparation.

The hydrophobic dye, Nile red, has a very low fluorescence in aqueous solution, but an enhanced fluorescence in a hydrophobic environment[32, 33], so only the hydrophobic shells of the vesicles are visualized in Figure 2.1a. Carboxyfluorescein is a water-soluble probe with green fluorescence. Vesicles containing both Nile red and carboxyfluorescein are shown in Figure 2.1b. The presence of the red shell and green fluorescence of carboxyfluorescein entrapped in the aqueous interior of the particles is direct evidence that hollow nanoparticles are present in aqueous solution.

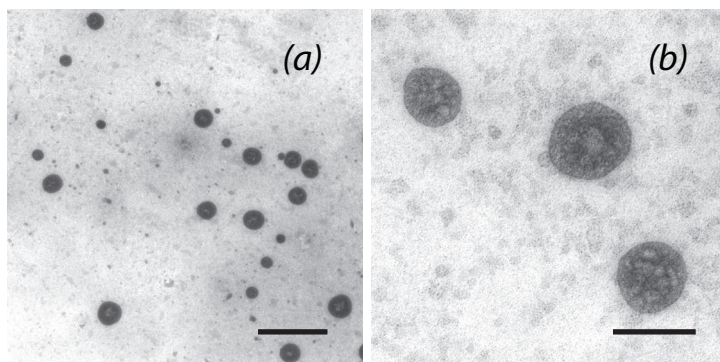


Figure 2.2: (a) TEM image of vesicles prepared by extrusion through an 100 nm membrane, scale bar 1 μm (b) higher magnification, scale bar 200 nm.

Detailed structural information was obtained by electron microscopy. Figure 2.2 shows TEM images of smaller vesicles. The vesicles were prepared with a 100 nm extrusion membrane. The two TEM images show circular particles having an average diameter of approximately 160 nm. The electron contrast of the deformed vesicles is so weak that the thickness of the vesicle walls can hardly be seen. This is typical for soft vesicles.[34] Some irregular features can be discerned on the surface of the polymerized vesicles, shown more clearly in Figure 2.2b. These are believed to come from irregularities formed during the polymerization of the PETA network. The interpenetrating network made up of polymerized PETA allows the Pluronic copolymers to remain associated by hydrophobic interactions of PPO with the polymerized PETA network and this association stabilizes the vesicle capsules.

Figure 2.3 shows a SEM image of vesicles obtained by extrusion through an 100 nm membrane. For TEM visualization, the sample was covered with 5 nm

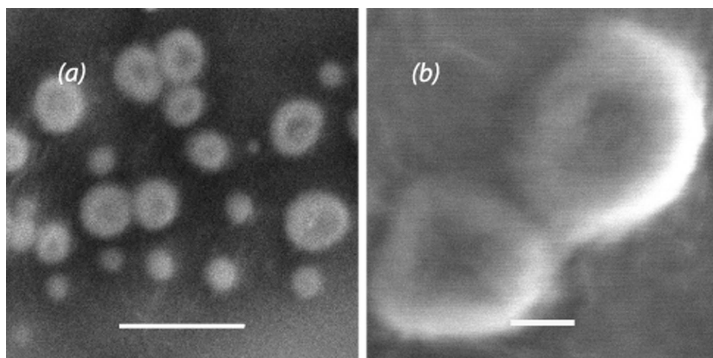


Figure 2.3: SEM image of vesicles obtained by extrusion through an 100 nm membrane, (a) scale 500 nm (b) 100 nm.

platinum. From this picture it is clearly seen that the particles are deformed by the drying process. The indentations in the center indicate that they are deflated hollow spherical particles. The particles are somewhat polydisperse. Some big aggregates attributed to the drying step were also observed (data not shown).

AFM images of the vesicles obtained by extrusion through an 100 nm membrane and deposited on mica are shown in Figure 2.4. From the height image we can extract information about the deformed vesicles. The height of the vesicles was in the range of 2-5 nm, much smaller than the average diameter of the vesicles (approximately 160 nm). This may have two reasons: (1) The height measured with tapping mode AFM may be lower than the real height of the vesicles due to the deformation of the vesicle surface by the AFM tip,[35] and (2) the vesicles were deformed as they were dried on the mica surface. The phase image (Figure 2.4b) shows something similar as the height image. The edge and the center of deformed vesicles have different responses to the force of the AFM probe. These features have been observed before and discussed in the literature.[34, 36] The height of the vesicles observed by AFM falls in the same range as the wall thickness of L121 vesicles estimated from cryo-TEM studies.[25] In combination with SEM, the data confirm that the vesicles are stable and detectable in the dry state. Both SEM and AFM yield consistent vesicle sizes of 160 nm, which is in agreement with DLS. The dried vesicles have slightly larger cross-sections than their diameter in solution.[34]

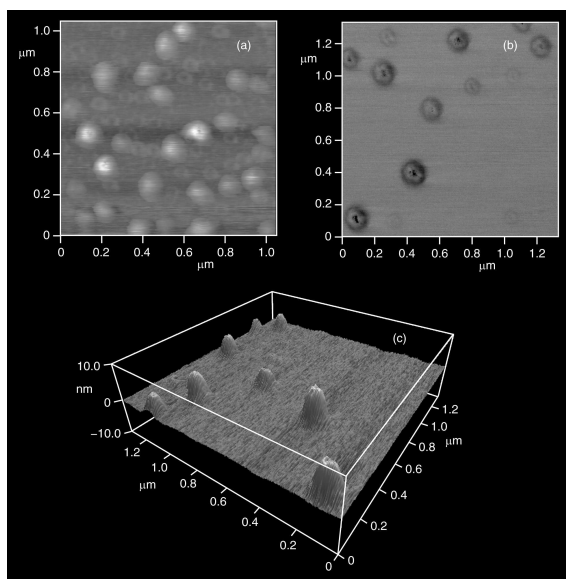


Figure 2.4: AFM image of stabilized vesicles obtained by extrusion through an 100 nm membrane. (a) height image, (b) phase image, (c) 3D height image area in Figure 2.4b.

2.2.2 Thermal stability study

All the samples used for the morphology study were usually between one day and two weeks old before the measurements. As shown in the images for AFM, TEM and SEM studies, they were deformed, but still retained their spherical shape after drying and under the measuring conditions. This means that at least a certain number of vesicles do not fall apart in time and under these conditions. Therefore, a more detailed study was performed of their stability as a function of time using dynamic light scattering (DLS).

A sample of stabilized vesicles prepared from extrusion through a 100 nm membrane was repeatedly analyzed by DLS over a period of 25 days after preparation. The relative scattering intensity and radius as a function of time obtained from the cumulant fits are shown in Figures 2.5a and 2.5b. This clearly shows that the PETA polymerized L121 vesicles are stable in time at 25 °C. A CONTIN analysis of the measurement after 25 days, shown in Figure 2.5c, shows a single peak. Similar CONTIN analyses were obtained for the measurements at other times. Therefore, the average size of the vesicles and their size distribution do not change during storage. So, the stability of the PETA polymerized L121 ve-

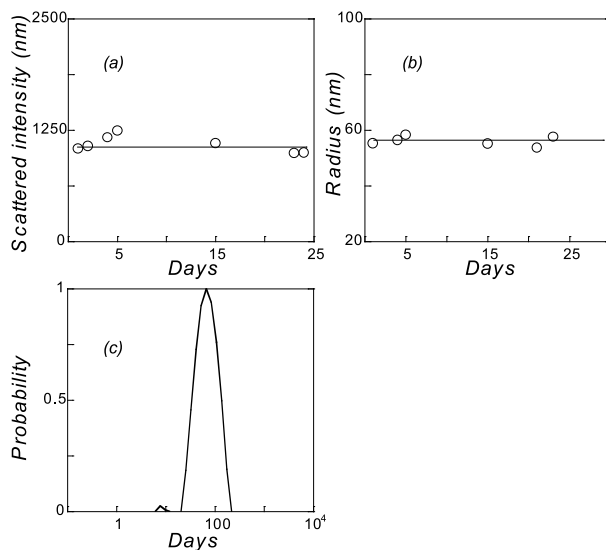


Figure 2.5: DLS measurements of stabilized vesicles obtained by extrusion through an 100 nm membrane (a) relative scattering intensity at 25 °C as a function of time (b) radius of hydration at 25 °C as a function of time (c) CONTIN analysis of the sample measured 25 days after preparation at 25 °C.

sicles is definitely increased as compared to the pure L121 vesicles: the latter were only stable for few hours, whereas the polymerized L121 vesicles remain stable for at least one month.

It is found that the size of the polymerized vesicles can be changed reversibly in a temperature range of 20-25 °C, as can be seen from Figures 2.6a and 2.6b. When the vesicle solution is slowly cooled down from 25 °C to 20 °C, the scattering intensity and the hydrodynamic radius of the particles decrease. Upon slow heating the radius and scattering intensity return again to their original value. The solubility of Pluronic (and also Pluronic L121) in water increases at low temperatures. Since the Pluronic are not covalently attached to the IPN and they are prepared at 25 °C, some molecules can slowly dissociate from the network upon cooling to 20 °C. Upon increasing the temperature they associate again with the vesicle, and this process is reversible.

In a similar experiment, the temperature of the vesicle solution was slowly decreased to 10 °C in 6 hours and the light scattering was measured (Figure 2.7). It is seen that the scattering intensity decreases strongly. It is found that at

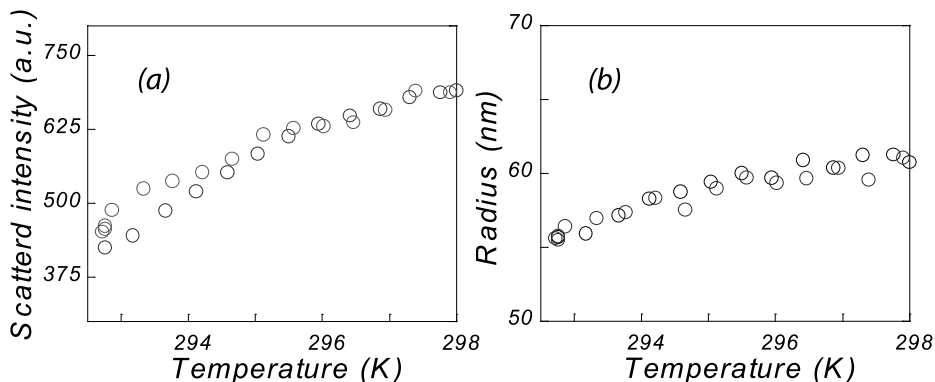


Figure 2.6: DLS measurements of stabilized vesicles obtained by extrusion through a 100 nm membrane as a function of temperature (a) scattered light intensity (arbitrary units) (b) hydrodynamic radius. The temperature was gradually increased from 20 °C to 25 °C in two hours, and subsequently reduced to 20 °C. Dark circles represents data upon temperature increase, light circles represent data upon temperature decrease.

about 14 °C, the vesicles start to disintegrate. When the temperature decreases, the Pluronic becomes more soluble and can dissociate from the permanent PETA network. The phase diagram of Pluronic L121 itself indicates that at a temperature below 14 °C, the surfactants prefer to form micelles instead of lamellar aggregates.[25, 26]

Loss of Pluronic molecules from the polymer network results in a decreased scattering intensity, while the free Pluronic molecules will partly self-assemble into small micelles, depending on the concentration and the exact temperature. When too many Pluronic molecules leave the network, the insoluble PETA networks will precipitate out of the solution. When the temperature is brought back to room temperature, a small fraction of the free Pluronic molecules will reassociate with the PETA network, and some of the capsules appear in solution again while stirring. The remaining Pluronic molecules will self-assemble into lamellar aggregates or vesicles as the pure Pluronic L121 molecules do.[26] These aggregates are not stable and their size grows very quickly in time (data not shown).

These observations indicate that the polymers can be removed from and associate again with the PETA capsules as a function of temperature. In view of the low amount of PETA that is used in relation to the amount of Pluronic, a picture emerges of stabilized vesicles that are held together by a loose polymeric network. Due to the self-aggregating properties of the Pluronics this is enough to stabilize

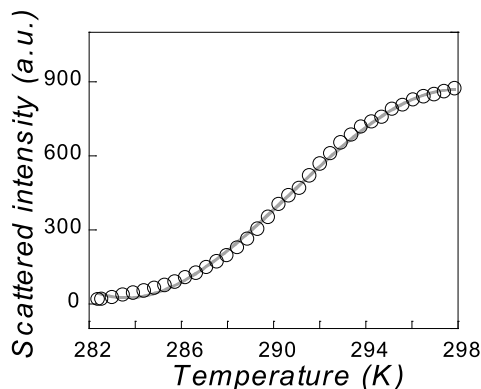


Figure 2.7: DLS measurements of 100 nm vesicles scattered light intensity value (with arbitrary units) The temperature was gradually decreased from 25 °C to 10 °C in six hours.

the vesicles for a long time. However, the Pluronic molecules are not covalently bound with the IPN, so when their solubility in water increases as happens when the temperature decreases they can reversibly dissociate from the polymer network. However, when too many Pluronics leave the network, precipitation of the network occurs. This temperature dependent behavior would also allow one to influence the permeability and thus release of entrapped species through the vesicle walls.

The easy and versatile preparation from inexpensive materials make these stabilized Pluronic L121 vesicles attractive for a broad range of possible applications. Clear advantages are the possibility to vary the strength of the network by using other acrylate network forming compounds and the possibility to modify the properties of the vesicles by using functionalized Pluronics. The easy control of vesicle size, the non-toxic nature of Pluronics and their long-term stability make these vesicles potentially interesting for drug delivery systems. We have shown that it is possible to load the vesicles with hydrophobic or hydrophilic dyes, which makes them potentially useful for molecular imaging, biological assays, as biomarker, for cell-labeling,[37] drug delivery and food applications.

2.3 Conclusions

Pluronic L121 vesicles were stabilized by means of a polymerized network of pentaerythritol tetraacrylate (PETA). Polymerization could not only be achieved by UV-irradiation but also by a thermal radical initiator. The permanent interpenetrating network allows the Pluronic L121 copolymers to reversibly associate with the vesicles. The size of the vesicles can easily be varied from 100 nm to 1 μ m, depending on the pore size of the extrusion membrane. CLSM, SEM, DLS and AFM studies prove that unilamellar vesicles are formed, and that the stabilized vesicles can retain their sizes for more than one month at room temperature.

Bibliography

- [1] D.E. Discher, A. Eisenberg, *Science*, **2002**, *297*, 967-973
- [2] Y. Kim, P. Dalhaimer, D.A. Christian, D.E. Discher, *Nanotechnology*, **2005**, *16*, S484-S491
- [3] S.A. Jenekhe, X.L. Chen, *Science*, **1998**, *279*, 1903-1907
- [4] T.A. Bronich, M. Ouyang, V.A. Kabanov, A. Eisenberg, F.C. Szoka, A.V. Kabanov, *J. Am. Chem. Soc.* **2002**, *124*, 11872-11873
- [5] B.M. Discher, Y.Y. Won, D.S. Ege, J.C.M. Lee, F.S. Bates, D.E. Discher, D.A. Hammer, *Science*, **1999**, *284*, 1143-1146
- [6] H. Kukula, H. Schlaad, M. Antonietti, S. Forster, *J. Am. Chem. Soc.* **2002**, *124*, 1658-1663
- [7] M.F. Mu, F.L. Ning, M. Jiang, D.Y. Chen, *Langmuir*, **2003**, *19*, 9994-9996
- [8] A. Napol, N. Tirelli, G. Kilcher, G.A. Hubbell, *Macromolecules*, **2001**, *34*, 8913-8917
- [9] R.P. Batycky, J. Hanes, J. Langer, D.A. Edwards, *J. Pharm. Sci.* **1997**, *86*, 1464-1477
- [10] S.A. Hagan, A.G.A. Coombes, M.C. Garnett, S.E. Dunn, M.C. Davies, L. Illum, S.S. Davis, *Langmuir*, **1996**, *12*, 2153-2161
- [11] M. Regenbrecht, S. Akari, S. Forster, H. Mohwald, *J. Phys. Chem. B*, **1999**, *103*, 6669-6675
- [12] A. Shen, A. Eisenberg, *J. Phys. Chem. B*, **1999**, *103*, 9473-9487

- [13] H. Shen, H. Zhang, A. Eisenberg, *J. Am. Chem. Soc.* **1999**, *121*, 2728–2740
- [14] S.M. Gravano, M. Borden, T. Von Werne, E.M. Doerffler, G. Salazar, A. Chen, E. Kisak, J.A. Zasadzinski, T.E. Patten, M.L. Longo, *Langmuir*, **2002**, *18*, 1938–1941
- [15] K. Yu, A. Eisenberg, *Macromolecules*, **1998**, *31*, 3509–3518
- [16] N.A.J.M. Sommerdijk, S.J. Holder, R.C. Hiorns, R.G. Jones, R. J. Nolte, *Macromolecules*, **2000**, *33*, 8289–8294
- [17] J. Ding, G. Liu, *Macromolecules*, **1997**, *30*, 655–657
- [18] M. Antonietti, S. Forster, *Adv. Mater.* **2003**, *15*, 1323–1333
- [19] M. Sauer, D. Streich, W. Meier, *Adv. Mater.* **2001**, *13*, 1649–1651
- [20] F. Liu, A. Eisenberg, *J. Am. Chem. Soc.* **2003**, *125*, 15059–15064
- [21] F. Ahmed, D.E. Discher, *J. Controlled Release*, **2004**, *96*, 37–53
- [22] P.P. Ghoroghchian, P.R. Frail, K. Susumu, D. Blessington, A.K. Brannan, F.S. Bates, B. Chance, D.A. Hammer, M.J. Therien, *Proc. Natl. Acad. Sci. U.S.A.* **2005**, *102*, 2922–2927
- [23] W. Meier, C. Nardin, M. Winterhalter, *Angew. Chem. Int. Ed.* **2000**, *39*, 4599–4602
- [24] A. Graff, M. Sauer, P.V. Gelder, W. Meier, *Proc. Natl. Acad. Sci. U.S.A.* **2002**, *99*, 5064–5068
- [25] K. Schillen, K. Bryske, Y.S. Melnikova, *Macromolecules*, **1999**, *32*, 6885–6888
- [26] K. Bryskhe, J. Jansson, D. Topgaard, K. Schillen, U. Olsson, *J. Phys. Chem. B*, **2004**, *108*, 9710–9719
- [27] A.V. Kabanov, P. Lemieux, S. Vinogradov, V. Alakhov, *Adv. Drug Deliv. Rev.* **2002**, *54*, 223–233
- [28] J. Jansso, K. Schillen, M. Nilsson, O. Soderman, G. Fritz, A. Bergmann, O. Glatter, *J. Phys. Chem. B*, **2005**, *109*, 7073–7083

- [29] P. Alexandridis, J.F. Holzwarth, T.A. Hatton, *Macromolecules*, **1994**, *27*, 2414-2425
- [30] P. Petrov, M. Bozukov, C.B. Tsvetanov, *J. Mater. Chem.* **2005**, *15*, 1481-1486
- [31] P. Petrov, M. Bozukov, M. Burkhardt, S. Muthukrishnan, A.H.E. Muller, C.B. Tsvetanov, *J. Mater. Chem.* **2006**, *16*, 2192-2199.
- [32] P. Greenspan, E.P. Mayer, S.D. Fowler, *J. Cell Biol.* **1985**, *100*, 965-973
- [33] M.M.G. Krishna, *J. Phys. Chem. A*, **1999**, *103*, 3589-3595
- [34] M. Yang, W. Wang, F. Yuan, X.W. Zhang, J.Y. Li, F.X. Liang, B.L. He, B. Minch, G. Wegner, *J. Am. Chem. Soc.* **2005**, *127*, 15107-15111
- [35] J. Tamayo, R. Garcia, *Langmuir*, **1996**, *12*, 4430-4435
- [36] M. Regenbrecht, S. Akari, S. Forster, H. Mohwald, *Surf. Interface Anal.* **1999**, *27*, 418-421
- [37] H. Kawaguchi, *Prog. Polym. Sci.* **2000**, *25*, 1171-1210

Chapter 3

Gentle immobilization of nonionic polymersomes on solid substrates

Vesicles from Pluronic L121(PEO₅-PPO₆₈-PEO₅) triblock copolymers were first stabilized by a permanent interpenetrating polymer network and then gently immobilized onto a glass or mica surface. Fluorescence-labeled μm -sized vesicles were visualized with confocal laser scanning microscopy and smaller sized capsules, around 100 nm, were probed by liquid atomic force microscopy. The immobilized vesicles were weakly attached to a negatively charged surface via negatively charged polyelectrolytes in combination with Mg^{2+} ions, and can be reversibly detached from the surface by slightly elevated temperatures. To illustrate that the immobilized vesicles remain responsive to external stimuli we show that it is possible to transform their shape from spherical to cylindrical by introducing a second Pluronic, namely, P123 (PEO₂₀-PPO₇₀-PEO₂₀). The detailed transition process has been recorded in real time by confocal laser scanning microscopy. Electron microscopy studies confirmed that a similar morphology change also occurs in the bulk.

In slightly modified form published as: F. Li, T. Ketelaar, A.T.M. Marcelis, F.A.M. Leermakers, M.A. Cohen Stuart, E.J.R. Sudhölter. *Langmuir* **2008**

3.1 Introduction

Polymersomes, that are vesicles composed of copolymer chains, have been studied extensively in the past ten years.[1-5] It is clear that they have many properties in common with surfactant or lipid vesicles. Even though the preparation of polymersomes might be somewhat more involved than the preparation of lipid vesicles, there are potentially significant advantages of polymersomes, e.g. with respect to their stability and freedom of choice of chemical composition. Despite their increased sturdiness, they may remain responsive towards external influences. Structural changes induced by mixing with other surfactants. e.g. biopolymer-induced structural transformations of vesicles have been observed.[6] In another study the formation of asymmetric polymersomes from a mixture of polymers and lipids was investigated.[7] Furthermore, the dynamics of formation of vesicles by mixing of surfactants was studied with sophisticated millisecond resolved SAXS experiments.[8]

Some of these experiments could probably have been much easier to perform if the vesicles would have been immobilized in one way or another. For example, it was recently shown that it is possible to track release processes of fluorescent species from vesicles immobilized in an agarose gel via fluorescent microscopy.[9] In this matrix the natural behavior of the vesicles, such as their shape fluctuations, were effectively suppressed. It would be more ideal when the immobilization could be somewhat more subtle, such that the vesicles themselves are not seriously altered by the constraints imposed by the matrix. In this paper we describe a method to gently immobilize vesicles onto a surface in such a way that the translational mobility is effectively absent while small local positional and vesicle shape fluctuations still remain possible.

Many examples have been worked out for adsorbing negatively charged objects like DNA onto negatively charged surfaces. (Poly)cations, polylysine or Mg^{2+} may for example be used to immobilize DNA onto a mica surface. In this case the (poly)cation binds simultaneously to both DNA and mica by electrostatic interactions. It appears that the polycation-induced binding dramatically increases the adsorption speed of these negatively charged species.[10, 11]

In our study we focus on vesicles composed of nonionic Pluronic block copolymers. Pluronic triblock copolymers are readily available and depending on the solvent, the size and the lengths of the blocks they form micelles or vesicles. Plu-

ronic L121 (PEO₅-PPO₆₈-PEO₅) for example, typically forms vesicles in water due to the short lengths of the EO blocks. Depending on the details of preparation, vesicles of approximately 100 nm in size are formed.[12-14] However, such L121 vesicles are not very stable and they aggregate and change their size in a few hours. Recently, we have described a way to stabilize Pluronic L121 vesicles with a permanent interpenetrating polymer network (IPN). We found that even though the Pluronic molecules are able to reversibly associate to and dissociate from the IPN stabilized vesicles,[12] the IPN stabilized L121 vesicles remain unaltered for over a month.

In this Chapter, we show that such IPN-stabilized nonionic vesicles can be (reversibly) bound to negatively charged surfaces. In short, Pluronic L121 is mixed with a few weight percent of high molecular weight polyacrylic acid (PAA), which is negatively charged at neutral pH. These vesicles are then stabilized with an IPN from pentaerythritol tetraacrylate (PETA). These stabilized PAA-containing Pluronic L121 vesicles are immobilized onto a glass or a mica surface by Mg²⁺ mediated electrostatic interactions, as illustrated in Figure 3.1. The interesting and important observation is that the vesicles gently attach to the surface at room temperature, and detach from the surface by increasing the temperature. As the vesicles are immobilized on the surface it becomes relatively easy to observe and follow many individual vesicles in time.

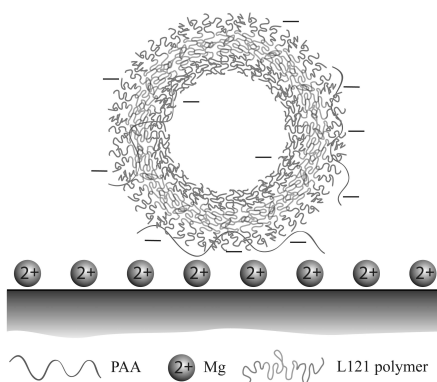


Figure 3.1: PAA charged Pluronic L121 vesicles gently immobilized on a weakly charged solid surface via Mg²⁺ bridges

The advantage of this approach is illustrated by showing that the vesicles can undergo a significant structural transition while they are immobilized. In more

detail, we have noticed a morphological transition of initially spherical vesicles into short cylindrical vesicles by introduction of a more hydrophilic Pluronic P123 in the IPN-stabilized vesicle system. Even though the morphological transition is used here to illustrate the immobilization technique, the effect of P123 on the IPN stabilized L121 vesicle is of interest by itself as it may be an interesting model for various shape transformations in biological cells where there is an elastic network connected to a lipid bilayer.[15, 16] At this stage we can not yet claim to have full insight in the mechanism of the structural transition, but we speculate that the addition of P123 induces an increase of the surface area which sets off the shape transitions.

The morphology of the immobilized vesicles was studied both by liquid atomic force microscopy (AFM) and confocal laser scanning microscopy (CLSM). The structural transition of IPN-stabilized spherical vesicles into cylindrical vesicles in bulk was characterized by negatively stained transmission electron microscopy (TEM) and dynamic light scattering (DLS). The morphological transition was studied in real time by CLSM.

3.1.1 Materials

Poly(ethyleneoxide)-*b*-poly(propyleneoxide)-*b*-poly(ethyleneoxide) (PEO₅-PPO₆₈-PEO₅) (Pluronic L121) was obtained as a kind gift from BASF Corp. Pluronic P123 (PEO₂₀-PPO₇₀-PEO₂₀), pentaerythritol tetraacrylate (PETA), and Nile red were purchased from Sigma. The thermal initiator 2,2'-azobis(4-methoxy-2,4-dimethyl valeronitrile) (V-70) was obtained from Wako. Polyacrylic acid (PAA, Mw = 28700 Da) was purchased from Polymer Sources. The extruder and the extrusion membranes were purchased from Avanti Polar Lipids.

3.1.2 Preparation of vesicles from PEO₅-PPO₆₈-PEO₅ copolymer

Details of the vesicle preparation are described in Chapter 2.[12] The procedure is only slightly modified to obtain negatively charged vesicles. The negatively charged capsules were made by adding 0.01 wt% PAA to the usual mixture of Pluronic L121 and PETA (0.2 wt% and 0.06 wt% respectively) and dissolved in a few milliliters of chloroform. The chloroform was evaporated under a nitrogen stream and the residue was dried under vacuum overnight. After hydration of the resulting thin film the mixture was freeze-thawed and extruded which resulted in

the formation of unilamellar vesicles. These were stabilized by UV- or thermally-induced polymerization of the PETA molecules. Small vesicles for AFM study were prepared by extrusion through a membrane with 100 nm diameter pores. Larger vesicles for fluorescent studies were made by extrusion through a membrane with 800 nm diameter pores. In this case Nile red was added to the vesicle solution containing PETA before the extrusion step. After extrusion the polymer network was formed by polymerization using the thermal radical initiator V-70. This mild procedure to form the IPN resulted in very much the same properties of the IPN-stabilized vesicles, but avoids the UV-photodegradation of Nile red.[12]

3.1.3 Electron Microscopy

IPN-stabilized L121 vesicles (without PAA) were engrossed on CuH and 1% formvar coated copper grids. The grids were submerged for 1 min into the sample solution, and then in an aqueous 1 wt% uranyl acetate solution. TEM measurements were performed on a JEOL 1200 EX electron microscope operating at 80 kV. Images were recorded with a 1k CCD camera.

3.1.4 ζ Potential measurements

The charge on the complex PAA-L121 vesicles was determined by electrophoretic mobility. The pH dependence on the electrophoretic mobility of the charged vesicles was measured in 10 mM KCl solution on a Malvern Zetasizer 2000. The mean values were averaged from five single measurements.

3.1.5 Dynamic light scattering

DLS was carried out on an ALV/DLS-5000 light-scattering apparatus (ALV, Langen, Germany), equipped with an argon ion laser (LEXEL, Palo Alto, CA) operating at a wavelength of 514.5 nm. All experiments were performed at scattering angles between 70° and 120°. Temperature was controlled at 25°C by using a Haake C35 thermostat.

3.1.6 Atomic force microscopy

Tapping-mode atomic force microscopy (AFM) experiments were carried out on a MFP-3D AFM from Asylum Research (Santa Barbara, CA). Height imaging

was done in the AC mode in an aqueous solution using OMCL-TR400PSA-1 silicon nitride triangular cantilevers (Olympus Corporation, Japan). The overall resonance frequency of the fluid cell and the probe assembly was 8 ± 1 kHz. For the surface immobilization, the PAA containing Pluronic L121 vesicles were mixed with 50 mM MgCl_2 . A few drops of this vesicle solution was deposited on a freshly cleaved mica surface at room temperature and equilibrated just a few minutes before imaging.

3.1.7 Confocal laser scanning microscopy

The solution with PETA-stabilized PAA-charged vesicles containing Nile red as fluorescent probe was mixed with 50 mM MgCl_2 and deposited on a glass(Menzel) surface, covered with a slide, and then visualized directly using a confocal laser scanning microscope (Zeiss LSM 510 Meta). Once the immobilized vesicles were detected, 40 mg/ml P123 solution was applied to these fixed vesicles via capillary forces. The structural transition process was recorded by the LSM Image Browser program.

3.2 Results and Discussion

3.2.1 Vesicles in solution

Detailed structural information of vesicles with no PAA co-assembled was obtained by electron microscopy. Figure 3.2a shows a negatively-stained TEM image of relatively small stabilized Pluronic L121 vesicles prepared using a 100 nm extrusion membrane. They have diameters of approximately 50 to 100 nm, which is in good agreement with light scattering measurements. The complete characterization of these vesicles was described in Chapter 2.[12] Similar negatively-stained TEM images of polymersomes were reported before.[17]

For the immobilization of the IPN-stabilized vesicles, we have mixed L121 with PAA during the preparation process. The electrophoretic mobility of the PAA - Pluronic L121 vesicles as a function of the pH is presented in Figure 3.3. At low pH, e.g. pH 3, PAA is barely charged, so there is almost no electrophoretic mobility. Above pH 5, the carboxylic groups in PAA are deprotonated, which makes the PAA-containing Pluronic L121 vesicles negatively charged at neutral pH. As seen from the figure, 0.01 wt% PAA-charged Pluronic L121 vesicles have a

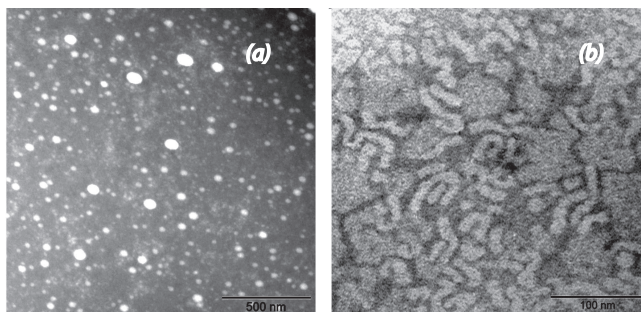


Figure 3.2: (a) Negatively stained TEM image of Pluronic L121 vesicles prepared by extrusion through an 100 nm membrane (b) Negatively stained TEM image of Pluronic L121 vesicles in the presence of Pluronic P123.

ζ potential of -35 ± 6 mV in 10 mM KCl. This value is consistent with Pluronic L121 and poly(lactic acid/glycolic acid) mixtures reported in the literature.[18] At present we do not know exactly how the PAA molecules are attached to the L121 vesicles. As depicted in Figure 3.1, we expect however that the PAA molecules are non-covalently and reversibly connected to the capsules and that hydrogen bond interactions of the carboxylic acid groups of the PAA to the oxygens of the polyether in the Pluronic chains exist. The terminal hydroxy group of the polyether may also stabilize the Pluronic L121 and PAA mixtures,[19] and this stabilization may well be improved further by the presence of the IPN with which the PAA may interact as well.

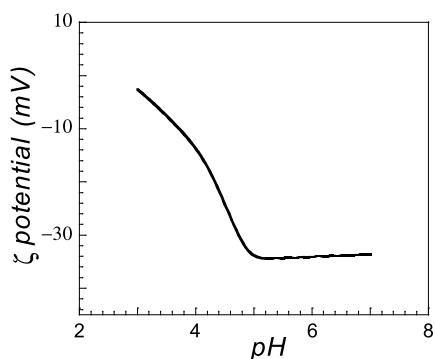


Figure 3.3: ζ potential of PAA-charged stabilized Pluronic L121 vesicles as a function of pH.

The negatively-charged vesicles can now be immobilized onto negatively char-

ged surfaces through a cationic intermediate employing electrostatic attraction. This is done by introducing Mg^{2+} ions. It is however well-known that ions like Mg^{2+} or Ca^{2+} may also induce vesicle fusion above a certain concentration. Magnesium ions, for example, can bridge between charged vesicles and thus induce aggregation. We found that this aggregation behavior is concentration dependent. Figure 3.4 shows the apparent diffusion coefficient, D_{app} , of the IPN-stabilized PAA-charged Pluronic vesicles as a function of q^2 for various concentrations of Mg^{2+} ions. Here q is the scattering vector which for a given wavelength is a function of the scattering angle and q may be interpreted as the probed length scale. From light scattering theory it is known that for spherical particles, D_{app} is constant irrespective of the angle of observation q . For non-spherical or asymmetric particles, however, D_{app} does depend on the scattering angle. As seen from Figure 3.4, at concentrations below 50 mM MgCl_2 , there is hardly any angular dependence detected, implying spherical particles, whereas at concentrations of 75 mM MgCl_2 and higher, the apparent diffusion coefficient clearly increases with increasing q . The latter indicates that asymmetric particles are present, probably through a linear aggregation of PAA-charged vesicles at relatively high Mg^{2+} ion concentrations. Therefore, we have chosen to use a concentration of 50 mM MgCl_2 for the immobilization of the vesicles on a surface to avoid significant aggregation.

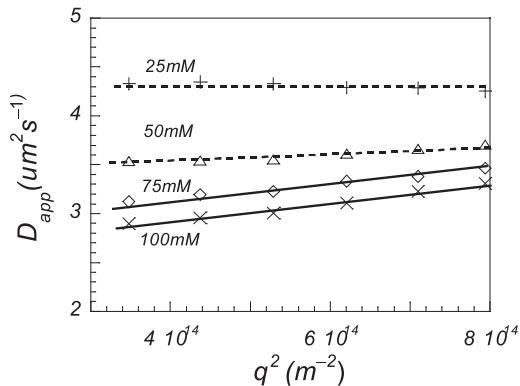


Figure 3.4: Apparent diffusion coefficient of PAA-charged stabilized Pluronic vesicles as a function of q^2 with different concentrations of Mg^{2+} : (+) 25mM, (Δ) 50mM, (\diamond) 75mM, (X) 100mM

As described in literature,[20] a mixture of Pluronic L121 and the more hy-

drophilic Pluronic P123 polymers in water forms more stable particles than those composed of pure L121. Pluronic P123 (PEO₂₀-PPO₇₀-PEO₂₀) itself is not a vesicle former in aqueous solution at ambient conditions. It forms multilamellar vesicles only in water and butanol mixtures.[21, 22] When P123 molecules are added to an aqueous solution of L121 vesicles, one observes that both the total scattered intensity as well as the particle size increases. This indicates that P123 is taken up in the L121 vesicles and causes them to swell. This behavior is similar as the effect of surfactants or detergents on polymersomes.[23] When sufficient P123 is added, the L121 vesicles are solubilized and mixed micelles are formed. Thus, at low P123 concentrations mixed micelles coexist with the L121-rich polymersomes and under these conditions the polymersomes also accommodate a certain amount of P123 molecules.

When Pluronic P123 (3 mg/ml) is introduced in a solution containing IPN-stabilized Pluronic L121 vesicles, remarkable features were observed with TEM, as seen in Figure 3.2b. This TEM image shows that most of the vesicles have changed their shape. Instead of spherical vesicles, elongated tubular objects are present in the system. The average contour length of the tubular vesicles in Figure 3.2b is close to 100 nm, and the aspect ratio of these particles is approximate 5. Since the Pluronics can freely associate to or dissociate from the IPN-stabilized L121 vesicles, because the network is not physically connected to the copolymers, addition of P123 will increase the number of Pluronic molecules associated with the PETA network and change the Pluronics composition. This change in composition may induce some stress in the IPN which may result in the formation of the asymmetric objects. Apart from the tubular vesicles also some irregular features can be seen in Figure 3.2b. There are some regions where larger objects are present that point to other types of aggregated matter. However, these may also have originated from drying artifacts or from the staining process.

Very similar features, i.e. the formation of elongated structures was also found upon mixing phospholipids with triblock copolymer vesicles.[7] However, this system differs considerably from ours. In our case the asymmetry is most likely linked to the induced stress originating from the polymeric network.

3.2.2 Vesicle immobilization

In order to visualize vesicles on a surface with liquid AFM, one typically has to equilibrate them for at least half an hour to get a sufficient number of vesicles adsorbed onto the surface.[24, 25] In the previous paragraph, it was shown that IPN-stabilized Pluronic L121 vesicles can be formed that have a negative charge at neutral pH due to the complexation (interaction) with PAA chains. In the presence of 50 mM Mg^{2+} ions we succeeded to immobilize the vesicles onto a negatively charged surface. A cartoon of this process is given in Figure 3.1.

A liquid AFM image of vesicles that were immobilized on a mica surface is shown in Figure 3.5a. Unlike for the non-electrostatic adsorption process,[24, 25] this immobilization procedure occurs within a few minutes. This also limits the amount of solvent evaporation and thus sample concentration during the experiments. The short equilibration time also minimizes thermal fluctuation effects, and provides images with good resolution even for the rather soft polymersomes. From Figure 3.5b it is seen that a height of approximately 15 nm is found for the stabilized vesicles with a diameter of about 80 nm. This is much more than the height found with AFM for a dried sample, which was only about 5 nm high.[12] In the absence of PAA and Mg^{2+} ions it is also possible to measure the height of adsorbed vesicles in the liquid cell, although, as explained, the procedure is much more tedious. The height then found does not differ much from the result obtained in the presence of PAA and Mg^{2+} , indicating that these additives do not strongly influence the measurements. The fact that it is now possible to easily immobilize the IPN-stabilized vesicles in an liquid AFM cell allows many more experiments to be done, such as deformation studies.

To study the immobilized vesicles in more detail, CLSM experiments were also done. For this purpose, larger vesicles were prepared, because these can be visualized directly by fluorescence microscopy. Instead of using a mica surface, we used a glass substrate for this study, which is also weakly negatively charged at neutral pH.

Figure 3.6 shows CLSM images of vesicles prepared by extrusion through an 800 nm membrane and subsequently immobilized by bringing the PAA-charged vesicles in a 50 mM $MgCl_2$ solution. These vesicles are visualized a few minutes after immobilization. As can be seen in Figure 3.6a, the vesicles are rather monodisperse and are all about 1 μm in size. These vesicles fluctuate relatively freely

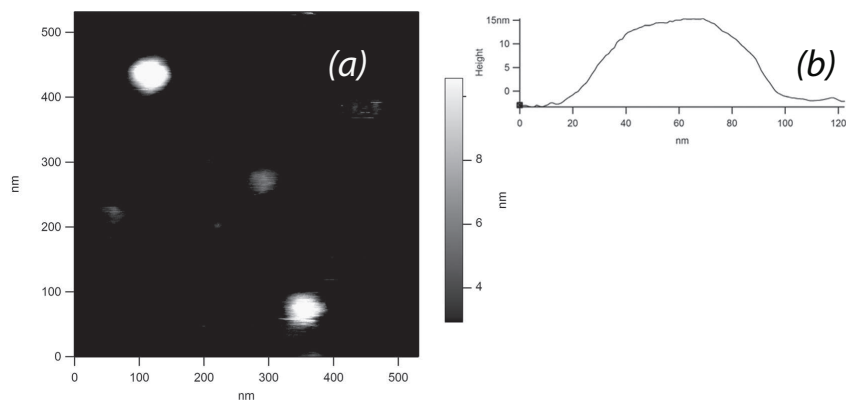


Figure 3.5: *Liquid AFM of PAA-containing vesicles extruded through a 100 nm membrane. (a) height image of immobilized vesicles in the presence of Mg^{2+} on mica (b) cross section analysis.*

around a certain average position, rather than showing Brownian motion. This indeed indicates that the vesicles are gently fixed onto the surface. A movie (available on line as the supporting information of this paper) shows the details of the restricted mobility. From this movie one can easily observe that the vesicle shapes fluctuate in time, but mostly remaining close to spherical. One can imagine various application for this system of surface immobilized vesicles, e.g. in nanotechnological applications.

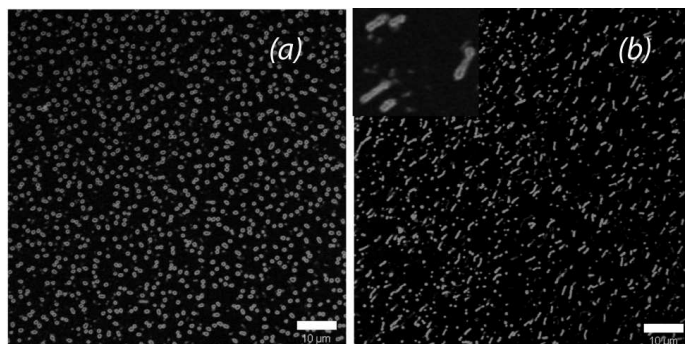


Figure 3.6: *CLSM images of vesicles extruded through an 800 nm membrane (a) immobilized vesicles containing membrane encapsulated Nile red (b) after adding Pluronic P123 to the immobilized vesicles.*

To illustrate the potential use of the surface-immobilization approach, we in-

roduced Pluronic P123 block copolymers into the system of the surface-immobilized IPN-stabilized vesicles. As was shown, such spherical vesicles transform under these conditions into tubular ones in the bulk. On the surface a similar structural transition takes place. In more detail, the Pluronic L121 vesicles that were immobilized on the glass surface are exposed to a 40 mg/ml micellar P123 solution. This more hydrophilic copolymer is applied into the system through the spaces between the support glass and the cover slide by capillary forces. A high concentration of P123 was selected to speed up the process and reduce the recording time.

When a certain threshold ratio of Pluronic L121 and P123 is reached the initially spherical L121 vesicles transform into cylindrical ones. A snapshot of the system just after this happened is shown in Figure 3.6b. The inset of Figure 3.6b gives an enlarged view, from which one may clearly see that tubular structures have been formed. One may wonder why the linear objects are all oriented in about the same direction. The reason for this is that the P123 is administered from one side and that there is a directional flow of liquid in the cell. This flow is sufficient to orient the tubular vesicles, but it is not strong enough to remove the vesicles from the surface. In the supporting information a movie of the shape transformation can be found. In this movie one can see that the vesicles first grow somewhat in size before they elongate. The elongated vesicles (cylindrical tubes) have a smaller width and a longer contour length as compared to the original L121 capsule diameter. This is consistent with the observations presented in Figure 3.2b, where the same process was visualized using TEM. Both experiments indicate that the aspect ratio of the cylindrical vesicles is approximately the same.

Comparison with negatively stained TEM clearly demonstrates that the structural transition detected by CLSM is not due to some artifact from the surface immobilization. Apart from the surface issue (used to immobilize the capsules in CLSM and only needed as a support in TEM), indeed the main difference between the CLSM and the TEM experiment is that in the first also PAA was present. Again the similar results for CLSM and TEM show that PAA does not change the properties of the IPN-stabilized vesicles. Indeed, this was also not expected, as there is only a few mass percent of PAA present in the vesicles, which will only slightly modify the elastic properties of the Pluronic L121 vesicles.

Pluronic L121 and P123 have a very similar central PPO block length, but differ with respect to the length of the PEO blocks. This longer PEO block of

P123 has the effect that the latter shows a significantly different self-assembling behavior from L121. We have shown previously that Pluronics are able to reversibly associate to and dissociate from the IPN-stabilized vesicles.[12] Upon introduction of P123 into the system, we can anticipate that L121 molecules are solubilized into the P123 micelles and that in turn some P123 molecules will be taken up in the IPN-vesicles. The net result of this may well be that the vesicular capsules are being modified with respect to their surface area.

In the Appendix we present a simple model based on the Helfrich bending energy of spherical and cylindrical vesicles in the presence of a spontaneous (optimal) curvature, a feature inherited from the formation of the IPN. According to this model a small increase in surface area, which will result in a non-optimal radius, can be tolerated and the vesicles remain spherical. However, at a 100% increase in area, the deviations from the preferred radius already cause so much bending stress in the network that a shape transformation becomes thermodynamically favorable. An inhomogeneously curved cylindrical vesicle becomes preferred over a homogeneously curved spherical one because the first has an average radius closer to the ideal radius of the network (that is the one given by the conditions under which the IPN was formed). In line with the experiments we calculate that the first stable tubular vesicles have an aspect ratio between 5 and 10.

Figure 3.6b only shows the effect of P123 on the IPN-stabilized vesicles shortly after the spherical to tubular phase transition took place. Due to the inflow of a high concentration of P123, the tubular vesicles are eventually completely solubilized. These transformations do not only occur at high concentrations of P123. When a much lower concentration of 3-4 mg/ml of P123 is used the same morphological transitions occur.

The results presented above show that the immobilization method is indeed very gentle. Additional arguments that the vesicles are only weakly bound come from the observation that the PAA-charged Pluronic L121 vesicles that are attached to the surface at room temperature spontaneously desorb from the surface when the temperature is increased. Indeed, almost all immobilized vesicles are released into the bulk at 35 °C. Again we do not exactly know why this effect takes place. We may speculate that the hydrogen bonds between PAA and the oxygen atoms of the Pluronic become slightly weaker at elevated temperatures, such that the PAA desorbs from the vesicles. It is also feasible that PAA be-

comes more soluble in water at higher temperatures and therefore does not tend to remain bound to the vesicles. Furthermore, Pluronic L121 is a temperature-sensitive block copolymer, for which the solubility typically decreases with increasing temperature.[12] When the solubility decreases however, one would expect a higher surface affinity. This provides additional evidence that a change of the vesicle-PAA interactions is responsible for the desorption process.

3.3 Outlook

Much synthetic effort has been put into making block copolymers containing PAA as part of the polymer. In many cases PAA is introduced in the system to create a biofunctional component that binds e.g. proteins.[26, 27] Conventional molecular chemistry, however, requires complex synthetic procedures and only in special cases, such PAA-containing copolymers can be used to generate vesicles with reasonable control over their size and morphology.

In the system presented here, the size of the vesicles can be tuned by simply selecting the size of the pores of the extrusion membrane. Then the vesicle size is fixed by the IPN formation. It was shown that PAA molecules can be associated with these capsules in such a way that the complex becomes charged. This renders them attractive for a broad range of possible (bio)applications. The PAA-coated capsules may be used to track proteins or other molecules adsorbing onto the vesicles in real time. These immobilized vesicles can be used as a tool to study single vesicle dynamics, such as release or fusion process,[9] and they can also provide a fast indication of morphological transitions or phase behavior in bulk.[8] Finally, it was shown that it is possible to generate asymmetrically shaped vesicles. The study of such morphological transitions may be of interest to understand the behavior of biological counterparts, e.g. blood cells.

3.4 Conclusions

Pluronic L121 vesicles in combination with PAA were stabilized by means of a network of polymerized PETA. The PAA-charged nonionic polymersome vesicles were immobilized onto glass as well as onto mica surfaces. Mg^{2+} ions are used as bridge between the two negatively charged components, polyelectrolyte and the surface. CLSM and liquid AFM studies show that the vesicles are indeed gently

immobilized on the weakly charged surface, because the capsules are bound to the surface at room temperature but are released at 35 °C, and the vesicles are able to move around an equilibrium position. The vesicles can change their shape to tubular vesicles upon addition of another block copolymer. The latter shape transition also occurs for corresponding conditions in the bulk. A simple model explains the thermodynamic stability of the tubular vesicles. It is argued that the IPN has a memory for a preferred radius and that by forcing the network to assume a larger area the cylindrical shape has an average curvature closer to the ideal one than the spherical shape.

3.5 Appendix

In this appendix a simple model is introduced that provides a possible mechanism for the structural transition seen in the IPN-stabilized L121 vesicles upon addition of P123. We will use thermodynamic arguments which explain in which direction changes take place. We stress that such free energy arguments are of use, even though the CLSM experimental observations for our system do not necessarily represent equilibrium because an excess of P123 is added. In the TEM experiments however we may be much closer to equilibrium. Lipid vesicles that are stressed by a pressure jump or by a sudden change of the temperature also show large transient shape changes.[28, 29] In these lipid vesicles however the hindered transport of water across the bilayer is an important factor. For our capsules we believe that the water transport is not very slow because the bilayer core is not as dense as that for the lipid vesicles. In our case the change in area is accompanied by water transport and also results in a change in volume.

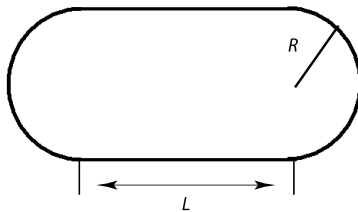


Figure 3.7: *Tubular vesicle with radius R and length L .*

The first observation is that by P123 addition there is an increase of the area of the vesicle from the initial value A_0 to the actual A . Important is the relative

increase in area, $A/A_0 > 1$. We may arbitrarily set $A_0 = 4\pi$ and use $A > 4\pi$ as an input parameter. The second experimental observation is that tubular vesicles are formed after P123 is added which is a motivation to focus on this geometry.

Referring to Figure 3.7 we assign the parameters R and L to the tubular vesicles. Using this geometry it is possible to express the radius R as a function of the length and the area, $R(L, A)$

$$R(L, A) = -\frac{L}{4} + \frac{1}{4}\sqrt{L^2 + 4\frac{A}{\pi}} \quad (3.1)$$

An important point is that the IPN gives the vesicles the memory of its initial radius $R_0 = 1$. In the following we will evaluate the difference in curvature energy of a closed surface for a given fixed surface area A . As the area is fixed the free energy per unit area (surface tension) is not important. Moreover as the topology does not alter, we do not need to include the Gaussian bending modulus. Following Helfrich we compute the free energy of curvature by

$$\Delta F = \int_{\Omega} \frac{1}{2}k_c (J - J_0)^2 \quad (3.2)$$

where the integration is over the whole surface. In this equation k_c is the mean bending modulus, and $J = 1/R_1 + 1/R_2$ is the mean curvature, where R_1 and R_2 are the two principle radii of curvature. J_0 is the curvature at the moment of the formation of the IPN, which is in our case $J_0 = 2/R_0$. Again, we will keep the area fixed and consider the result of eqn (3.2) keeping R (and related to this L) as the control variable

$$\frac{\Delta F}{k_c} = 2\pi R^2 \left(\frac{2}{R} - \frac{2}{R_0} \right)^2 + \pi RL \left(\frac{1}{R} - \frac{2}{R_0} \right)^2 \quad (3.3)$$

The first term on the right hand side of eqn (3.3) gives the curvature energy in the spherical end caps of the cylinder. The second term gives the curvature energy in the cylindrical body. It is easily checked that when the area increase vanishes, i.e. when $A = 4\pi$, the length of the cylinder must be zero, the radius $R(L, A) = R_0$ and the change in the curvature energy vanishes. We are not interested in the absolute value of the curvature energy, but focus on the R (or equivalently L) dependence. For this dependence the absolute value of the bending modulus is not important.

$\Delta F/k_c$ is plotted in Figure 3.8 for various values of $A > 4\pi$ as a function of L . For very small increases in area, i.e. $A/A_0 < 1.7$, the curvature energy is an increasing function of L . This means that the spherical vesicle is the ground state (lowest in energy). However, when $A/A_0 > 1.7$ the curvature energy becomes non-monotonic and a second minimum appears. This minimum represents the possible stabilization of cylindrical vesicles. In the regime $1.7 < A/A_0 < 2.0$ the tubular vesicle remains meta-stable and the spherical capsule remains the stable one. However when $A/A_0 > 2.5$ the tubular vesicle is the lowest in energy and the spherical one becomes metastable. The energy barrier between the two states that can coexist at $A/A_0 \sim 2.5$ (bimodal condition) indicates that the transition is abrupt. As the height of this barrier scales with the area of the initial vesicle, it diverges in the limit of very large vesicles. For mesoscopic vesicles however, the barrier height is finite and the transition is only first-order like. In the language of phase transition, the first appearance of the meta-stable state at $A/A_0 = 1.7$ may be identified as a spinodal point. The second spinodal point associated with the loss of the metastable spherical vesicle occurs only in the limit of infinite A .

The aspect ratio of the tubular vesicles L at the bimodal is approximately 10. This is in good agreement with the experiments.

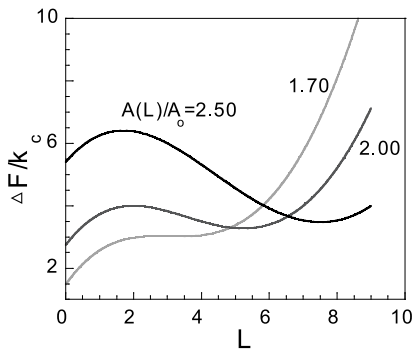


Figure 3.8: *Bending energy difference of cylinder vesicles versus spherical vesicles against the length of the cylinder tube at different sizes.*

Bibliography

- [1] D.E. Discher, A. Eisenberg, *Science* **2002**, *297*, 967-973
- [2] Y. Kim, P. Dalhaimer, D.A. Christian, D.F. Discher, *Nanotechnology* **2005**, *16*, S484-S491
- [3] S.A. Jenekhe, X.L. Chen, *Science* **1998**, *279*, 1903-1907
- [4] B.M. Discher, Y.Y. Won, D.S. Ege, J.C.M. Lee, F.S. Bates, D.E. Discher, D.A. Hammer, *Science* **1999**, *284*, 1143-1146
- [5] H. Kukula, H. Schlaad, M. Antonietti, S. Forster, *J. Am. Chem. Soc.* **2002**, *124*, 1658-1663
- [6] J.H. Lee, V. Agarwal, A. Bose, G.F. Payne, S.R. Raghavan, *Phys. Rev. Lett.* **2006**, *96*, 048102
- [7] T. Ruysschaert, A.F.P. Sonnen, T. Haefele, W. Meier, M. Winterhalter, D. Fournier, *J. Am. Chem. Soc.* **2005**, *127*, 6242-6247
- [8] T.M. Weiss, T. Narayanan, C. Wolf, M. Gradzielski, P. Panine, S. Finet, W.I. Helsby, *Phys. Rev. Lett.* **2005**, *94*, 038303
- [9] U. Borchert, U. Lippardt, M. Bilanz, A. Kimpfler, A. Rank, R.P. Suss, R. Schubert, P. Lindner, S. Förster, *Langmuir* **2006**, *22*, 5843-5847
- [10] J.V. Noort, S. Verbrugge, N. Goosen, C. Dekker, R.T. Dame, *Proc. Natl. Acad. Sci. U.S.A* **2004**, *101*, 6969-6974
- [11] P. Hinterdorfer, Y.F. Dufrêne, *Nature Methods* **2006**, *3*, 347-355

- [12] F. Li, T. Ketelaar, A.T.M. Marcelis, F.A.M. Leermakers, M.A. Cohen Stuart, E.J.R. Sudhölter, *Macromolecules* **2007**, *40*, 329-333
- [13] K. Schillen, K. Bryske, Y.S. Melnikova, *Macromolecules* **1999**, *32*, 6885-688
- [14] K. Bryske, J. Jansson, D. Topgaard, K. Schillen, U. Olsson, *J. Phys. Chem. B* **2004**, *108*, 9710-9719
- [15] W.B. Huttner, J. Zimmerberg, *Curr. Opin. Cell Biol* **2001**, *13*, 478-484
- [16] J. Käs, E. Sackmann, *Biophys. J* **1991**, *60*, 825-844
- [17] J.H. Lee, S.R. Yang, E.J. An, J.D. Kim, *Macromolecules* **2006**, *39*, 4938-4940
- [18] N. Csaba, L. Gonzalez, A. Sanchez, M.J. Alonso, *J. Biomater. Sci. Polym. Ed.* **2004**, *15*, 1137-1151
- [19] T.G. Park, S. Cohen, R. Langer, *Macromolecules* **1992**, *25*, 116-122
- [20] K.T. Oh, T.K. Bronich, A.V. Kabanov, *J. Controlled Release* **2004**, *94*, 411-422
- [21] J. Zipfel, P. Linder, M. Tsianou, P. Alexandridis, W. Richtering, *Langmuir* **1999**, *15*, 2599-2602
- [22] J. Zipfel, J. Berghausen, G. Schmidt, P. Linder, P. Alexandridis, M. Tsianou, W. Richtering, *Phys. Chem. Chem. Phys.* **1999**, *1*, 3905-3910
- [23] V. Pata, F. Ahmed, D.E. Discher, N. Dan, *Langmuir* **2004**, *20*, 3888-3890
- [24] S.L. Li, A.F. Palmer, *Macromolecules* **2005**, *38*, 5686-5698
- [25] X.M. Liang, G.Z. Mao, K.Y. Simon Ng, *J. Colloid Interface Sci.* **2005**, *285*, 360-372
- [26] A. Wittemann, T. Azzam, A. Eisenberg, *Langmuir* **2007**, *23*, 2224-2230
- [27] V. Bromberg, M. Temchenko, G.D. Moeser, T.A. Hatton, *Langmuir* **2004**, *20*, 5683-5692
- [28] C. Nicolini, A. Celli, E. Gratton, R. Winter, *Biophys. J* **2006**, *91*, 2936-2942
- [29] T. Baumgart, S.T. Hess, W.W. Webb, *Nature* **2003**, *425*, 821-824

Part II

Polymer co-assembly

Chapter 4

Small monodisperse unilamellar vesicles from binary copolymer mixtures

Small unilamellar vesicles are formed spontaneously by simple mixing of lamellae-forming diblock copolymer PB₁₀PE₁₀ (PB is a butylene oxide block, and PE an ethylene oxide block) with micelle-forming diblock copolymer PB₁₀PE₁₈. Small angle neutron scattering (SANS) measurements show that the average vesicle radius may be as small as 30 nm with a polydispersity index of 0.15. From the SANS measurements it can also be deduced that the vesicles have a 3.4 nm thick hydrophobic membrane core and a 1.2 nm hydrophilic corona. Furthermore, it is seen that the vesicles coexist with spherical micelles. The influence of the mixing ratio as well as the concentration of the polymeric components is studied. Results of the micelle size, the vesicle size and the shell structure are confirmed by cryo-TEM measurements.

In slightly modified form published as: F. Li, S. Prévos, R. Schweins, A.T.M. Marcelis, F.A.M. Leermakers, M.A. Cohen Stuart, E.J.R. Sudhölter. *Soft Matter* **2009**

4.1 Introduction

Vesicles composed of block copolymers, also called polymersomes, have been studied extensively in the past few years due to their stimuli responsiveness and chemical diversity.[1] Many amphiphilic block copolymers can self-assemble into vesicles at low concentrations.[2-5] Often some processing trick is needed to form polymersomes. For example, one may start with dissolving the copolymer in a solvent that is good for both blocks (e.g. THF) and then add a selective solvent (e.g. water). Typically, the sizes of such polymersomes are not easily controlled below a radius of 100 nm. In addition, they are relatively polydisperse implying that the thermodynamic status is uncertain. For applications, e.g. in drug delivery, there is a strong desire for particles with a diameter around 40-50 nm.[6, 7] Structures larger than 100 nm will be cleared quickly from the blood stream (typically within 48 h after administering).[6] Conceptually, there are no fundamental reasons that prevent polymersomes with a sub 100 nm size to form. Indeed, upon strict thermodynamic control, one can arrive at small entities.[8] Alternatively, small objects may be expected in a process of self assembly by precisely tuning the hydrophilic/hydrophobic balance. However, it is hard to find the proper driving and stopping forces for this process.

An interesting route to regain control over the vesicle size is to work with mixtures of associating copolymers. Such a procedure may be referred to as co-assembly. Although co-assembly has been investigated before, these studies often were concerned with mixtures with a highly asymmetric composition. For example, bilamellar vesicles have been reported, which were formed by mixing unilamellar vesicles with a biopolymer.[9] Asymmetric polymersomes were found in mixtures of polymers and lipids.[10] The properties of such objects can be readily modified by tuning the mixing ratios of the various components. One may then easily end up with very complex systems so that sophisticated techniques are required to probe the detailed properties and to explain the mechanisms behind these.[11]

In this Chapter the formation of small unilamellar vesicles is reported, which are generated by systematically mixing two chemically and compositionally similar block copolymers, namely poly(butylene oxide)-co-poly(ethylene oxide), abbreviated by PB_nPE_m , in water. As such, the formation of polymersomes in such a system may qualify as a process of co-assembly. Several examples of

self-assembled PB_nPE_m vesicles have been reported previously. In most cases, large vesicles are formed, having a radius in the micrometer range.[12, 13] Only upon extrusion of the polymersomes through a filter with small pores, the vesicle size can be reduced to the nanometer range.[14] In the system described here, we simply combine lamellae-forming nonionic block copolymers, $PB_{10}PE_{10}$, with micelle-forming ones, $PB_{10}PE_{18}$, in an aqueous solution. In well-chosen mixing ratios, rather monodisperse small vesicles with well-defined dimensions are formed. By itself, the vesicle-forming $PB_{10}PE_{10}$ block copolymer forms very unstable vesicles. They quickly fuse and aggregate into micrometer-size, multilamellar vesicles,[12] proving that the lamellar phase is the equilibrium state. Copolymers with the larger PE block, $PB_{10}PE_{18}$, spontaneously forms spherical micelles at room temperature.[15] Upon mixing, the two block copolymers co-assemble into vesicles as small as 30 nm in size with a narrow size distribution. Apparently, the presence of the PE_{18} tails prevents aggregation of the formed vesicles. Hence a solution of polymersomes is obtained that remains stable in time. The systems were characterized both by SANS and cryo-TEM. The results are in good agreement with each other and from this we have detailed information on the properties of the polymersomes. In Chapter 5 we present the molecular modeling of this system.[17] Our simple approach to form stable polymersome opens a flexible route in designing controlled nano-containers with excellent opportunities for drug delivery applications.

4.1.1 Materials

The diblock copolymers $PB_{10}PE_{10}$ and $PB_{10}PE_{18}$ were synthesized by anionic polymerization of 1,2-butylene oxide and ethylene oxide. We obtained these polymers as a kind gift from Dr. Harris of the Dow Chemical Company. Details on the polymer synthesis and characterization can be found elsewhere.[12]

4.1.2 Preparation of vesicles from $PB_{10}PE_{10}$ and $PB_{10}PE_{18}$ copolymer

Block copolymers with indicated mixing ratios were added to water (D_2O for the SANS studies). The samples were frozen to -20 °C and subsequently thawed to room temperature, while stirring. This freeze-thaw cycle helps both components to get intimately homogenized which speeds up the equilibration of the vesicles. We note that there is no filtration process involved in the whole sample prepara-

tion procedure. All samples were allowed to stand for more than 48 h before the experiments were performed.

4.1.3 Small Angle Neutron Scattering (SANS)

Small angle neutron scattering experiments were performed at the Institut Max von Laue-Paul Langevin (ILL), Grenoble, France, on the D11 instrument. Three sample-to-detector distances were chosen to cover a wide q -range of 0.019-2.073 nm^{-1} , with an incident wavelength of 0.6 nm and a wave-vector resolution $\Delta q/q$ of 10%. Samples were contained in quartz cuvettes with a neutron pathway of 1 mm, placed in a thermostated sample-holder at 25 °C with a precision of 0.1 °C. Data were accumulated on a two dimensional detector with an active counting area of 64 x 64 pixels with a pixel size of 1 x 1 cm^2 . Scattering patterns were isotropic and subsequently radial-averaged. The spectra were treated according to standard ILL procedures, and the scattering cross-sections are expressed in cm^{-1} . Normalisation was achieved by measuring H_2O as secondary calibration standard. The SANS data are modeled by a combination of two particular species, namely small spheres (representing micelles) admixed with bilayer vesicles, using the SASfit software written by Joachim Kohlbrecher, which is available from ETH.[16] The mathematical background for the fitting is also described at this website.

4.1.4 Cryo-Transmission Electron Microscopy (cryo-TEM)

A few microliters of sample were placed on a holey carbon film supported on a TEM grid. A filter paper was then used to blot the drop so as to create a thin film. This sample was cryo-fixed by rapidly immersing into liquid ethane cooled to -170 to -180 °C. The specimen was inserted into a cryo-transfer holder and then transferred to a JEOL JEM2100 TEM. Examinations were carried out at temperatures around -170 °C. The TEM was operated at an acceleration voltage of 200 kV. Zero-loss filtered images were taken under low dose conditions (1000-2000 nm^2).

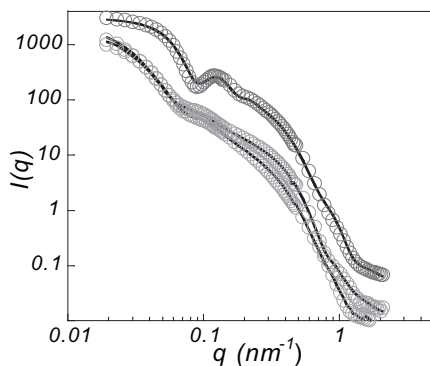


Figure 4.1: SANS data from $PB_{10}PE_{10}$ and $PB_{10}PE_{18}$ mixtures. From top to bottom: 40 mg/ml $PB_{10}PE_{10}$ and 20 mg/ml $PB_{10}PE_{18}$, 4 mg/ml $PB_{10}PE_{10}$ and 6 mg/ml $PB_{10}PE_{18}$, 4 mg/ml $PB_{10}PE_{10}$ and 2 mg/ml $PB_{10}PE_{18}$

4.2 Results and Discussion

Polymer mixtures at low concentrations (4 mg/ml $PB_{10}PE_{10}$ admixed with 6 mg/ml $PB_{10}PE_{18}$) and at high concentration (40 mg/ml $PB_{10}PE_{10}$ mixed with 20 mg/ml $PB_{10}PE_{18}$) were studied with SANS. These SANS profiles are fitted using a combined model of a solid sphere (representing micelles) and a detailed vesicle model. The fits to the data are shown in Figure 4.1 as solid lines. All fits are in excellent agreement with the scattering data, especially in the low q range of the scattering curve. This indicates that the form factors are fully consistent with the co-existence of small unilamellar vesicles and (effectively) spherical micelles. At higher q ($0.9 < q < 1.0 \text{ nm}^{-1}$) there is a very small discrepancy between the data and the model. This possibly points to the complexity of the vesicle membrane, for example the fact that the membrane leaflet will feature thickness fluctuations.[14] Alternatively, the small deviations at higher q may point to fluctuations of the micelle shape away from the spherical geometry which was also not accounted for.

Detailed information about our systems, which apparently are composed of both spherical micelles and unilamellar vesicles, was obtained from the fitting results. The effective micelle radii are as follows: 4.9 nm, 5.4 nm for the mixtures at low concentrations (4:2 and 4:6) and 6.0 nm for the mixture at high concentration (40:20). The corresponding aggregation numbers increase from 13 to 53 and even up to 190 for the most concentrated case. These relatively large changes of the micelle size and aggregation numbers with polymer concentrations is remarkable

as in the case of micelles composed of $PB_{10}PE_{18}$ only, the size of the micelles does not depend much on concentration.[15] Indeed, the differences in micelle size and aggregation number that were extracted from the SANS measurements can not simply be attributed to an increased polymer concentration. In principle, the micellization may be sensitive to the temperature, but during these experiments, the temperature was hold constant at 25 °C, which excluded this parameter as a possible cause of the micelle size growth. We therefore are left with the scenario that mixed micelles must form in this system and that the size apparently depends on the polymer composition.

Table 4.1: Vesicle dimensions (radius of vesicle upto the core, R_{ves} membrane core thickness, t_{core} and membrane corona thickness, t_{corona} and polydispersity determined from the SANS model for three different mixtures of $PB_{10}PE_{10}$ and $PB_{10}PE_{18}$).

$PE_{10}: PE_{18}$	R_{ves} (nm)	t_{core} (nm)	t_{corona} (nm)	polydispersity
4:2	33.7	3.2	1.5	0.30
4:6	38.5	3.9	1.4	0.32
40:20	31.0	3.4	1.1	0.15

Molecularly realistic self-consistent field theory studies indicate that upon adding $PB_{10}PE_{18}$ to $PB_{10}PE_{10}$ aqueous solution, the aggregates of the amphiphilic mixtures do not simply change gradually from spherical vesicles into spherical micelles (Chapter 5). Instead, we find that for a range of copolymer compositions, spherical micelles coexist with vesicles and that upon an increase in $PB_{10}PE_{18}$, the amount of copolymers in micelles increases at the expense of that in vesicles. Indeed, the micelles consist of both block copolymers and their size and composition may easily vary upon a change of the overall polymer concentration and mixing ratio.

As mentioned, the mixture of $PB_{10}PE_{10}$ and $PB_{10}PE_{18}$ not only gives rise to mixed micelles, but also to stable mixed vesicles. This is remarkable as well, because in the absence of $PB_{10}PE_{18}$ the vesicles of $PB_{10}PE_{10}$ are not stable. In the small unilamellar vesicles composed of the binary mixture of polymers, both block copolymers have the same hydrophobic block length and hence we do expect that both surfactants mix well. It is further expected that the inner and outer leaflets of the vesicle walls have slightly different dimensions due to the difference in the hydrophilic chains, which leads to small differences of the membrane core and corona thicknesses with composition and concentration, as shown in Table

4.1. With increasing ratio $PB_{10}PE_{18}$ to $PB_{10}PE_{10}$, the overall membrane thickness increases slightly which may be related to the larger average size of the PE block.

In Figure 4.2 the results of the fitting procedure are displayed where we plot volume fraction (number density times R^3) as a function of the radius R of the two species. Indeed, upon mixing of 2 % (w/w) $PB_{10}PE_{18}$ with 4 % $PB_{10}PE_{10}$ highly monodisperse small unilamellar vesicles are spontaneously generated. The small polydispersity index of 0.15 indicates that the vesicles are under thermodynamic control. For such a vesicle solution one should expect that the vesicle radius and perhaps also the polydispersity index are a function of both the overall polymer concentration and the mixing ratio. Indeed, when the concentration is reduced ten fold, the sample shows a significantly larger polydispersity index of 0.30. This response to a reduction of the concentration from 4 % to 0.4 % $PB_{10}PE_{10}$, is shown in Figure 4.2.

Both samples with relatively low polymer concentrations (0.4 % $PB_{10}PE_{10}$ with 0.2 % $PB_{10}PE_{18}$ and 0.6 % $PB_{10}PE_{18}$) have similar size distribution profiles and in both situations the vesicles (and the micelles) are more polydisperse (Figure 4.2a), than for the higher polymer concentration (Figure 4.2b). The explanation of this phenomenon is very likely found from realizing again that our sample contains two copolymers.

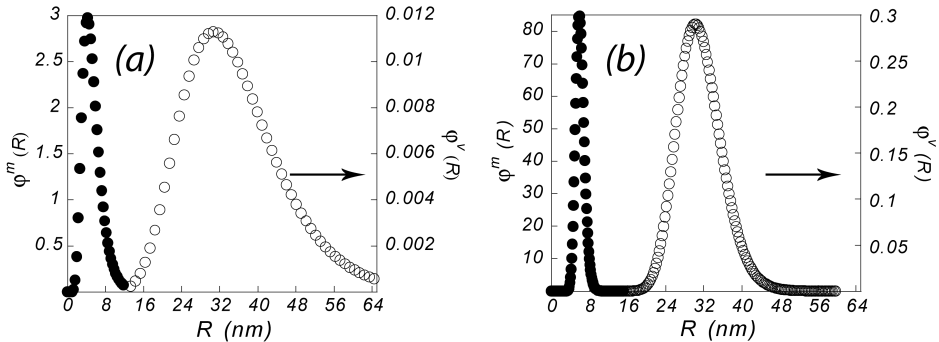


Figure 4.2: Lognormal distribution of mixed micelle and vesicle volume fraction as a function of particle radius for combination of (a) 4 mg/ml $PB_{10}PE_{10}$ and 2 mg/ml $PB_{10}PE_{18}$ and (b) 40 mg/ml $PB_{10}PE_{10}$ and 20 mg/ml $PB_{10}PE_{18}$; left sharp peak indicated with filled circle comes from mixed micelle and right broad peak indicated with open circle belongs to small unilamellar vesicle.

In Chapter 5[17] we present results of a molecularly realistic self-consistent field theory aimed to model the present system. From this study it follows that

there is a window of compositions for which it is possible that vesicles coexist with spherical micelles. With increasing loading of the vesicles with $PB_{10}PE_{18}$ it appears necessary to decrease the vesicle size dramatically. At the same time the micelle concentration that coexists with the vesicles increases exponentially and become more monodisperse. These predictions correlate well with the experimental findings.

A more definite proof that mixed micelles co-exist with small unilamellar mixed vesicles comes from cryo-TEM experiments. The experimental conditions for the neutron scattering experiments apply here as well. Because for cryo-TEM relatively high concentrations are needed, the results for the polymer mixtures at the highest concentration, i.e. 2 % $PB_{10}PE_{18}$ mixed with 4 % $PB_{10}PE_{10}$ are presented here. Figure 4.3 shows some typical cryo-TEM images. In these images, the vesicles are clearly visible, and the much smaller micelles can also be identified. In line with the SANS data, the images show relatively monodisperse vesicles. Also the average radius of 34 nm is comparable to the SANS data. In Figure 4.3b an magnified image is presented from which a value of about 3 nm for the vesicle wall thickness can be measured. Indeed, this corresponds quite well with the thickness of the hydrophobic core of the membrane of the vesicle as deduced from SANS. Apparently, the hydrophilic corona of the membrane has too little contrast for cryo-TEM. From Figure 4.3b a micelle core radius of approximately 5 nm can also be obtained which is consistent with the SANS data.

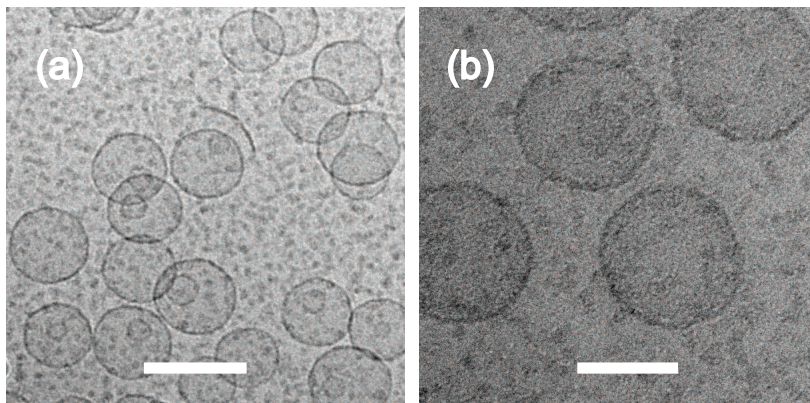


Figure 4.3: Cryo-TEM image of a mixture of 40 mg/ml $PB_{10}PE_{10}$ and 20 mg/ml $PB_{10}PE_{18}$ (a) representative image of small unilamellar vesicles coexistent with mixed micelles, scale bar 100 nm (b) enlarged image, scale bar 50 nm

The combination of SANS and cryo-TEM data confirm that the vesicles that are found in the mixed systems are rather monodisperse with a small size of about 30 nm. The vesicles are stable in time as found experimentally, since both the SANS and the Cryo-TEM samples were measured one week after sample preparation. Two main factors contribute to this stability. First, two copolymer species were used for which the hydrophobic parts exactly match. This ensures that both polymers mix well. The second point is that one of the polymers has a slightly larger PE block. This forms a stabilizing corona layer that gives steric stabilization. Interestingly, the temperature stability of PB-PE vesicles is very good and stable vesicles of this type have been reported upto 80 °C.[14]

To our mind the method that is advanced of making stable vesicles from the mixture of two copolymers is novel and has important implications. Normally, one expects that a finite solubility of the amphiphiles may disturb potential applications, e.g., for their use in drug delivery. In the present system, this problem may not necessarily be so prominent because upon dilution one will first dissolve the micelles, and only in the limit that all micelles have disappeared the vesicles will disintegrate. In other words, the reduction of the micelle concentration will prevent in first order the drop of the chemical potential of the surfactants when the system is diluted.

The addition of a micelle-forming surfactant to a lamellae-forming lipid is known to strongly reduce the mean bending modulus of the composite vesicle.[18] From this, one may speculate that it is natural to expect small vesicles to become stable with increasing concentration of surfactants. We note however, that the present system differs from the surfactant/lipid mixtures. The theoretical modeling of the current system[17] shows that the mean bending modulus is virtually unaffected by the ratio $PB_{10}PE_{18}$ to $PB_{10}PE_{10}$. The reason for this is that both polymeric components have the same length of the hydrophobic block. The increase of the average head group size (with increasing composition of $PB_{10}PE_{18}$) does not affect the mean bending modulus much because the effects of the increase of the corona size and the decrease of the core size compensate each other.[19] The mechanism behind the formation of small vesicles in mixtures of lamellae forming and micelle forming copolymer thus does not rely on the change in the bending modulus. It is however not completely unrelated to the value of the bending modulus. Indeed, the value should be small to prevent the bending energy in the vesicles to be excessively large. A low bending modulus corresponds to a low

value of the membrane persistence length which in turn facilitates the formation of small vesicles. Our calculations also show that the total curvature energy of vesicles is not excessively high.

Assisted by a freeze-thaw cycle, the spontaneous formation of small unilamellar vesicles from a simple mixture of lamellae and micelle forming copolymers, will be of interest for a broad range of possible applications. It is believed that the formation of stable vesicles by using a pair of copolymers is a general feature, which may apply to other amphiphilic mixtures as well. The interest in polymeric species to design nanocapsules using different components may add more than one functionality to those nanocapsules. More specifically, our capsules may already provide interesting opportunities for *in vivo* drug delivery and food applications. The small size is an attractive feature as for such capsules the circulation time in the blood stream may be sufficiently long to start thinking about the introduction of a successful targeting functionality. Finally, due to the ethylene oxide corona, these capsules probably exhibit stealth behaviour.

4.3 Conclusions

Small unilamellar vesicles spontaneously form in simple mixtures of a lamellae-forming block copolymer PB₁₀PE₁₀ with a micelle-forming block copolymer PB₁₀-PE₁₈. SANS and cryo-TEM studies prove that the co-assembled vesicles are rather monodisperse with a core radius down to 30 nm and that under these conditions the polymeric species coexist with mixed spherical micelles. The polydispersity of the vesicles as well as their sizes are well controlled by the mixing ratio of the components as well as by the polymer concentrations used.

Bibliography

- [1] D.E. Discher, A. Eisenberg, *Science* **2002**, 297, 967-973
- [2] T.A. Bronich, M. Ouyang, V.A. Kabanov, A. Eisenberg, F.C. Szoka, A.V. Kabanov, *J. Am. Chem. Soc.* **2002**, 124, 11872-11873
- [3] B.M. Discher, Y.Y. Won, D.S. Ege, J.C.M. Lee, F.S. Bates, D.E. Discher, D.A. Hammer, *Science* **1999**, 284, 1143-1146
- [4] H. Kukulka, H. Schlaad, M. Antonietti, S. Forster, *J. Am. Chem. Soc.* **2002**, 124, 1658-1663
- [5] Y. Kim, P. Dalhaimer, D.A. Christian, D.E. Discher, *Nanotechnology* **2005**, 16, S484-S491
- [6] N. Ishiyama, *Nature Nanotechnology* **2007**, 2, 203-204
- [7] W. Jiang, B.Y.S. Kim, J.T. Rutka, W.C.W. Chan, *Nature Nanotechnology* **2008**, 3, 145-150
- [8] F. Li, T. Ketelaar, A.T.M. Marcelis, F.A.M. Leermakers, M.A. Cohen Stuart, E.J.R. Sudhölter, *Macromolecules* **2007**, 40, 329-333
- [9] J.H. Lee, V. Agarwal, A. Bose, G.F. Payne, S.R. Raghavan, *Phys. Rev. Lett.* **2006**, 96, 048102
- [10] T. Ruysschaert, A.F.P. Sonnen, T. Haefele, W. Meier, M. Winterhalter, D. Fournier, *J. Am. Chem. Soc.* **2005**, 127, 6242-6247
- [11] T.M. Weiss, T. Narayanan, C. Wolf, M. Gradzielski, P. Panine, S. Finet, W.I. Helsby, *Phys. Rev. Lett.* **2005**, 94, 038303

- [12] J.K. Harris, G.D. Rose, M.L. Bruening, *Langmuir* **2002**, *18*, 5337
- [13] G. Battaglia, A.J. Ryan, *J. Am. Chem. Soc.* **2005**, *127*, 8757-8764
- [14] Norman, A. I.; Ho, D. L.; Lee, J. H.; Karim, A. *J. Phys. Chem. B* **2006**, *110*, 62-67
- [15] A.I. Norman, D.L. Ho, A. Karim, E.J. Amis, *J. Colloid Interface Sci.* **2005**, *288*, 155-165
- [16] <http://kur.web.psi.ch/sans1/SANSSoft/sasfit.html>
- [17] F. Li, A.T.M. Marcelis, F.A.M. Leermakers, M.A. Cohen Stuart, E.J.R. Sudhölter; *Soft Matter* *10.1039/b904525b*
- [18] M.M.A.E. Claessens, B.F. van Oort, F.A.M. Leermakers, F.A. Hoekstra, M.A. Cohen Stuart, *Physical Review E* **2007**, *76*, 011903
- [19] Y. Lauw, F.A.M. Leermakers, M.A. Cohen Stuart, *J. Phys. Chem. B* **2003**, *117*, 10912-10918

Chapter 5

Field Theoretical Modeling of the Coexistence of Micelles and Vesicles

Using the self-consistent field (SCF) theory for inhomogeneous polymer systems, we elaborate a molecular model on a united atom level and discuss the possibility of coexistence of spherical micelles and small unilamellar vesicles in binary copolymer mixtures in a selective solvent. Our analysis is in line with recent neutron scattering and Cryo-TEM results for the mixture of two members of the poly(butylene oxide)-*b*-poly(ethylene oxide) (referred to as PB_nPE_m) family, namely the $(n, m) = (10, 10)$ and $(10, 18)$ species in water that clearly pointed towards such coexistence. The $-PE_{18}$ is a micelle forming and the $-PE_{10}$ a lamellae forming copolymer. Upon increasing concentration of $-PE_{18}$ the micelle concentration that coexists with the vesicles increases dramatically. In this situation the micelles determine the chemical potentials of the copolymers and with increasing fraction PE_{18}/PE_{10} the vesicle size becomes dramatically smaller. The selection of vesicle size indicates its thermodynamic stability. The strategy to

In slightly modified form published as: F. Li, A.T.M. Marcelis, M.A. Cohen Stuart, E.J.R. Sudhölter, F.A.M. Leermakers. *Soft Matter* **2009**

arrive at thermodynamically stable vesicles with sizes much smaller than 100 nm is of interest for a wide range of applications.

5.1 Introduction

Amphiphilic block copolymers in selective solvents are known to self-assemble into various association colloids ranging, e.g., from vesicles,[1] rods,[2] small disks,[3] to micelles.[4] Vesicles composed of block copolymers have been studied extensively, because of their stimuli responsiveness to physiochemical stimuli and their chemical diversity. Micelles have been studied for many years as well, for example to learn about their ability to solubilize hydrophobic molecules, and to take up active ingredients.[5] Phase diagrams of amphiphilic molecules are fascinatingly complex, and this complexity even increases for mixed amphiphilic systems. This paper deals with a binary copolymer solution that spontaneously forms a mixture of vesicles and micelles.

There are various reports in the literature that point to the possibility of coexistence between different types of aggregates in one system, suggesting that phase transitions between different types of aggregates are possible. For example, early experimental observations of (cylindrical) micelle-vesicle coexistence in lipid-surfactant systems were published more than two decades ago.[6, 7] More recently, the coexistence of disklike micelles and vesicles received some attention.[8] In a phenomenological model, Andelman and coworkers [9] it was argued that in mixed dilute solutions a phase transition from cylindrical micelles to vesicles can occur when there is a large difference in preferred geometry of aggregation between the lipid and the surfactant. In their model these authors did not consider the size (nor size selection) of the vesicles and avoided all issues regarding the thermodynamic stability. Of a more recent date there are computer simulations[10] that focus on the structural transition from micelles to vesicles and point to a possible coexistence of aggregates.

Experimentally, it is easiest to consider such structural transitions in binary amphiphilic mixtures. Most of these studies therefore have focused on mixtures of a pair of amphiphiles that differ dramatically in chemical structure, i.e. mixtures of short, relatively polar micelle-forming surfactants with very apolar lipid species that prefer vesicles [11]. No systematic experimental nor theoretical studies are known that focused on the vesicle-to-micelle transition in a binary mixture with

relatively little difference in molecular architecture between the constituent amphiphiles. In polymeric surfactants, however, there exist interesting possibilities to implement such an investigation.

In Chapter 4, small angle neutron scattering (SANS) measurements were performed, which indicate that in mixtures of two block copolymers that are chemically and compositionally similar to each other, vesicles and micelles can coexist. More specifically, we focused on two members of the poly(butylene oxide)-*b*-poly(ethylene oxide), PB_nPE_m , copolymer family in aqueous solutions, namely $(n, m) = (10, 10)$ which is a lamellae forming copolymer, and $(10, 18)$, which forms spherical micelles. We found that for a certain mixing ratio, small unilamellar mixed vesicles with an average radius of 30 nm and narrow polydispersity index 0.15 coexist with a relatively concentrated solution of spherical micelles with a radius of approximately 5 nm.[12] These results were confirmed by Cryo-TEM images on the same samples.

We have evidence that these systems represent true thermodynamic equilibrium. For example, we find that the structural features did not change for long storing times, that both the vesicles as well as the micelles have a narrow size distribution, and that the size as well as the polydispersity is a function of the polymer composition and the concentration. We used a freeze-thaw method to accelerate the equilibration, but the results were not sensitive to the details of the preparation procedure.

Hence, the question should be considered why such small vesicles form, why they are highly monodisperse and how they can coexist with much smaller micelles. The fairly small differences between the two copolymer species makes it difficult to distinguish between them experimentally, e.g., labeling the polymers is likely to perturb the co-assembly significantly. That is why progress on the experimental side is difficult.

Fortunately, the evidence that these systems are in a free energy minimum justifies a theoretical analysis aimed at understanding the equilibrium properties of these vesicle-micelle systems. With the above questions in mind we embarked on a detailed self-consistent field (SCF) analysis of this problem. The model that is used is tailored to the PB_nPE_m system, but we stress that our results are more generally applicable. In line with the early model of Andelman [9], it appears relatively straightforward to show that it is possible to find a regime where the mixing ratio between $PB_{10}PE_{10}$ and $PB_{10}PE_{18}$ is such that the respective chemi-

cal potentials for these species assembled in micelles is equal to that in vesicles. Hence, this allows us to confirm that these two states of assembly can indeed coexist. The size selection of the vesicles, however, is a more delicate issue. We present evidence that one should expect that the size of the vesicles is a strongly decreasing function of the PE_{18}/PE_{10} ratio, giving support for the findings and interpretations of the SANS and Cryo-TEM data. Although it is not yet possible to make strong quantitative predictions, we stress that many experimental aspects of these polymer mixtures are recovered by the model, e.g., regarding issues such as the size and size distribution of the micelles and the micelle concentration that coexist with the vesicles. Hence, the field theoretical modeling confirms our viewpoint that in these systems the small unilamellar vesicles are thermodynamically stable.

The remainder of this Chapter is organized as follows. First, we will briefly outline the SCF theory and mention its approximations. This part is followed by a short section on the thermodynamic arguments that are used to analyze the stability of the association colloids. The model and its parameters are presented before the results are discussed. Again we stress that we exclusively focus on the binary PB_n - PE_m systems, trying to model the experimental system.[12] In the concluding remarks we will put our predictions in a broader perspective.

5.1.1 SCF theory

Here we present the SCF theory for (polymeric) self-assembly using the discretization scheme of Scheutjens and Fleer [13, 14] and apply this to a molecularly detailed model where the segments in the polymer chain are described on an united-atom level (the united atoms are referred to as segments below). The theory has been extensively discussed in the literature, and we refer to this for most of the details.[15, 16] Here, we will only mention the main characteristics and approximations used. The parameters that are used for the PB_nPE_m copolymers in an aqueous solution are the same as those used for corresponding modeling of Pluronic polymers (also modeled on the united-atom level).[17, 18] Instead of propylene-oxide units in the latter, we now have polybutylene-oxide units with just one CH_2 (united) atom extra in the side chain. One consequence of this is, obviously, that the PB unit is more hydrophobic than poly(propylene oxide). All molecular details (the model) and the parameters used are collected in a small

paragraph presented below.

At the basis of the SCF theory is the mean-field free energy density $f[\{\varphi\}, \{u\}](r)$ (we will reduce all energies by the thermal energy $k_B T$). This notation implies that the free energy is a function of two conjugated quantities, namely the volume fraction $\varphi(r)$ (dimensionless concentration), and the corresponding segment potential $u(r)$. Both quantities are a function of the radial coordinate in the system $r = 1, 2, \dots, M$ (we focus on the spherical geometry and trust that the modifications for other geometries are obvious), and thus f is a function of this radial coordinate as well. The curly brackets indicate that for each segment type in the system the (φ, u) pair is present. In our system segments are referred to with the index A . The solvent S (water): $A = 1$, segment C2 (representing CH_2): $A = 2$, segment C3 (representing CH_3): $A = 3$, segment O (representing oxygen atom and the terminal OH group): $A = 4$.

The mean-field free energy is written as $F[\{\varphi\}, \{u\}] = \sum_r L(r) f[\{\varphi\}, \{u\}](r)$, where $L(r)$ is the dimensionless volume of the lattice layer (number of lattice site) r . We will reduce all lengths by the size of a lattice site b . For the spherical coordinate system we have $L(r) \propto r^2$. In all our calculations $r = 0$ will coincide with the center of mass of a spherical micelle or a spherical unilamellar vesicle (the two main target species of the calculations).

The free energy F is formally given by:

$$F[\{\varphi\}, \{u\}] = -\ln Q(\{u\}) - \sum_r L(r) \sum_A u_A(r) \varphi_A(r) + F^{\text{int}}(\{\varphi\}) + \sum_r u'(r) \left(L(r) \sum_A \varphi_A(r) - 1 \right) \quad (5.1)$$

The first term of Eqn 5.1 features the partition function $Q(\{u\}, V, T)$, which can be computed from the segment potentials. The second term in Eqn 5.1 is a Legendre transformation such that the first two terms essentially give the dimensionless entropy in the classical $(\{n\}, V, T)$ ensemble. The third term is the contribution that specifies all possible interactions between the different segments, and between segments and the solvent. The last term of eqn 5.1 decouples the volume fractions of the components, where the Lagrange parameter $u'(r)$ is linked to the incompressibility constraint $\sum_A \varphi_A(r) = 1$, implemented locally for each coordinate r .

In our model we will only account for short-range nearest-neighbor interactions

and use the well-known Bragg-Williams approximation to estimate the number of (A - B) contacts (here the index B refer to the segments similarly as A).[19] For each contact between unlike segments, there is a Flory-Huggins interaction parameter χ_{AB} , which is positive for repulsion and negative for attraction.[19] It is possible to write $F^{\text{int}} = \sum_r L(r)f^{\text{int}}(r)$, where the free energy density for the interactions $f^{\text{int}}(r)$ can be written as

$$f^{\text{int}}(r) = \sum_A \sum_{B>A} \chi_{AB} \varphi_A(r) (\langle \varphi_B(r) \rangle - \varphi_B^b) \quad (5.2)$$

Here, $\varphi_A(r)$ is the fraction of sites in layer r occupied by segments of type A and φ_A^b is the corresponding fraction in the bulk (a region far away from the micelle or the vesicle, where no inhomogeneities in concentrations exist). The angular brackets imply a three-layer average:

$$\langle \varphi(r) \rangle = \lambda(r, r-1)\varphi(r-1) + \lambda(r, r)\varphi(r) + \lambda(r, r+1)\varphi(r+1) \quad (5.3)$$

where the *a priori* step probabilities $\lambda(r, r')$ specify the fraction of contacts a segment at coordinate r has with segments at coordinate r' . These quantities depend on the spatial coordinates because they must obey the internal balance equation $L(r+1)\lambda(r+1, r) = L(r)\lambda(r, r+1)$. Obviously, these transition probabilities are normalized $\sum_{r'=r-1, r, r+1} \lambda(r, r') = 1$.

The optimization of the free energy leads to the self-consistent field conditions:

$$\frac{\partial F}{\partial \varphi_A(r)} = -u_A(r) + u'(r) + \chi_{AB} \langle \varphi_B(r) - \varphi_B^b \rangle = 0 \quad (5.4)$$

$$\frac{\partial F}{\partial u_A(r)} = -\frac{\partial \ln Q}{\partial u_A(r)} - L(r)\varphi_A(r) = 0 \quad (5.5)$$

$$\frac{\partial F}{\partial u'(r)} = \sum_A \varphi_A(r) - 1 = 0 \quad (5.6)$$

The Eqns 5.4-5.6 are solved numerically up to high precision[16, 14] and the result is known as the SCF solution. For such SCF solution it is possible to evaluate the grand potential $\epsilon_m = F - \sum_i \mu_i n_i$, where i refers to a molecular species (Water: $i = 1$, PB₁₀PE₁₀: $i = 2$ and PB₁₀PE₁₈: $i = 3$) and μ_i is the corresponding chemical potential for species i . In first order the chemical potentials of the molecular components are found from the bulk volume fractions $\mu_i \approx \ln \varphi_i^b$. More accurate values, available from Flory-Huggins theory, are implemented for the computation of ϵ_m . It turns out that it is possible to write $\epsilon_m = \sum_r L(r)\omega(r)$, where the dimensionless grand potential density ω is given by:

$$\omega(r) = - \sum_i \frac{\varphi_i(r) - \varphi_i^b}{N_i} + \ln \frac{\varphi_S(r)}{\varphi_S^b} - \frac{1}{2} \sum_A \sum_B \chi_{AB} (\varphi_A(r) \langle \varphi_B(r) \rangle + \varphi_B(r) \langle \varphi_A(r) \rangle - \varphi_A^b \varphi_B^b) \quad (5.7)$$

Here the degree of polymerisation N_i specifies the total number of lattice sites that are occupied by each molecule i .

At this point we did not yet explain how we evaluate the partition function $Q = \prod_i q_i^{n_i} / n_i!$, where q_i is the single-chain partition function, nor how we can compute the volume fractions from the segment potentials (other than the formal definition given by eqn 5.5). We have implemented a Markov approximation for this. This implies that the chain connectivity is accounted for, in such a way that the memory of the path of the chains is lost after each 'propagating' step. This means that it is not excluded that chains self-intersect. The combined statistical weight of all allowed walks is found by solving the Edwards diffusion equation (effectively, this leads to the Gaussian chain model). [20] On a lattice this procedure transforms into a set of complementary propagators, and the chain model is that of a freely-jointed chain. The propagator equations are very efficient in computing the volume fractions, because the number of operations is of order N . However, these propagators become somewhat involved for branched molecules, and therefore we sketch what is exactly done. We refer to the literature for full details.[21, 22]

In short, the propagators generate the set of all allowed conformations, $\{c\}$, of the (branched) polymer (solvent) i , with segment ranking numbers $s = 1, \dots, N_i$ and enumerates for each conformation c the sum of its segment potentials $u_i^c = \sum_s u_i^c(s)$ (where $u_i^c(s)$ is the segment potential felt by segment s of molecule i being in conformation c). For a given conformation the coordinates of all segments, r_s^c , are specified and from the primary sequence of segments of the chain we know the segment type A of segment s (this is an input) and thus the value of u_i^c is evaluated straightforwardly using the segment potentials specified in Eqn 5.4. Next, the statistical weight of each conformation c is found by applying the Boltzmann law $G_i^c = \exp -u_i^c$. From these weights it is then possible to generate the volume fraction profiles $\varphi_A(r)$ without further approximations. The volume fraction distributions are normalized such that the total number of chains in the system is consistent with the imposed value (in a closed system) or that the bulk

volume fraction of the component equals the imposed value (semi-open system).

In summary, the SCF formalism specifies how to compute the volume fractions for given potentials and how the segment potentials follow from the volume fractions. The SCF solution is found iteratively. Routinely, we obtain a numerical accuracy better than 7 significant digits. As a result, we have detailed information on the (radial) volume fraction profiles of all molecular species in the system, and we have exact numerical values for the mean-field free energy of the system. The latter information is used to analyze the thermodynamic status of a particular SCF solution, which is explained next.

5.1.2 Thermodynamics of association colloids

From a classical thermodynamic analysis of mixtures of amphiphiles in a selective solvent one cannot obtain details on the molecular level on how molecules interact with each other. Instead it gives well-known laws for macroscopic equilibrium, for example, that there can be no spatial gradients in the chemical potential of the components in the system. Our interest is in the case that copolymers partition between a free state in solution, being assembled into spherical (or worm like) micelles and/or in vesicles. This can only happen if the chemical potential of the molecular species in all these states is identical. We will use this criterion below.

To make further progress, one has to focus on what happens in the system on a length scale of the micelles or vesicles. This is the realm of the thermodynamics of small systems and statistical thermodynamics.[23] In SCF modeling one has to start by choosing the geometry of the coordinate system. For example, a spherical coordinate system is used to study spherical micelles and vesicles, the cylindrical coordinate system is used to model the linear micelles (worm like micelles) and the (ordinary) flat coordinate system is applicable for bilayers. When our interest is in knowing which of the aggregate types is thermodynamically the most favorable, one has to consider the chemical potentials of the molecules that are observed in all these cases. The aggregates with the lowest chemical potentials are the preferred ones. Hence, in an SCF calculation it is possible, by choosing, e.g., the wrong geometry to obtain detailed information on the aggregation properties of the copolymers that would not have formed spontaneously. Inversely, it is possible that in an SCF analysis a particular aggregation type is claimed to be most favorable, while the best aggregated state has been overlooked. A full analysis is

therefore not trivial and various complementary calculations are always needed before strong conclusions can be drawn.

To judge equilibrium, it appears that the grand potential ϵ that is associated to the presence of the aggregates is a key quantity of interest. The grand potential of a self-assembled object is the intensive variable conjugated to the number of such objects. It is important to mention that this number is not fixed and optimizing the system free energy with respect to the number of objects leads to the conclusion that $\epsilon = 0$. [24, 25] In other words, the free energy of the micellar system must be equal to $F = \sum_i n_i \mu_i - pV$.

In the computational volume of a typical SCF analysis a micelle as well as a vesicle has no translational degrees of freedom, as these are fixed with their center of mass to the center of the coordinate system. The grand potential that is evaluated after solving the SCF equations is, for a single object, given by ϵ_m . As the micelles are fixed to the center of the coordinate system, we must insist that $\epsilon_m > 0$. Assuming that only translational degrees of freedom on the micelle or vesicle length scale are ignored we may write (recall, all terms are reduced by $k_B T$):

$$\epsilon = \ln \phi + \epsilon_m = 0 \quad (5.8)$$

Here ϕ is the volume fraction of micelles (vesicles). Alternatively, ϵ may be interpreted as the excess chemical potential that can be associated to a micelle (which must be zero), $\ln \phi$ is $-TS_{\text{translation}}/k_B T$ and ϵ_m is the free energy of formation of the micelle. As the excess chemical potential per micelle is zero, we have $\phi = \exp(-\epsilon_m)$. [24]

Of course eqn 5.8 has only limited applicability. In the context of a micellar system, we clearly ignored the entropy associated with size and shape distributions. For vesicles, the main extra approximation is that eqn 5.8 ignored the entropy that is present in the membrane undulations. Hence, the application of eqn 5.8 gives only an indicative value of the micelle/vesicle volume fractions. Therefore, we will not insist on the accuracy of the book keeping in terms of the full distribution of polymers over the micelles, vesicles and freely floating in solution. Hence, strong quantitative predictions are, at the current state of matter, out of reach. Instead we will use Eqn 5.8 to obtain an order of magnitude of the micelle/vesicle concentrations.

Even though the SCF modeling focuses on most-likely micelles/vesicles, and

although in the 'simulation' volume just one micelle/vesicle is present, we can estimate, e.g. the fluctuations in the micelle size from evaluating how much the aggregation number changes with small changes in the chemical potential(s). In multi-component systems such analysis is already more complex than in single component systems so we will only qualitatively apply this information.

5.1.3 The model and the parameters

The molecules in our system are modeled on a united-atom level. Following previous calculations on Pluronic self-assembly, we have good estimates of the interaction parameters.[17, 18] We will therefore not discuss the parameters but justify them *a posteriori* by the correlation of the calculations with the experimental data.

There are three molecular entities in our model: water plus two diblock copolymer species PB_nPE_m :

- 1 Water molecules are modeled as small (compact) objects that occupy 5 lattice sites. These sites are arranged in a 'star' configuration, i.e. a central 'segment' is surrounded by 4 neighbors. The motivation for doing this is to mimic the fact that water forms, through its H-bonding capabilities, small clusters. These clusters are invariably larger than, e.g., a united atom CH_2 . We arbitrarily have chosen for a size ratio of 5. We haste to mention that this is a very primitive model for water. In the model the 'segment' type of water is denoted by S.

The copolymers have three segment (united atom) types: CH_2 , CH_3 and O. The PB block has the following structure: $PB = O-(C2[C2-C3]-C2-O)_n-$, where the part in the square bracket is a side chain (which thus occurs n times). The PE block is a linear sequence of united atoms $-(C2-C2-O)_m$.

- 2 For ($n = 10$, $m = 10$) copolymer, the backbone of the hydrophobic part is as long as that of the hydrophilic part. We will prove that (with the current set of interaction parameters) this copolymer prefers the lamellar topology.
- 3 The ($n = 10$, $m = 18$) copolymer has an almost twice as long hydrophilic block than the hydrophobic one. Due to this, this surfactant is a strongly micelle forming species and even refuses to make linear micelles at high concentrations.

Table 5.1: List of Flory-Huggins interaction parameters used the model.

χ	S	C3	C2	O
S	0	1.5	1.1	-0.7
C3	1.5	0	0.5	2
C2	1.1	0.5	0	2
O	-0.7	2	2	0

Note that both copolymers have an equal length of the hydrophobic part. This is an important property of our system. The similar length of the PB part will guarantee that the two copolymers mix ideally with each other. We thus may not expect that the two copolymers form separate phases inside one aggregate, i.e., no patches are expected nor strong partitioning of copolymers between inner and outer leaflets in the vesicle, etcetera. This simplifies the theoretical modeling significantly.

The list of FH χ parameters used in the study are collected in table 5.1. The interaction parameters with the solvent S are most relevant for the starting and stopping mechanism of self-assembly. The C3 unit (the final segment in the side groups) is taken somewhat more hydrophobic than the C2 ones. The negative value of χ_{SO} indicates that the oxygen really likes to be solvated by water. In a previous study we argued that this parameter is the one that responds to the temperature, a more negative value implies a lower temperature. The current value is chosen so that the self-assembly is somewhere in between the critical micellisation temperature (CMT) and the cloud point temperature (CPT). We further implemented a small repulsion between C2 and C3, which is the same as in previous studies. There is further a significant repulsion between O and the apolar units $\chi_{OC3} = \chi_{OC2} = 2$. This repulsion helps to separate the PE block from the PB one and this repulsion adds to the stability of the micelles/vesicles. Again, these parameters have been used before to model the self-assembly of Pluronic polymers. They reproduced the proper trends, e.g., for the CMC as a function of the lengths of the PPO and PEO blocks and also the trends for CMT and CPT.[17, 18] We haste to mention however, that the present set is not necessarily the best possible one. Although small changes in the parameters will give quantitatively different results, we have checked that the qualitative effects remain the same when the parameters are modified (within reasonable limits of course).

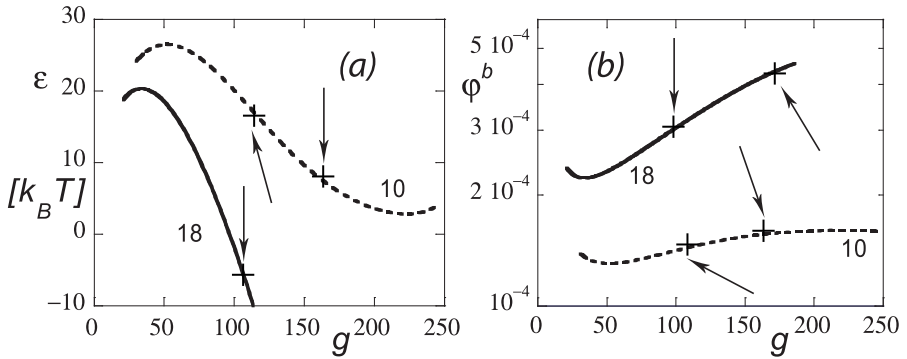


Figure 5.1: a) The grand potential ϵ_m as a function of the aggregation number g for two systems, the (10, 10) copolymer (dashed line) and the (10,18) copolymer (solid line). The arrow pointing downward is discussed in the text and points which micelle coexists with worm-like micelles. b) the bulk volume fraction of copolymers as a function of the aggregation number g on a log-lin scale. The dashed line is for the (10, 10) copolymer, the solid line for the (10, 18) one. The arrows pointing downward is discussed in the text and points to the aggregation number of the spherical micelle that coexist with long linear micelles. The upward arrow points to the point where a flat bilayer would coexist with spherical micelles.

5.2 Results and interpretation

The result section is organized in the following parts. We will begin with a presentation of the self-assembly characteristics of copolymers separately. We will see that $PB_{10}PE_{18}$ forms spherical micelles and that $PB_{10}PE_{10}$ strongly prefers the lamellar topology. We then move on to the binary mixtures, establish a diagram of states, and identify the region of micelle/vesicle coexistence. The remainder of the results will focus on the properties of the system when coexistence is possible and elaborate on the size selection of the vesicles.

5.2.1 Single copolymer assemblies

In the SCF theory one has to choose the system volume (and geometry) and specify the number of copolymers that are in this volume. Next, one needs to present the numerical procedure with some initial guess. In most cases a small (local) disturbance away from the homogeneous solution is sufficient to arrive at a unique non-trivial SCF solution.[16] For such a result we find that a fraction of the molecules has accumulated in the micelle/vesicle and the remainder is floating

freely in solution. The concentration of the latter is invariably close to the critical micelle concentration. From this it is clear that not all compositions that are used will lead to meaningful micelles or vesicles. We need the thermodynamic arguments to select the relevant cases. More specifically we need to analyze the grand potential and the chemical potentials.

At this stage it is important to mention that the aggregation number g_i of copolymers of type i in an aggregate is given by the excess amounts in the aggregate:

$$g_i = \frac{1}{N_i} \sum_r L(r) (\varphi_i(r) - \varphi_i^b) \quad (5.9)$$

In Figure 5.1a we present the grand potential ϵ_m as a function of the aggregation number found for the (translationally restricted) spherical micelles, for both PB₁₀PE₁₈ as well as PB₁₀PE₁₀. The accompanying Figure 5.1b gives the corresponding bulk volume fractions of polymers that are in equilibrium with the micelles on a log-lin scale. The quantities plotted in panels *a* and *b* are related through the Gibbs-Duhem relation $\partial\epsilon_m/\partial\ln\varphi^b = -g$. As the fluctuations in the aggregation number in the micelle size are necessarily positive, we should focus on the aggregation numbers for which $\partial g/\partial\mu > 0$. This coincides with the requirement $\partial\epsilon_m/\partial g < 0$. There are a number of important predictions that can be extracted from these graphs: [17]

- 1 *Theoretical CMC.* The maximum in $\epsilon_m(g)$ corresponds to the first appearance of stable micelles in the system. The corresponding minimum in $\varphi^b(g)$ thus corresponds to the (theoretical) CMC. The volume fraction of micelles at this theoretical CMC may be computed from Eqn 5.8 and is much smaller for the PE₁₀ than for the PE₁₈ copolymers. The aggregation numbers for these first micelles appears to be roughly the same for the two copolymers ($g \approx 50$); it is slightly smaller for the PE₁₈ species than for the PE₁₀ one.
- 2 *Experimental CMC.* Depending on the measuring technique, we expect that one can experimentally see micelles above some threshold ϕ (below some threshold ϵ_m). Quite arbitrarily one may choose micelles with $\epsilon_m < 10$ as micelles that are experimentally observable. Following this criterion we thus expect that the first micelles that can be measured for the PE₁₈ polymer have a twice lower aggregation number than those of PE₁₀.
- 3 *The CMC.* The CMC is to first order a function of the length of the hydrophobic block. As both copolymers have the same 'tail' length, we expect the

CMC to be roughly the same. To second order it should be an increasing function of the length of the polar block. Hence we expect the CMC to be lower for the PE₁₀ than for the PE₁₈ copolymer. Indeed this is what is observed (cf. Figure 5.1b): there is a difference in CMC by a factor of about two.

- 4 *The CPT.* The minimum in $\epsilon_m(g)$ found for the PE₁₀ around $g \approx 225$ indicates that it is not possible to obtain a high concentration of those micelles: application of Eqn 5.8 implies that ϕ goes through a maximum. This indicates that this system is close to the cloud point.[18] For sufficiently high copolymer concentrations one must expect a condensed phase of copolymers (often this is the lamellar phase). A similar minimum does not appear for the PE₁₈ copolymer system, indicating that the longer hydrophilic block keeps the micelles stable up to higher micelle concentrations. This system is well below its cloud point temperature.
- 5 *Fluctuation in micelle size.* From Figure 5.1b we can directly estimate the fluctuations of the micelle size for micelles with a given average g , by taking the inverse of the slope of the curves (at the specified g).[17] Clearly the PE₁₀ micelles have significantly larger size fluctuations than the PE₁₈ ones. We will return to this property below.
- 6 *The second CMC.* From Figure 5.1b we find that with increasing polymer concentrations the micelles will grow slightly (only by a factor of approximately two) and at the same time the chemical potential increases slightly as well, but the micelle concentration increases exponentially ($\epsilon_m(g)$ decreases linearly with g). At some threshold polymer concentration the chemical potential will reach the value for which worm-like micelles become stable. In Figure 5.1b we have indicated these bulk volume fractions of the copolymers by the arrows that point downwards. These concentrations were obtained from analyzing micellisation in the cylindrical coordinate system (not shown). In Figure 5.1a one can find the grand potential of the micelles that coexist with the worm-like micelles. To first order this grand potential is equal to the so-called end-cap energy.[26] Around the appearance of the worm-like micelles the system switches its strategy (instead of increasing the number of micelles, it increases the length of the worm-like micelles). This change in strategy is easily seen in experiments and the concentration

of copolymers where this happens is known as the second CMC. Worm-like micelles should have a positive value for the end-cap energy and we conclude that only for the PE₁₀ species the spherical micelles can potentially coexist with worm-like micelles. The PE₁₈ polymer has a negative end cap energy and thus these copolymers form spherical micelles up to very high polymer concentrations.

7 *Stability of tensionless bilayers.* For both copolymers we have also considered the stability of tensionless flat bilayers.[27] The bulk volume fractions of the surfactants that are found in this case are also presented in 5.1b, i.e., by the arrow pointing upward. We note that large vesicles exist at virtually the same chemical potential ($\ln \varphi^b$) as the tensionless flat bilayers and thus, we may already speculate on the possible coexistence of spherical micelles with vesicles (similarly as worm-like micelles coexist with spherical micelles). However, from Figure 5.1b we conclude that, for the PE₁₈ polymer, the bulk concentration of polymers that co-exists with bilayers (arrow pointing upward) is even higher than that for the worm-like micelle. Hence, there is no possibility to have coexistence between spherical micelles and vesicles. Indeed, when we model spherical vesicles composed of PE₁₈ only (not shown), we find that the curvature energy of the vesicle is negative (Figure 5.3c). This clearly points to the instability of the bilayer configuration for the PE₁₈ chains. The situation is completely different for the PE₁₀ copolymer. In this case the bulk concentration of surfactant that coexists with bilayers is lower than that for worm-like micelles. Hence, it is not possible to form worm-like micelles for this surfactant, as speculated above. Instead, bilayers should form first. The volume fraction of micelles (as can be estimated from using eqn 5.8) that coexists with bilayers (vesicles) is extremely low (below the experimental CMC), so that in practice it will be very difficult to observe such coexistence. This might explain why this phenomenon has not been discussed in the literature.

We have seen that the interpretations based on the results of Figure 5.1 are in close correspondence with known behavior for surfactant and copolymer micellisation in general.[28] More specifically, the results prove to be in excellent agreement with experimental observations that the PE₁₈ copolymer readily forms micelles and that the micelles are rather monodisperse up to very high copolymer

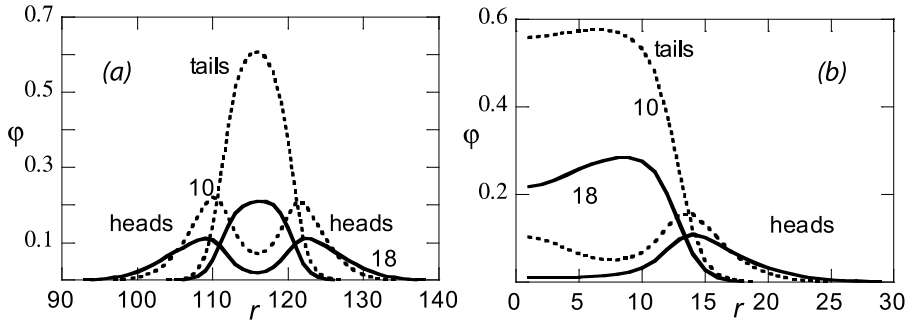


Figure 5.2: Radial volume fraction profile for tail (PB) and head group (PE) segments of $PB_{10}PE_{10}$ and $PB_{10}PE_{18}$ in: a) mixed vesicles and b) mixed micelles with a radius $R \approx 50$. Both systems have same chemical potentials for all species and thus correspond to the situation that the vesicles coexist with the micelles: $\varphi_{10}^b = 1.217 \times 10^{-4}$ and $\varphi_{18}^b = 6.2167 \times 10^{-5}$. The $PB_{10}PE_{10}$ polymer is indicated as dashed lines the $PB_{10}PE_{18}$ copolymer by solid line.

concentration. On the other hand, the PE_{10} polymer is just forming lamellae and in the absence of repulsion between the membranes (not shown), we should expect that a lamellar phase, or an onion phase (multilamellar vesicles) is formed. We will see next that the analysis becomes slightly more involved in binary polymer mixtures.

5.2.2 Binary copolymer assemblies

In binary systems it appears necessary to define how much of the (10, 10) and (10, 18) copolymers we have in the assemblies. This can be done in various ways. Here, we choose to do this by computing the amount θ_i^σ of segments of each type that is in excess in the micelles. The ratio of these is computed from

$$\frac{\theta_{18}^\sigma}{\theta_{10}^\sigma} = \frac{\sum_r L(r) (\varphi_2(r) - \varphi_2^b)}{\sum_r L(r) (\varphi_1(r) - \varphi_1^b)} \quad (5.10)$$

where copolymer $i = 1$ (10, 10) is given the subindex (10), and $i = 2$ (10, 18) the subindex (18) for obvious reasons (the same we do for other quantities below).

Mixing the two copolymers with fractions x_{18} and x_{10} (sum is unity) may to first order be a way to mimic the performance of a copolymer with an intermediate head-group size $\langle m \rangle = 18x_{18} + 10x_{10}$. However, there are various issues that complicate matters, namely that the partitioning of the two copolymers between micelle and bulk, or between vesicle and bulk is not the same. Nor do we expect

that at a given set of chemical potentials the ratio $\theta_{18}^\sigma/\theta_{10}^\sigma$ in the micelle is identical to that in the vesicle. For this reason we choose to work explicitly with copolymer mixtures rather than to mimic the mixture with some 'effective' copolymer.

In the present system it appears not so difficult to find situations where vesicles coexist with micelles. Let us first present typical radial volume fraction profiles for such a system. Radial profiles for mixed vesicles and mixed micelles are shown in Figure 5.2a,b, respectively. An important point is that in both systems the chemical potentials match; in both systems the bulk concentration of $PB_{10}PE_{18}$ and $PB_{10}PE_{10}$ are identical, $\varphi_{18}^b(\text{micelle}) = \varphi_{18}^b(\text{vesicle})$ and $\varphi_{10}^b(\text{micelle}) = \varphi_{10}^b(\text{vesicle})$. This system corresponds to the points indicated by the arrows in Figure 5.3.

In Figure 5.2a we present a radial distribution through a curved bilayer (vesicle). The center of the vesicle is at $r = 0$ hence in this example we have chosen for a vesicle with a very small radius of $R \approx 50$. This is done deliberately because it allows us to discuss several features of curved bilayers in binary copolymer mixtures. For example, it is found that the PE_{18} chains extend slightly further out away from the core, while the PE_{10} chain remains closer to the core. From polymer brush theory these effects are well known.[29] As compared to the homodisperse systems, the PE_{10} has a compressed conformation and the PE_{18} is somewhat over-stretched in a so-called flower conformation. More important for the present system, are the differences in profile found for the inner and outer membrane leaflet. Such differences are attributed to the curvature of the bilayer. Intuitively one would expect the PE_{18} to be preferentially in the outer leaflet and the PE_{10} in the inner one. Indeed this is the case, but the differences in composition between inner and outer leaflet are minute. Secondly, focusing again on the PE part, we expect the overall volume fraction to be higher on the inside leaflet than on the outer one. Because of the high curvature, one can indeed observe this in Figure 5.2a. The higher packing density in the inner leaflet causes the PE_{18} tails to be more clearly in the flower-conformation. They extend further away from the core in the inner leaflet than in the outer one. In the core there are also salient features that can be attributed to the curvature. For example the core-density is not exactly homogeneous; it is slightly higher on the outside than on the inside. Such effects are well known and we do not discuss these effects here further.[30, 31, 32]

The radial volume fraction profiles of mixed micelles, shown in Figure 5.2b,

also have several noteworthy features that need to be discussed. In a small spherical micelle there is a strong curvature of the interface. Hence, we expect that the micelle is preferentially populated by the PE₁₈ chains and that the PE₁₀ chains are suppressed, e.g., in comparison to the composition in the vesicles (recall that the chemical potentials are fixed). This is indeed the case, but again, the partitioning is far from complete and clearly we have an example of a mixed micelle. Focusing once more on the corona of the micelle, we see qualitatively the same phenomenon as already discussed for the vesicle. The PE₁₈ chain extends further away from the core than the PE₁₀ one. Again the PE₁₈ have the flower-conformation and these chain parts force the PE₁₀ parts to remain near the core. Quite unexpectedly, it is observed that some of the PE groups of the (10, 10) copolymers are pushed into the core. This does not happen with the PE₁₈ chain parts. The occurrence of head groups inside the core in a non-trivial distribution is often the sign that the spherical micelle has a problem and that there might be significant micelle-shape fluctuations (which allow the micelles to prevent the head groups to be in the core). We extensively looked for these. Indeed we found that small disks may be generated for which the copolymers have nearly the same chemical potentials as those of the current micelles. The same is true for small dumbbells (short worms). Hence these type of shapes should occur as fluctuations. However, also in the disk edges as well as in the end-caps of the worms the same phenomenon is observed, namely that PE₁₀ chains are partitioned inside the core. We thus conclude that this is a feature of the present mixture of copolymers. We may attribute this to the finite miscibility of PE groups in PB rich region. The fact that the two monomer units only differ with respect to the (rather small) side group may possibly facilitate this. Apparently, the PB and PE are not as strongly segregating as is the case, e.g., in charged surfactant systems where head and tail regions are strictly separated.[33]

At this point we may speculate that the presence of PE chain parts in the micelle center is one of the reasons that the system chooses for a coexistence between micelles and vesicles. Upon an increase in loading of the (10, 18) spherical micelle with (10, 10) copolymers, the PE₁₀ chain parts are 'pushed' into the micelle core. This gradually destabilizes the spherical micelle, so that the micelle-to-vesicle transition starts.

It turns out that by varying the ratio between the two polymers, one can precisely enter the region where only vesicle, only micelle or both aggregates are

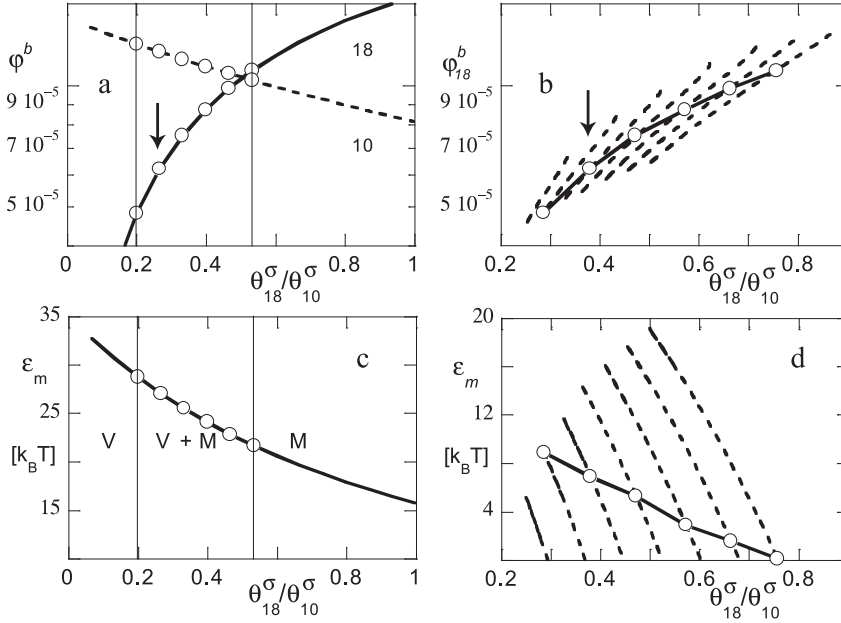


Figure 5.3: (a) Bulk volume fraction of $PB_{10}PE_{10}$, dotted line, and $PB_{10}PE_{18}$, solid line, as a function of the fraction $\theta_{18}^{\sigma}/\theta_{10}^{\sigma}$ in mixed vesicles with a radius $R \approx 100$. (b) Bulk volume fraction of $PB_{10}PE_{18}$ as a function of the ratio between amounts of $PB_{10}PE_{18}$ and $PB_{10}PE_{10}$ in mixed micelles. The different curves (dashed lines) correspond to systems for which φ_{10}^b is fixed to values between 1.2728×10^{-4} to 1.033×10^{-4} . The solid line connects points for which micelle-vesicle coexistence is possible, i.e. where φ_{10}^b and φ_{18}^b values in the micelle system coincide with those in mixed vesicles. (c) The grand potential of mixed vesicles (corresponding to panel a) plotted as a function of the ratio between amounts of $PB_{10}PE_{18}$ and $PB_{10}PE_{10}$ in the vesicle. With vertical lines we give the position of the boundaries where vesicle can coexist with micelles. Here V stands for vesicle phase only (left hand side), M stands for micelle phase only (right hand side), in between the vertical lines ($V+M$) both species can exist simultaneously. (d) The grand potential of mixed micelle is plotted (corresponding to panel b) as a function of the $\theta_{18}^{\sigma}/\theta_{10}^{\sigma}$ ratio in micelles (dashed lines). Again, the solid line connects points where micelle-vesicle coexistence is possible. The arrows (in panel a and in b refer to a system of which the radial profiles are shown in Figure 5.2.

present and the relevant compositions of the vesicles is such that the (10, 18) is in the minority, i.e., $\theta_{18}^\sigma < \theta_{10}^\sigma$. Again, as in a given SCF calculation there is just one (most-likely) aggregate present, one has to identify these regions from analyzing the thermodynamic information of these systems. In Figure 5.3a,c data for the vesicles and in Figure 5.3b,d the information for mixed micelles is presented. The first two panels (*a*, *b*) focus on the bulk volume fractions (chemical potentials), whereas panels *c* and *d* present the corresponding grand potentials.

Conceptually, it is more easy to understand how the calculations proceed for the vesicle case and therefore we will explain these results first. As discussed above already, it suffices to specify for a given volume of the system (with spherical geometry) the number of molecules of all components to obtain a unique SCF solution. In this case we first estimate how many molecules we need for the vesicle to have a radius of approximately $R \approx 100$, and then do a series of calculations for which x_{18} and x_{10} is varied. We then compute the ratio of the excess quantities and evaluate the grand potential as well as the chemical potentials. These quantities are presented in Figure 5.3a,c.

As is seen in Figure 5.3a the bulk volume fraction of (10, 18) increases, and that of (10, 10) decreases upon an increase of the ratio of amounts of PB₁₈/PB₁₀ in the vesicle. The increase of the bulk volume fraction of (10, 18) is expected, because when $\theta_{18}^\sigma \ll \theta_{10}^\sigma$, the amount of (10, 18) in the system is initially very small (sub CMC) and grows towards CMC-values. The decrease of the bulk volume fraction of (10, 10) is less trivial. Indeed, upon the gradual loading of the vesicles with (10, 18), the membrane thickness decreases gradually and this is favorable for the packing of the (10, 10). More specifically, this molecule does not need to stretch as much as in the pure (10, 10) bilayers. Correspondingly, the grand potential of the vesicle decreases with increasing presence of (10, 18), i.e. with increasing $\theta_{18}^\sigma/\theta_{10}^\sigma$ as is shown in Figure 5.3c. For spherical vesicles the grand potential can be decomposed into $\epsilon_m = 4\pi(2k_c + \bar{k})$, where k_c is the mean and \bar{k} the Gaussian bending modulus.[34, 35] Hence, we see that the effective bending modulus $\tilde{k} = 2k_c + \bar{k}$ is decreasing by about a factor of two upon an increase of the loading of (10, 18) into (10, 10), up to the 1:1 ratio. This does not necessarily mean the same change in respective values of k_c or \bar{k} . We will return to this below.

We now would like to identify those vesicles that coexist with micelles. As in the calculations of the micelles, one needs to specify the amount of molecules

for at least one component, we choose for the following strategy. Using results presented in Figure 5.3a we select a relevant value for the bulk concentration of PB₁₀PE₁₀, and then fix this value in the calculations of micelles. The number of copolymers of the type PB₁₀PE₁₈ is varied in an attempt to find a matching bulk volume fraction of surfactant for the (10, 18) copolymer. Upon increasing loading of PB₁₀PE₁₈ in the micelles we obtain data similarly as given in Figure 5.1. Here we choose to present the results in Figure 5.3b where the dotted line gives the bulk volume fraction of PB₁₀PE₁₈ as a function of the ratio $\theta_{18}^\sigma/\theta_{10}^\sigma$ in the micelle. The corresponding curve of $\epsilon_m(\theta_{18}^\sigma/\theta_{10}^\sigma)$ is presented in Figure 5.3d. This procedure is repeated several times for (slightly) different values of the bulk concentration of PB₁₀PE₁₀. In favorable cases there exists one point along a given (dotted) curve of Figure 5.3b for which the bulk volume fraction of PB₁₀PE₁₈ exactly matches the value needed for coexistence. The points for which a successful match of chemical potentials was found are connected by the solid line in Figure 5.3b. In Figure 5.3d the corresponding grand potential curves are presented, and again the solid line connects those points on the curves for which a successful match of the chemical potentials was possible.

Focusing on the solid line in Figure 5.3b, we see that with increasing loading of the micelles with (10, 18), the bulk volume fractions of (10, 18) increase as expected. It appears that we can only find a match of the chemical potentials in a specific composition regime. The upper and lower limits of coexistence are presented as vertical lines in Figure 5.3c. Turning our attention to the grand potentials of the micelles for which the matching was possible, we see that the grand potential decreases almost linearly with increasing $\theta_{18}^\sigma/\theta_{10}^\sigma$, Figure 5.3d. More striking is the fact that the grand potential of the micelles is rather low: the grand potential equals $\epsilon_m \approx 10$ for the first time we can find coexistence ($\theta_{18}^\sigma/\theta_{10}^\sigma \approx 0.3$), and it vanishes ($\epsilon_m = 0$) around $\theta_{18}^\sigma/\theta_{10}^\sigma \approx 0.75$. Using again Eqn 5.8 we see that the micelle concentration ϕ , initially is still fairly low (near the CMC $\phi \approx 10^{-4}$, but with increasing amounts of (10, 18) copolymers in the system the volume fraction of micelles that coexists with the vesicles becomes very high indeed. A key observation is that in this situation most of the copolymers reside in micelles and only a minority in the vesicles. When the concentration of micelles approaches unity ($\epsilon_m \rightarrow 0$), all aggregates must be micelles and no vesicles can form. This is the upper boundary of vesicle-to-micelle coexistence.

Let us summarize by discussing the diagram of states. Referring to Figure 5.3c,

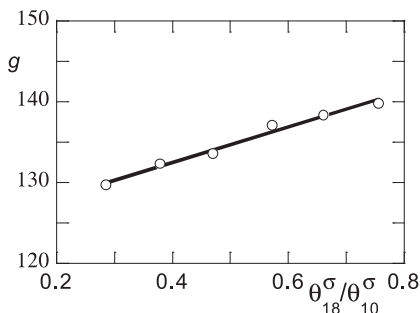


Figure 5.4: Overall aggregation number of mixed micelle $g = g_{18} + g_{10}$ as a function of $\theta_{18}^{\sigma} / \theta_{10}^{\sigma}$ in the micelle. The points corresponds to systems for which $(\varphi_{10}^b, \varphi_{18}^b)$ is fixed to values between $(1.2728 \times 10^{-4}, 4.8248 \times 10^{-5})$ and $(1.033 \times 10^{-4}, 1.0901 \times 10^{-4})$ as in Figure 5.3.

the vesicle with a low loading of (10, 18), (indicated by the letter V), is found when only vesicles are present. Above a threshold fraction of (10, 18) chains in the system we only have micelles (indicated by M). At intermediate cases we have micelle-to-vesicle coexistence (indicated by V + M). The fact that vesicles coexist with a relatively high concentration of micelles is consistent with the experimental data.

Turning once again to results of Figure 5.3 we notice that, at coexistence, the molecular composition of the micelles and that of the vesicles differ significantly. More specifically, we find $\theta_{18}^{\sigma} / \theta_{10}^{\sigma}(\text{micelle}) \approx 1.4 \theta_{18}^{\sigma} / \theta_{10}^{\sigma}(\text{vesicle})$. This result was already discussed in Figure 5.1, but we see that the difference in composition is significant for all the coexisting micelle/vesicle systems. The fact that the micelles are relatively rich in (10, 18) and the vesicles are rich in (10, 10) might have been expected from rather general considerations.[36]

Above we have seen that upon an increase of the fraction (10, 18) in the system the grand potential of the micelles that coexist with vesicles decreases. At the same time the chemical potential (bulk volume fraction) of (10, 18) increases. On the other hand, the chemical potential of the (10, 10) copolymer decreases (slightly). At this stage it is not trivial to ascertain whether the size of the micelle, in terms of the total amount of copolymers ($g = \theta_{18}^{\sigma} / N_{18} + \theta_{10}^{\sigma} / N_{10}$), is an increasing function of the (10, 18) concentration or not. As can be seen in Figure 5.4 the model predicts that the overall molecular weight of the micelle increases with increasing ratio $\theta_{18}^{\sigma} / \theta_{10}^{\sigma}$, and hence the overall micelle aggregation number

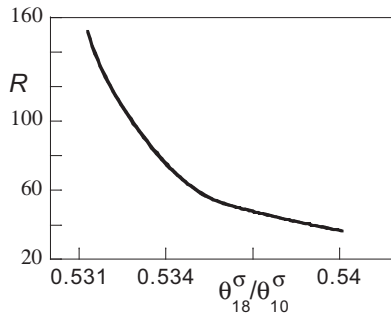


Figure 5.5: Radius of mixed vesicles plotted as a function of $\theta_{18}^{\sigma}/\theta_{10}^{\sigma}$ in the vesicle. For all vesicles the bulk volume fractions of both copolymers was assumed to be fixed (and set by the predominantly available mixed micelles): $\varphi_{10}^b = 0.00010330$ and $\varphi_{18}^b = 0.00010901$.

increases with increasing overall micelle concentration (cf Figure 5.3d). Again, this result is in line with the experimental data,[12] albeit that in the experiments the increase in micellar mass is somewhat more pronounced. The reason for this is discussed below.

From the experiments we further know that the width of the micelle size distribution is somewhat larger for lower polymer concentrations. We may understand this from our results as well. For a lower overall polymer concentration the micelle concentration is lower and the composition of the coexisting micelles shifts to a lower loading with (10, 18). From Figure 5.1 we know that micelles rich in (10, 10) have a higher degree of polydispersity than micelles rich in (10, 18).

Above, we have extensively discussed the possibility that micelles and vesicles can coexist. At this stage we must realize that we have limited our analysis thus far to vesicles with a size of approximately $R \approx 100$. There is nothing special about this particular size and, indeed, we can repeat the complete analysis for another vesicle size. It will not be a surprise that we obtained very similar result for this. Here we stress the word similar, because important differences are found too, with major consequences. From our experiments [12] we know that the vesicle size appears to be a strong function of the ratio (and concentration) PB_{18}/PB_{10} in the system. Although a full analysis of why there is a strong reduction of the vesicle size is involved, we propose the following argument. From Figure 5.3d we know that it is possible to arrive at a situation that the concentration of micelles in the system is relatively high. In this regime it is reasonable to assume that the chemical potentials are determined by the micellar species rather than the vesicles.

We therefore decided to search for vesicles with a fixed set of chemical potentials (bulk concentrations) of the two polymers. Indeed, for each vesicle size R we can find the requested match of bulk volume fractions (not exactly, but in very high accuracy). It appears, however, that all these vesicles have a systematically different polymer composition. In Figure 5.5 we plot the radius of the vesicle R as a function of the copolymer ratio in the vesicle, $\theta_{18}^\sigma/\theta_{10}^\sigma$, where we explicitly implemented the constraints that $\varphi_{10}^b = 0.00010330$ and $\varphi_{18}^b = 0.00010901$. As such Figure 5.5 is thus only a result with a 'proof of principle' status, because we could have chosen any other set of bulk volume fractions to illustrate our arguments.

Inspection of Figure 5.5 shows that with decreasing radius, the vesicles become slightly richer in the (10, 18) species. As in these graphs the chemical potentials of both surfactants are fixed, we also find that the grand potential of the vesicles is (virtually) constant. Hence, the free energy density is not altered while the composition shifts slightly as a response to an applied curvature. The result of Figure 5.5 now suggests that upon an increase in the amount of the (10, 18) polymer in the system, the system can choose to keep the chemical potentials unaltered, and to populate the vesicles with (slightly) more (10, 18) copolymers. As evident from Figure 5.5, these vesicles have a smaller radius R . Hence, we conclude that once the chemical potentials are buffered by means of a strong dominance of small mixed micelles, the vesicle radii are a decreasing function of the amount of (10, 18) in the system. From Figure 5.5 we notice that the dependence of R on the $\theta_{18}^\sigma/\theta_{10}^\sigma$ is extremely strong and therefore we conclude that, in line with the experimental data, there is a very strong *size selection* of the vesicles. Inspection of Figure 5.5 shows that the vesicle size levels off at an $R \approx 40$. It is reasonable to take a value of $b \approx 0.5\text{nm}$ as the characteristic size of a lattice layer. On this basis our results predict that the size of the vesicles can reduce to approximately $R \approx 20\text{ nm}$ (which is only reached at very high overall polymer concentrations). In any case, the predictions are in very good agreement with the observation that in the experimental system the vesicle size is as small as 30 nm.[12]

The robust size selection in these systems also suggests that the vesicle size distribution must be narrow. Experimentally it was shown that the vesicle size distribution becomes more narrow with increasing overall polymer concentration.[12] This is in full agreement with the prerequisite of the present argument, i.e., that

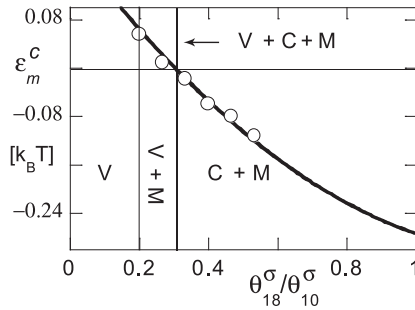


Figure 5.6: The grand potential of mixed cylinder micelle per unit length ϵ_m^c (plotted as a function of the ratio between amounts of $PB_{10}PE_{18}$ and $PB_{10}PE_{10}$ in the cylindrical micelle). With vertical lines we give the position of the boundaries where vesicle can coexist with micelles. Here V stands for vesicle phase only, M stands for micelle phase, and C stands for cylindrical micelles. The bulk volume fractions of both copolymers was assumed to match those of the mixed vesicles and for the points (cf. Figures 5.3 and 5.4) the match with mixed spherical micelles is possible.

the concentration of micelles must be large (so that the micelles buffer the chemical potentials) to have an effective size selection and thus a narrow size distribution. Reducing the polymer concentration reduces the micelle concentration, and then the size selection is expected to be less effective and the vesicle size distribution should become broader. This is also found experimentally.[12]

Up to this point we have focused on assemblies with spherical geometry, namely spherical vesicles and corresponding micelles. In the introduction we already pointed out that one of the complicating issues of the present type of SCF theories is that one needs to consider all possible geometries before one can decide what the most probable aggregate type is. We also discussed that by mixing the (10, 10) and (10, 18) copolymers, one can end up with an effective copolymer (10, $\langle m \rangle$) where $10 < \langle m \rangle < 18$. In such a situation we can expect that the worm-like micelles become the dominant species in the system at some intermediate copolymer mixing ratios. At this stage we need to estimate where this occurs in the current system. The simplest way to obtain this information is to consider the association into long linear micelles using the one-gradient cylindrical coordinate system. The Ansatz that we use is the following. We have seen in Figure 5.3a which sets of copolymer bulk volume fractions for both the (10,10) as well as the (10,18) copolymers are consistent with mixed vesicles. We use these sets of bulk concentrations once again in the cylindrical coordinate system. In Figure

5.6 we present the grand potential of the worm-like micelles (per unit length) as a function of the ratio $\theta_{18}^\sigma/\theta_{10}^\sigma$ in the worm like micelles, where we have explicitly imposed these matching bulk volume fractions (with the vesicles). The circles indicated in Figure 5.6 correspond to the same points used in Figures 5.3 and 5.4, which indicates that, in addition, the coexistence with mixed spherical micelles is possible.

In Figure 5.6 we can see that the linear micelles that are rich in PB₁₀PE₁₈ have a negative grand potential, whereas the ones that have relatively low levels of PB₁₀PE₁₈ have positive values of this grand potential. Physically, one can interpret the grand potential per unit length as the lateral tension in the worm-like micelles. A positive value means that it is unfavorable to have long worms and such worms should shrink and transform into spherical micelles. On the other hand, a negative grand potential per unit length implies that it is favorable to have worms. Hence the system likes to make linear micelles as long as possible. The imposed chemical potentials are in the latter regime higher than necessary for the worm like micelles, and we conclude that linear micelles should dominate at high polymer concentrations (and are in fact not coexisting with vesicles, but only with mixed spherical micelles). Only in the case that the system is not too concentrated in PB₁₀PE₁₈, we can confirm, now with even more confidence, that coexistence of spherical vesicles and spherical micelles is the thermodynamic stable state (first two points in Figures 5.3, 5.4 and 5.6).

Returning to Figure 5.5 we must point to the fact that the aggregation numbers reported in this figure are underestimates, except for the aggregation numbers with the lowest $\theta_{18}^\sigma/\theta_{10}^\sigma$ values. By the same token we must return to Figure 5.3 and mention that upon the increase of micelle concentration (Figure 5.3d) the transition from spherical to worm-like micelles takes place for $\theta_{18}^\sigma/\theta_{10}^\sigma > 0.4$. These worm-like micelles, however, do coexist only in a very narrow concentration regime with the vesicles. Indeed, the fact that both vesicles as well as linear micelles consist of a large number of polymers, the vesicle-to-linear micelle transition assumes close to first-order characteristics.

The diagram of states presented in Figure 5.3a,c now needs to be modified, because in this figure we overestimated the region where micelle-vesicle coexistence is possible. The improved phase boundaries are presented in Figure 5.6 by the vertical lines. With increasing PB₁₀PE₁₈ concentration it is expected that the PB₁₀PE₁₀ lamellar phase first transforms into unilamellar vesicles (letter V

in Figure 5.6). Then, with the appearance of many small mixed micelles in the system the vesicle size decreases dramatically and these vesicles are under thermodynamic control. This region is indicated in Figure 5.6 by the letters V+M. Above a given micelle concentration, the spherical micelles give way to worm-like micelles (second vertical line in Figure 5.6 labeled by V+C+M indicates that at this point vesicles, cylindrical micelles and spherical micelles coexist). At higher $\text{PB}_{10}\text{PE}_{18}$ concentrations the coexistence of micelles with vesicles disappears very quickly. Instead we will have a coexistence of spherical micelles with worm like micelles only, as indicated in Figure 5.6 by the letters C+M. Further increase of $\text{PB}_{10}\text{PE}_{18}$ will transform the linear micelles back into spherical micelles when the amount of $\text{PB}_{10}\text{PE}_{10}$ is the minority component in the system (not indicated in Figure 5.6).

In the present model the hydrophilic/hydrophobic balance (which depends on temperature) can be tuned by the Flory-Huggins parameter χ_{SO} . A more negative value implies a lower temperature and a less negative value implies a higher temperature of the system. With increasing temperature the system approaches the CPT. Another way to say the same is that the packing parameter [28] increases with temperature. Hence, the tendency to form worm like micelles increases with increasing temperature, and, consequently, the preponderance of spherical micelles decreases. On the basis of the current calculations we conjecture that with increasing temperature it should be possible to switch from a coexistence of spherical vesicles with spherical micelles to a coexistence of spherical vesicles with worm-like micelles. Evidence for such types of coexistence has been obtained by simulations.[10]

5.3 Discussion and outlook

The above results clearly point to a mechanism which facilitates the appearance of small vesicles with a narrow size distribution. The results leave little doubt that in these systems the vesicle formation is thermodynamically controlled. Both the mechanism by which the stabilization occurs, as well as the level of detail in which we are able to mimic the properties of the binary $\text{PB}_{10}\text{PE}_{10}$, $\text{PB}_{10}\text{PE}_{18}$ mixtures are unique. We argued above that the results are not limited to the PB-PE block copolymer systems, but some of the properties of this system certainly contribute to the equilibration:[12]

- 1 *The polymers have a low degree of polymerization.* Although the hydrophobicity of PB is higher than that of Poly(propylene oxide), we still must expect that the solubility of the two copolymers in water is not extremely low. The prediction of the CMC is $\varphi^b \approx 10^{-4}$. The corresponding concentration in mol/L is of the same order of magnitude. This is not extremely low and thus we may expect that equilibration between micelles and vesicles is possible through the transport of freely floating copolymers.
- 2 *Both species have the same tail length.* Both copolymers have the same hydrophobic length and this helps the full miscibility of the copolymer inside the aggregates. Especially when there is a tail length disparity one may find non-ideal mixing of the copolymer species and vesicles composed of such copolymers may develop a non-zero spontaneous curvature (the spontaneous curvature is discussed below as well). The present system does not suffer from such problem.
- 3 *Micelles help equilibration.* When vesicles coexist with a large number of small micelles, we must anticipate a rapid equilibration of the polymers throughout the system. The small micelles diffuse very rapidly and when they are near a much larger vesicle, the exchange of polymers must be relatively efficient. We cannot imagine that in systems with many small dynamic micelles, vesicles that have not equilibrated their size can persist. Equilibration through the presence of monomeric species is of course also possible.

It is important to realize that the unilamellar mixed vesicles must coexist with mixed micelles and that it is impossible to remove the micelles while keeping the vesicles in tact. This must be contrasted to classical first-order phase transitions, e.g. in a gas-liquid two-phase state. In this case it is possible to remove one phase while keeping the chemical potentials fixed and keep the other phase in the system. The vesicle to micelle transition is only a first order like transition and strictly speaking the chemical potentials change slightly when by addition of micelle forming copolymers the vesicles are gradually transformed into micelles. The translational entropy of the micelles and the vesicles cause this subtle effect.

Our SCF model predicts that the overall bending energy stored in the vesicles is of order $20 k_B T$. This is still a relatively high value and we expect that translational entropy alone cannot entirely compensate for the bending energy. As

argued above we must anticipate that shape fluctuations also contribute to the entropy that is ignored in the SCF analysis. In any case, it seems likely that the vesicles are thermodynamically stable, implying that the ignored entropy (translation and undulation) compensates for the curvature energy. Direct application of eqn 5.8 leads to very low volume fractions of vesicles, but a renormalization of the curvature energy (implementing the undulations) may help to increase the vesicle concentration to the levels seen in experiments.[37, 38]

In the literature it is generally expected that the mean bending modulus of a (lipid) bilayer is reduced when (micelle-forming) surfactants are added.[38] In fact, this is implemented in procedures where surfactants (e.g., Triton) are used to disrupt lipid bilayers in an attempt to harvest membrane proteins.[39] Bilayers with a low value for the bending modulus will also have a low value of the membrane persistence length ξ as $\xi \propto \exp k_c/k_B T$. [37] The membrane is expected to remain flat on length scales smaller than ξ , but it can bend away in arbitrary directions on larger length scales. It was argued therefore that thermodynamically stable vesicles should have a radius $R \propto \xi$. [38] If we apply this argument to the present system, the dramatic reduction of the vesicle size R with increasing amount of PB₁₈ copolymers would suggest a significant reduction of the bending modulus. This appears incompatible with the current SCF predictions. Within the SCF model we can compute the bending modulus of mixed bilayers accurately[15] and we found (results not shown) that the bending modulus is a very weakly *increasing* function of the amount of PB₁₈-blocks in the vesicles. The Gaussian bending modulus is negative and decreases slightly more, so that the overall curvature energy decreases. From previous calculations we learned that the bending modulus mostly depends on the length of the hydrophobic part of the copolymer and it is remarkably insensitive to the length of the corona block.[23] This trend was interpreted by the cancellation of compensating effects. A longer corona block leads to a reduction of the dimension of the core. Hence the increase of the bending modulus through the increasing dimension of the corona is compensated by the reduction of the bending modulus due to the reduction of the core size. We thus conclude that we cannot explain the size reduction of the vesicles by a decrease of the bending modulus of the bilayer upon the increase of PB₁₈ copolymers.

We realize that the proposed mechanism of having thermodynamically stable mixed vesicles coexisting with a high concentration of mixed micelles is non-classical. Intuitively, one could argue that the uneven distribution of the two

amphiphiles between the inner- and outer leaflet of the vesicle results in a non-zero spontaneous curvature. Again, using the method of Oversteegen et al. [?], while computing the bending moduli discussed above, we found $J_0 = 0$ in all our systems, even though the inner- and outer layers have slightly different polymer compositions. Indeed, a non-zero J_0 is only expected for systems wherein the two amphiphiles have a solubility gap. In this case the inner-leaflet can be strongly enriched by the amphiphile with a small head group and the outer leaflet by the amphiphile with a larger head group. For a given composition the demixing is optimal for a well-defined vesicle radius corresponding to the spontaneous curvature. Obviously, this situation does not occur in the present system and thus the simple argument that an uneven distribution induces a non-zero J_0 does not apply.

In true first-order phase transition the coexistence between two phases is limited to a fixed value of the chemical potentials of the molecules involved. For micelles that are composed of a limited number of copolymers and having a concentration-dependent entropic contribution, the transition is only first-order like. Hence, the coexistence of spherical vesicles with spherical micelles, as elaborated above, occurs in a narrow window in chemical potentials. Unlike in true first-order transitions, the two species that coexist are subject to compositional and size changes while the system is pushed through the transition window. The model further suggests that the type of coexistence may be a strong function of the temperature. It is of considerable interest to find experimental support for the latter prediction.

Small unilamellar vesicles that are thermodynamically stable may find many applications. For example, small vesicles $R < 100\text{nm}$ have a much longer blood circulation time than larger vesicles.[40, 41] For this type of applications it is also relevant that the corona of the vesicle bilayer has a stealth property[42] in the sense that the immune system does not notice small particles that have a poly(ethylene oxide) brush on its surface. Most likely this is due to the fact that proteins do not penetrate this PE layer. One can argue that the vesicles of the PB-PE system are less suitable for drug delivery vehicles because its constituents are relatively soluble in water (CMC is finite). Hence, upon dilution the bulk concentration may fall below the CMC (even though the CMC is a decreasing function of temperature) and the aggregates must fall apart. However, the presence of the large concentration of micelles in these systems may protect the disintegration of the

vesicles to some extent. It is expected further that the micelles will dissolve first (and replenish the PB-PE bulk concentration to remain near the CMC) before the vesicles disintegrate. This is because the (10, 18) chains are more soluble than the (10, 10) ones, and the micelles are rich in the (10, 18) species.

5.4 Conclusions

A detailed self-consistent field theory is used to study the self-assembly characteristics of binary polymer mixtures in a selective solvent. We mimic the binary mixture of the lamellae forming copolymer $PB_{10}PE_{10}$ mixed with the micelle forming $PB_{10}PE_{18}$ species.[12] It is possible to choose a mixing ratio where small unilamellar vesicles coexist with many spherical micelles. We argued that the vesicle size can be tuned by the copolymer mixing ratio. For still modest PE_{18}/PE_{10} ratios, one enters a regime where the micelles are the dominant species, and these micelles buffer the chemical potential of the copolymers in the system. In such a situation one can store more PE_{18} chains in smaller vesicles than in larger ones. Hence upon an increase of the amount of PE_{18} in the system, the vesicles evolve towards small sizes. The predictions are in line with SANS and Cryo-TEM data.[12] In addition, the SCF model explains many other salient properties of these systems. Hence, the SCF analysis gives strong support for the expectation that in binary polymer mixtures it is possible to have thermodynamically stable small unilamellar vesicles.

Bibliography

- [1] D.E. Discher, A. Eisenberg; *Science*, **2002**, *297*, 967-973.
- [2] Y. Won, H.T. Davis, F.S. Bates; *Science*, **1999**, *283*, 960-963.
- [3] S.U. Egelhaaf, P. Schurtenberger; *Phys. Rev. Lett.*, **1999**, *82*, 2804-2807.
- [4] Z. Li, E. Kesselman, Y. Talmon, M.A. Hillmyer, T.P. Lodge; *Science*, **2003**, *306*, 98-101.
- [5] R. Savic, L. Luo, A. Eisenberg, D. Maysinger; *Science*, **2003**, *300*, 615-618.
- [6] P. Fromherz, D. Ruppel; *FEBS Lett.*, **1985**, *179*, 155.
- [7] S. Almog, B.J. Litman, W. Wimley, J. Cohen, E.J. Wachtel, Y. Barensholz, A. Ben-Shaul, D. Lichtenberg; *Biochemistry*, **1990**, *29*, 4582.
- [8] T.M. Weiss, T. Narayanan, C. Wolf, M. Gradzielski, P. Panine, S. Finet, W. T. Helsby; *Phys. Rev. Lett.*, **2005**, *94*, 038303.
- [9] D. Andelman, M.M. Kozlov, W. Helfrich; *Europhys. Lett.* , **1994**, *25*, 231-236.
- [10] X.H. He, F. Schmid; *Macromolecules*, **2006**, *39*, 2654-2662.
- [11] S. Schmölzer, D. Gräßner, M. Gradzielski, T. Narayanan; *Phys. Rev. Lett.*, **2002**, *88*, 258301.
- [12] F. Li, S. Prévost, R. Schweins, A.T.M. Marcelis, F.A.M. Leermakers, M.A. Cohen Stuart, E.J.R. Sudhölter; *Soft Matter* [10.1039/b904522h](https://doi.org/10.1039/b904522h).
- [13] J.M.H.M. Scheutjens, G.J. Fleer; *J. Phys. Chem.*, **1979**, *83*, 1619.

- [14] G.J. Fleer, M.A. Cohen Stuart, J.M.H.M. Scheutjens, T. Cosgrove, B. Vincent; *Polymers at Interfaces*. Chapman and Hall, London, **1993**.
- [15] S.M. Oversteegen, F.A.M. Leermakers; *Phys. Rev. E.*, **2000**, *62*, 8453.
- [16] O.A. Evers, J.M.H.M. Scheutjens, G.J. Fleer; *Macromolecules*, **1990**, *23*, 5221.
- [17] F.A.M. Leermakers, J.C. Eriksson, J. Lyklema; *Fundamentals of Interface and Colloid Science, Vol. V: Soft Colloids*. Elsevier, Amsterdam, **2005**.
- [18] V.G. de Bruijn, L.J.P. van den Broeke, F.A.M. Leermakers; *Langmuir*, **2002**, *18*, 10467.
- [19] P. Flory; *Principles of Polymer Chemistry*, Cornell University Press, Ithaca, N.Y. **1953**.
- [20] S.F. Edwards; *Proc. Phys. Soc.*, **1965**, *95*, 613.
- [21] F.A.M. Leermakers, P.A. Barneveld, J. Sprakel, N.A.M. Besseling; *Phys. Rev. Lett.*, **2006**, *97*, 066103.
- [22] R.A. Kik, J.M. Kleijn, F.A.M. Leermakers; *J. Phys. Chem. B*, **2005**, *109*, 14251.
- [23] Y. Lauw, F.A.M. Leermakers, M.A. Cohen Stuart; *J. Phys. Chem. B*, **2003**, *107*, 10912.
- [24] D.G. Hall, B. A. Pathica; *Nonionic Surfactants*. Marcel Dekker, New York, **1967**.
- [25] T.L. Hill, *Thermodynamics of Small Systems, Part 1 and Part 2*, Dover Publications, N.Y. (1991) and (1992).
- [26] A.B. Jodar-Reyes, F.A.M. Leermakers; *J. Phys. Chem. B*, **2006**, *110*, 18415.
- [27] F.A.M. Leermakers, J.M.H.M. Scheutjens; *J. Chem. Phys.*, **1988**, *89*, 3264.
- [28] J.N. Israelachvili, B.W. Ninham; *J. Chem. Soc Faraday Trans II.*, **1976**, *72*, 1525.
- [29] W.M. de Vos, F.A.M. Leermakers; *Polymer*, **2009**, *50*, 305.

- [30] F.A.M. Leermakers, J.M.H.M. Scheutjens; *J. Phys. Chem. B*, **1989**, *93*, 7417.
- [31] Y. Jiang, T. Chen, F.H. Ye, H.J. Liang, A.C. Shi; *Macromolecules*, **2005**, *38*, 6710.
- [32] X. Li, P. Tang, F. Qiu, H. Zhang, Yu, Yang; *J. Phys. Chem. B*, **2006**, *110*, 2024.
- [33] D.F. Evans, H. Wennerström; *The colloidal Domain Where Physics, Chemistry, Biology and Technology Meet*, VGH, **1994**.
- [34] W. Helrich; *Z. Naturforsch*, **1973**, *28c*, 693.
- [35] S.A. Safran; *Statistical Thermodynamics of Surfaces, Interfaces, and Membranes*, Addison-Wesley Publishing Company, U.S.A. **1994**.
- [36] S. Jain, F.S. Bates; *Science*, **2003**, *300*, 460-464.
- [37] S.A. Safran, P. Pincus, D. Andelman; *Phys. Rev. A*, **1991**, *43*, 1071.
- [38] M.M.A.E. Claessens, F.A.M. Leermakers, F.A. Hoekstra, M.A. Cohen Stuart; *J. Phys. Chem. B*, **2007**, *111*, 7127.
- [39] C. Bordier; *J. Biol. Chem.* **1981**, *256*, 1604.
- [40] N. Ishiyama; *Nat. Nanotechnol.* **2007**, *2*, 203.
- [41] W, Jiang, B.Y.S. Kim, J.T. Rutka, W.C.W. Chan; *Nat. Nanotechnol.* **2008**, *3*, 145.
- [42] F. Gu, L.F. Zhang, B.A. Teply, N. Mann, A. Wang, A.F.R. Moreno, R. Langer, O.C. Farokhzad; *Proc. Nat. Acad. Sci. U.S.A.* **2008**, *105*, 2586.

Chapter 6

Formation of nanotapes by co-assembly of polypeptide and polythiophenes

Nanotapes are formed by the co-assembly of triblock peptide copolymers with an amino acid-substituted polythiophene derivative (PTT). The driving force for the assembly is ionic interaction (complex coacervation). These nanotapes were visualized by atomic force microscopy and confocal laser scanning microscopy. The interactions between the triblock peptide copolymers and the PTT are also expressed in the steady state and time resolved fluorescence spectra. The steady state spectra indicate that upon interaction with the peptide copolymer the backbone of the PTT adopts a rather twisted, and definitely less, aggregated conformation. The time-resolved fluorescence decay studies further confirm this interpretation. The structure of these nanotapes at the mesoscopic scale depends, among other physical chemical parameters, on the concentrations of its constituents.

In slightly modified form published as: F. Li, A.A. Martens, A. Åslund, P. Konradsson, F.A. de Wolf, M.A. Cohen Stuart, E.J.R. Sudhölter, A.T.M. Marcelis, F.A.M. Leermakers. *Soft Matter* **2009**

6.1 Introduction

Conjugated polymers that have useful conductive properties can be used in optical sensors and electronic devices. In particular, polythiophenes (PTs) with various side chains have been studied for this reason.[1-6] Recently, water-soluble nanowires have been described that are formed by self-assembly of a low molecular weight organogelator and a conjugated threonine substituting polythiophene, PTT.[7] The latter compound has side chains with zwitterionic amino acid groups, which make it remarkably water-soluble. The zwitterionic group has the interesting property that it binds to charged objects irrespectively of the sign of the charge.[4] Among those chargeable objects, bioinspired peptide block copolymers have received significant attention recently, due to their biocompatibility. Particularly, fiber formation of peptide block copolymers has been studied thoroughly.[8, 9] A few examples of chemical synthetic triblock peptide copolymers have been studied to understand the basic rules of nanoscale self-assembly and ways of controlling the nanostructures.[10, 11] The photo-physical properties of fluorophore-containing peptides have also been studied lately through peptide-driven self-assembly.[12] In addition to these chemicosynthetic peptide block copolymers, biosynthetic peptide block copolymers, biologically expressed from a designed DNA template, have been studied extensively. These block copolymers all have identical designed length and primary structure, while chemically synthesized polymers usually lack these features, i.e. they typically are polydisperse.[13, 14]

In the present paper, we describe the co-assembly of a PT (PTT) with biosynthetic positively or negatively charged triblock peptide copolymers, leading to organized conjugated nanotapes. Both components that give rise to the co-assembled tape formation are water-soluble and thus do not aggregate on their own. Only upon mixing the assembly takes place. We therefore refer to this case of assembly as complex coacervation driven assembly or simply as co-assembly. The integrity of the tapes fundamentally depends on the presence of both components. Therefore, we expect the tapes to be continuous in PTT, and thus a possibility for good conductive properties arises for these tapes.

The fluorescence spectrum of PTT is very sensitive to its spatial conformation. When the side-groups are charged, i.e., at high or low pH, the thiophene backbone adopts a planar conformation. In the uncharged state (around the isoelectric point pH 5.7) the PT adopts a non-planar conformation. These structural changes in

the backbone are reflected in changes in the fluorescence spectra. Consequently, PTs have been used as optical probes for monitoring peptide conformations.[3-6]

The two variants of the peptide copolymers that are used have many aspects in common (Scheme 1). Both variants have a symmetric triblock structure and are produced by the expression of a designed DNA template in yeast.[15, 16] The two ‘collagen-like’ outer blocks, refer to by C, which are nearly neutral and hydrophilic, form random coils in aqueous solutions at all pH values. The middle block is in one case positively charged at low pH because of the presence of histidine groups, and in the other case, negatively charged at high pH because of the presence of glutamic acid residues, we refer to this block by S, which is originated from silk-like repeats. When the middle blocks are charged, electrostatic repulsion keeps the triblock peptide copolymers molecularly dissolved in water; the peptide copolymers do not aggregate and thus do not form any linear objects. However, when the charges in the middle blocks are quenched, the middle block orders as it forms secondary structures as silk does, through intra-molecular interactions. Above a concentration of approximately 0.3 mg/ml, they subsequently stack (due to hydrophobic interactions) into nanotapes within 12 hours.[16] In the absence of PTT we can find long linear objects for the histidine containing peptide copolymers, but only at a high pH. Similarly, for the glutamate containing peptide copolymers linear objects form at a low pH.[16] In the present study, however, the triblock peptide copolymer solutions are prepared at a pH that prevents the central blocks from aggregating by themselves. By addition of PTT, the charges from the central blocks interact with the zwitterionic groups of PTT, therefore triggering the formation of the nanotapes.

6.1.1 Materials

The synthesis of the threonine-substituted polythiophene, PTT, has been reported previously.[18] The synthesis of the triblock peptide copolymers ($CS^E S^E C$ / $CS^H S^H C$, E and H stands for glutamate and histidine, respectively, C stands for collagen-like blocks and S stands for silk like blocks, with molecular weight of 65 kDa, and exactly 49 chargeable amino acids per polymer) has been reported elsewhere.[15, 16] Tablets for preparing phosphate buffer solutions (10 mM, pH 7.4) were from Sigma. Triblock peptide copolymers solutions, 0.33 mg/mL (5 μ M, equal to 250 μ M in chargeable amino acids units), were prepared in a

0.33 mM NaOH or HCl solution. These amounts are slightly more than required for deprotonation or protonation of the side groups. Up to 30 $\mu\text{g}/\text{mL}$ (300 μM in thiophene units) PTT was added gradually as a concentrated solution to the above peptide solution while stirring, until the specific ratio of each measurement was obtained. After preparation these mixtures were used immediately for the various experiments. In the remaining part of the paper the molar concentration of the triblock peptide copolymer is used, whereas for the PTT the concentration of thiophene units will be used.

```

YVEFGLGAGAPGEPGNPSPGNQGQPQGNKGSPPG
NPGQPQNEGQPGQPQGNQGPPEPSPGNSGPPGSSQ
GNPGKNGQPSPGSGSPGNQGSPPGQPQGNPQGPQ
PGEQKQKPGNQGPAGEPGNPSPGNQGPQGNKGS
SPGNPQGPQNEGQPGQPQGNQGPPEPSPGNSGPPQ
GSQGNPGKNGQPSPGSGSQSPGNQGSPPGQPQGN
PGQPPEQKQKPNQGPAGEGAGAGACEGAGAGAGAG
GEGAGAGAGEGAGAGAGEGAGAGACEGAGAGAGAG
GEGAGAGAGEGAGAGAGEGAGAGACEGAGAGAGAG
GEGAGAGAGEGAGAGAGEGAGAGACEGAGAGAGAG
GEGAGAGAGEGAGAGAGEGAGAGACEGAGAGAGAG
GEGAGAGAGEGAGAGAGEGAGAGACEGAGAGAGAG
GEGAGAGAGEGAGAGAGEGAGAGACEGAGAGAGAG
GEGAGAGAGEGAGAGAGEGAGAGACEGAGAGAGAG
GEGAGAGAGEGAGAGAGEGAGAGACEGAGAGAGAG
GEGAGAGAGEGAGAGAGEGAGAGACEGAGAGAGAG
GEGAGAGAGEGAGAGAGEGAGAGACEGAGAGAGAG
GEGAGAGAGEGAGAGAGEGAGAGACEGAGAGAGAG
GEGAGAGAGEGAGAGAGEGAGAGACEGAGAGAGAG
GEGAGAGAGEGAGAGAGEGAGAGACEGAGAGAGAG
GEGAGAGAGEGAGAGAGEGAGAGACEGAGAGAGAG
GEGAGAGAGEGAGAGAGEGAGAGACEGAGAGAGAG
GEGAGAGAGEGAGAGAGEGAGAGACEGAGAGAGAG
NQGQPQGNKGSPPGNPQPNEGQPGQPQGNQGNQGP
GEPSPGSPQGSQGNPQGNQGPQGPSPGSGSQSPPGN
QGSPPGQPQGNPQPNEGQKPGNQGPAGEPGNPQ
SPGNQGPQGNKGSPPGNPQPNEGQPGQPQGNQGN
GQGPPEPSPGNSGSPGNSPQGNKNGQPQSPGSGSQ
SGNQGSPGQPQGNPQGPQGNQGPQGNQGPAGEGAG
  
```

```

YVEFGLGAGAPGEPGNPSPGNQGQPQGNKGSPPG
NPGQPQNEGQPGQPQGNQGPPEPSPGNSGPPGSSQ
GNPGKNGQPSPGSGSPGNQGSPPGQPQGNPQGPQ
PGEQKQKPGNQGPAGEPGNPSPGNQGPQGNKGS
SPGNPQGPQNEGQPGQPQGNQGPPEPSPGNSGPPQ
GSQGNPGKNGQPSPGSGSQSPGNQGSPPGQPQGN
PGQPPEQKQKPNQGPAGEGAGAGAGHAGAGAGAG
CHGAGAGAGHAGAGAGHAGAGAGAGHAGAGAGAG
CHGAGAGAGHAGAGAGHAGAGAGAGHAGAGAGAG
CHGAGAGAGHAGAGAGHAGAGAGAGHAGAGAGAG
CHGAGAGAGHAGAGAGHAGAGAGAGHAGAGAGAG
CHGAGAGAGHAGAGAGHAGAGAGAGHAGAGAGAG
CHGAGAGAGHAGAGAGHAGAGAGAGHAGAGAGAG
CHGAGAGAGHAGAGAGHAGAGAGAGHAGAGAGAG
CHGAGAGAGHAGAGAGHAGAGAGAGHAGAGAGAG
CHGAGAGAGHAGAGAGHAGAGAGAGHAGAGAGAG
CHGAGAGAGHAGAGAGHAGAGAGAGHAGAGAGAG
CHGAGAGAGHAGAGAGHAGAGAGAGHAGAGAGAG
CHGAGAGAGHAGAGAGHAGAGAGAGHAGAGAGAG
CHGAGAGAGHAGAGAGHAGAGAGAGHAGAGAGAG
CHGAGAGAGHAGAGAGHAGAGAGAGHAGAGAGAG
CHGAGAGAGHAGAGAGHAGAGAGAGHAGAGAGAG
CHGAGAGAGHAGAGAGHAGAGAGAGHAGAGAGAG
CHGAGAGAGHAGAGAGHAGAGAGAGHAGAGAGAG
CHGAGAGAGHAGAGAGHAGAGAGAGHAGAGAGAG
CHGAGAGAGHAGAGAGHAGAGAGAGHAGAGAGAG
CHGAGAGAGHAGAGAGHAGAGAGAGHAGAGAGAG
CHGAGAGAGHAGAGAGHAGAGAGAGHAGAGAGAG
CHGAGAGAGHAGAGAGHAGAGAGAGHAGAGAGAG
CHGAGAGAGHAGAGAGHAGAGAGAGHAGAGAGAG
CHGAGAGAGHAGAGAGHAGAGAGAGHAGAGAGAG
GNQGPQGNKGSPPGNPQPNEGQPGQPQGNQGNQGP
GEPSPGSPQGSQGNPQGNQGPQGPSPGSGSQSPPGN
QGSPPGQPQGNPQPNEGQKPGNQGPAGEPGNPQ
SPGNQGPQGNKGSPPGNPQPNEGQPGQPQGNQGN
GQGPPEPSPGNSGSPGNSPQGNKNGQPQSPGSGSQ
SGNQGSPGQPQGNPQGPQGNQGPQGNQGPAGEGAG
  
```

$$\text{CS}^{\text{E}}\text{S}^{\text{E}}\text{C}$$

$$\text{CS}^{\text{E}}\text{S}^{\text{E}}\text{C} \text{ or } \text{CS}^{\text{H}}\text{S}^{\text{H}}\text{C}$$

C = collagen-like uncharged oligopeptide blocks

$\text{S}^{\text{E}}\text{S}^{\text{E}}$ = AGEGAGAGAG sequence (x 49)

$\text{S}^{\text{H}}\text{S}^{\text{H}}$ = AGHGAGAGAG sequence (x 49)

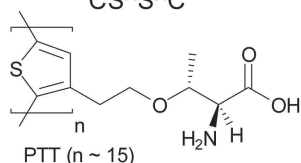
$$\text{CS}^{\text{H}}\text{S}^{\text{H}}\text{C}$$


Figure 6.1: Structures of the compounds used in this study. The protein-polymers (top) have a tri-block structure. The outer blocks are collagen-like and are referred to by C. The central block is silk-like and referred to by S. Only in the central S block the two variants of the protein polymers differ, namely there are either glutamic acid (E) residues or histidine (H) ones. The PTT has a degree of polymerization of approximately $n = 15$ and is zwitterionic in its side group. The PTT is fluorescent and conductive.

6.1.2 Atomic force microscopy

Tapping-mode atomic force microscopy (AFM) experiments were carried out with a JEOL JSPM-5400 scanning probe microscope (JEOL Europe BV). Height images were obtained in the AC mode in air using NSC35/AIBS ultra sharp cantilevers (MikroMasch Europe). 10 μL of the nanotape-containing solution were deposited on a freshly cleaved mica surface at room temperature and dried overnight before imaging. The AFM tip broadening effect on nanotapes' width measurement was corrected by using the WinspmII processing software.

6.1.3 Steady state and time-resolved fluorescence spectroscopy

Steady state and time-resolved emission measurements were done using a FLS 920 spectrophotometer (Edinburgh Instruments, UK) fitted with a cooled MCP PMT detector (Hamamatsu, R3809U-50). For the steady state measurements the samples were excited with a pulsed xenon lamp. For the time-resolved measurements the samples were excited ($\lambda_{exc} = 372 \text{ nm}$) with a pulsed diode laser (LDH-PC-375; PicoQuant GmbH, Germany; fwhm = 39 ps), controlled by a pulse controller (PDL 800-B; PicoQuant GmbH, Germany). The instrument response function (fwhm of IRF = 87 ps) was determined and calibrated from scattering experiments using colloidal silica Ludox (Sigma-Aldrich). The decay curves were analyzed using "Fast" software (Edinburgh Instruments, UK).

The co-assembled nanotapes were prepared in water with triblock peptide copolymer / PTT ratio to 1:2 (5 μM : 10 μM) and diluted five times in 10 mM phosphate buffer of pH 7.4 for the measurements. The reference sample, 5 μM PTT, was prepared in water and diluted five times in 10 mM phosphate buffer of pH 7.4. All samples were equilibrated two hours in the dark before doing the fluorescence measurements.

6.1.4 Confocal laser scanning microscopy (CLSM)

Confocal fluorescence images of the PTT/triblock peptide copolymer nanotapes were recorded with an confocal laser scanning microscope (Zeiss LSM 5 EXCITER), with an excitation wavelength of 458 nm and a long band pass of 560 nm. The PTT/triblock peptide copolymer nanotapes were aligned through molecular combing on a hydrophobic surface. The substrates used in this study were cover slips for fluorescence microscopy. In order to get a lower surface energy of the

substrates to enable the alignment of the fibrils, a PDMS stamping procedure was undertaken. A PDMS stamp was placed onto the substrate for 60 min, which resulted in transfer of PDMS oligomers from the stamp and a hydrophobic pattern on the substrate was obtained. On the PDMS-modified surface, a droplet (30 μL) of the PTT/peptide triblock copolymer complex (5 μM : 300 μM) was incubated for 30 min and then gently blown off in one direction with nitrogen gas. The surface was then carefully rinsed in deionized water.

6.1.5 Circular Dichroism

Samples for CD measurements were prepared from stock solutions of 3 mg/ml protein in a 3 mM NaOH or HCl solution or a mixture of protein stocks and 9 mM PTT. A dilution to 0.1 mg/ml protein for all samples was made in water. For the measurement at pH 10 and pH 2, the solutions were adjusted with 1 M NaOH and 1M HCl respectively. The above solutions were permitted to age for 72 h in a refrigerator at 4 $^{\circ}\text{C}$ before measurement.

CD spectra were acquired on a CD Jasco J-715 Spectropolarimeter. Spectra were recorded in the far-UV region (190-260 nm) at 20 $^{\circ}\text{C}$ at a speed of 10 nm/min and a sampling interval of 0.2 nm in a quartz cuvet with diameter 0.1 cm. 20 repeating measurements were made for all the samples. The background was subtracted for all the samples.

6.2 Results and Discussion

The proposed mechanism for the co-assembling of the nanotapes is shown in Figure 6.2. Triblock peptide copolymers that are initially charged are dissolved as a molecular solution under slightly acidic (for the histidine-containing peptide) or slightly basic conditions (for the glutamate-containing peptide). Addition of the zwitterionic PTT polymer results in ionic interactions with the charged block of the polypeptide. Together with hydrogen bonding and hydrophobic interactions this overcomes the electrostatic repulsion and leads in both cases to co-assembly and formation of the nanotapes.[16]

At a concentration of 5 μM of peptide, the length of the nanotapes increases with increasing PTT concentration until the ratio of charged units between peptide and thiophene is about 1:1. Figure 6.3 shows AFM images of samples in

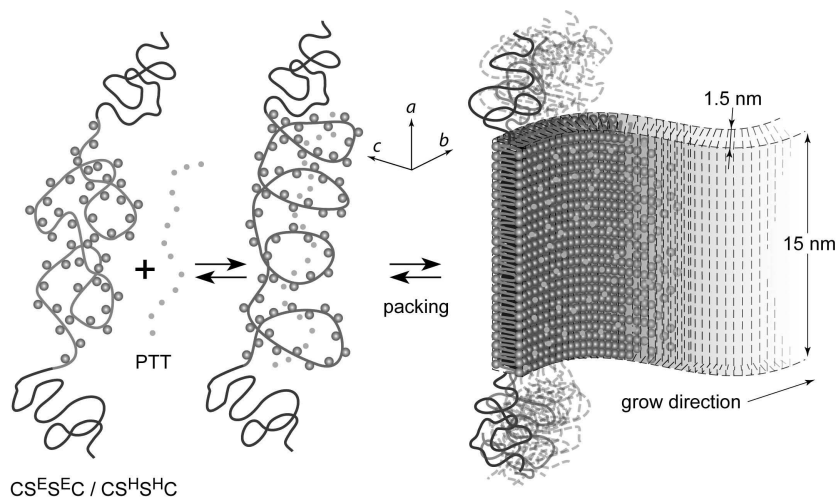


Figure 6.2: *schematic representation of triblock peptide copolymers that co-assemble with PTT leading first to a conformationally ordered central block of the peptides (as it occurs in Silk), which subsequently aggregate and pack into long nanotapes with specified dimensions. The collagen-like outer blocks remain in a random coil conformation acting as a protective layer against aggregation on the exterior of the nanotapes.*

which the ratio of the triblock peptide copolymer / thiophene units in PTT are 1:2 ($5 \mu\text{M} : 10 \mu\text{M}$) and 1:20 ($5 \mu\text{M} : 100 \mu\text{M}$) ($5 \mu\text{M}$, equal to $250 \mu\text{M}$ in chargeable amino acids units). It is clearly seen that the length of the fibers increases with increasing PTT content. In Figures 6.3c and 6.3d, nanotapes up to several micrometer long are clearly visible.

Above a charge ratio of about 1:1, however, we find bundles of nanotapes. As mentioned before, each triblock peptide copolymer has exactly 49 amino acids that potentially can carry a charge. When an excess of PTT is added, this can induce attractive interactions between the aggregates through the bridging mechanism with bundle formation as one of the consequences. Indeed when more PTT is added, the peptide/PTT aggregates gradually precipitate from the solution.

A triblock peptide copolymer / PTT ratio of 1:60 ($5 \mu\text{M} : 300 \mu\text{M}$), which is slightly higher than a 1:1 charge ratio, resulted in highly viscous solutions for which it was hard to get a clear AFM image. Fluorescent images of the structures in these mixtures were obtained with confocal laser scanning microscopy on polydimethylsiloxane (PDMS) modified glass surfaces, Figure 6.4. The images indicate that some of the primary nanotapes assemble into organized bundles,

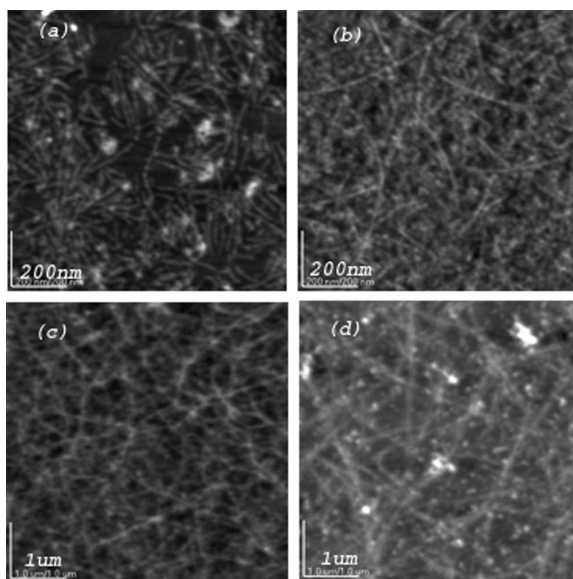


Figure 6.3: AFM images of co-assembled protein fibers. (a) 1:2 (mol/mol) $CS^E S^E C$: PTT; (b) 1:2 (mol/mol) $CS^H S^H C$: PTT; (c) 1:20 (mol/mol) $CS^E S^E C$: PTT; (d) 1:20 (mol/mol) $CS^H S^H C$: PTT.

particularly in the presence of excess PTT. These tens of micrometer long, green fluorescent tapes further confirm the co-assembly of triblock peptide copolymers with PTT. Again, in the absence of PTT no organized (fluorescent) structures are present under the experimental conditions.

The sample with the same PTT/protein ratio (60:1) as used in Figure 6.4 was studied with circular dichroism. Relevant CD spectra are presented in Figure 6.5, where we combine information for random coil proteins (when the S block is charged), the spectra for the protein copolymers when they form long ribbons after a pH adjustment and corresponding spectra for the current linear objects triggered by the addition of PTT. In Figure 6.5a the positively charged proteins and in Figure 6.5b the negatively charged variants are used. The CD data indicate that upon interacting with PTT, the secondary structure of both positively charged and negatively charged proteins evolve from the random coil towards β -turn secondary structures (as seen from the combination of a negative band around 208 nm and the tendency to go towards positive bands around 200 and 225 nm). Especially for the negatively charged protein case, the CD signal

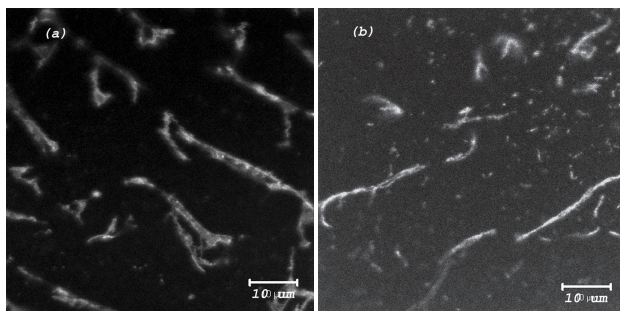


Figure 6.4: CLSM images of co-assembled protein fibers. (a) 1:60 (mol/mol) $CS^E S^E C$: PTT (with pH 8.36) (b) 1:60 (mol/mol) $CS^H S^H C$: PTT (with pH 4.36).

resembles the CD signal of the nanotapes that were formed by adjusting the pH only.[16] Thus, the PTT assisted aggregation of the protein copolymers allows the silk-like repeats to adopt secondary structures similarly as what happens after a pH shift.[16] The differences in the spectra between the pH induced and PTT induced tape formation indicates that the organization of the S block of the protein copolymer in terms of the total fraction of S block ordering, depends on the method used. We may attribute some of the differences in the structure also to the differences in experimental conditions. Namely, the pH value used in the CD experiments in the presence of PTT is far from the pH where the protein aggregation starts spontaneously. As a result the co-assembly of proteins by the PTT addition showed much slower kinetics and although the samples were aged for three days before the CD spectra were recorded, we can not exclude that relaxation processes were still in process. Hence, we do not expect exactly the same CD signals for the nanotapes formed under these two different conditions.

In summary, the direct observation of the linear aggregates discussed above based on AFM and CLSM, and the clear non-random coil signals in the CD, proves that PTT co-assembles with these protein copolymers and together organize into organized linear structures.

Co-assembly at lower overall concentrations is possible, but occurs at lower peptide/PTT ratios. For example, at a ten times lower concentration of peptide, we could only detect fiber formation with AFM for peptide/PTT ratios lower than 1:60, i.e. with an excess of thiophene units. In Figure 6.6, AFM images are presented for systems with a peptide/PTT ratio of 1:60 ($0.5 \mu\text{M} : 30 \mu\text{M}$). Figure 6.6a shows nanotapes from negatively charged triblock peptide copolymers and

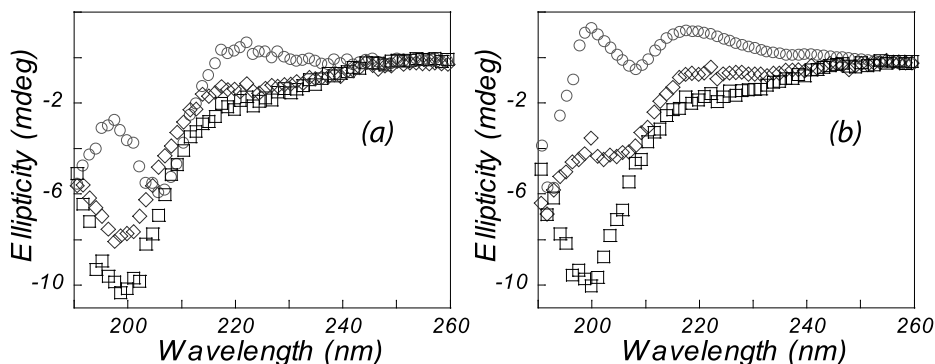


Figure 6.5: CD spectrum of co-assembled protein fibers. (a) (\square) $1.7 \mu\text{M } \text{CS}^{\text{H}} \text{S}^{\text{H}} \text{C}$ at pH 2; (\diamond) $1.7 \mu\text{M} : 100 \mu\text{M } \text{CS}^{\text{H}} \text{S}^{\text{H}} \text{C} : \text{PTT}$ (pH4); (\circ) $1.7 \mu\text{M } \text{CS}^{\text{H}} \text{S}^{\text{H}} \text{C}$ at pH 10 (b) (\square) $1.7 \mu\text{M } \text{CS}^{\text{E}} \text{S}^{\text{E}} \text{C}$ at pH 9; (\diamond) $1.7 \mu\text{M} : 100 \mu\text{M } \text{CS}^{\text{E}} \text{S}^{\text{E}} \text{C} : \text{PTT}$ (pH8); (\circ) $1.7 \mu\text{M } \text{CS}^{\text{E}} \text{S}^{\text{E}} \text{C}$ at pH 2.

PTT at a mole ratio of 1:60. Figure 6.6b shows nanotapes that are formed by PTT added to positively charged triblock peptide copolymers with a mole ratio of peptide/PTT 1:60. The dimensions of nanotapes are seen in the cross section analysis. In both images the nanotapes have a width of 15-20 nm and a height of 1-1.5 nm, which is in good agreement with previous studies.[16] We note that the lateral resolution is influenced by AFM tip, the number mentioned above is found after proper corrections performed by the JEOL software. From AFM, electron microscopy and SAXS studies on the pH-mediated triblock peptide copolymer nanotapes it was estimated that the width of the $\text{GS}^{\text{E}} \text{S}^{\text{E}} \text{G}$ nanotapes is around 15 nm, with a height of 2 nm.[16] Here, instead of using a pH adjustment to promote the formation of tapes, we use the zwitter-ionic PTT polymer to induce the nanotape formation. We note that the AFM samples are dried on the mica surface, which may explain the measured heights being slightly lower than their actual values in solution.

From the presented AFM and CLSM images, we conclude that the triblock peptide copolymers co-assemble with the PTT into well-structured nanotapes. More information on how exactly the PTT-oligomers are organized on the molecular level when they interact with the triblock peptide copolymers was obtained from steady state fluorescence spectroscopy. In this experiment, the ratio between the triblock peptide copolymers and PTT was set to 1:2 ($5 \mu\text{M} : 10 \mu\text{M}$), to minimize the influence of the non-assembled PTT. Figure 6.7 shows the fluorescence

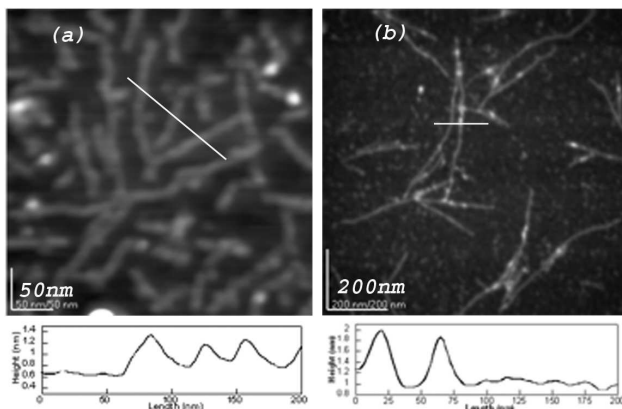


Figure 6.6: AFM images of co-assembled protein fibers. (a) $0.5 \mu\text{M} : 30 \mu\text{M CS}^E S^E C$: PTT and cross section analysis of the line indicated; (b) $0.5 \mu\text{M} : 30 \mu\text{M CS}^H S^H C$: PTT and cross section analysis of the line indicated.

emission spectrum of the co-assembled nanotapes in comparison with the spectrum of freely dissolved PTT molecules. The maximum emission of $10 \mu\text{M}$ PTT is blue-shifted from 618 nm to 598 nm upon addition to the positively-charged triblock peptide copolymer at $5 \mu\text{M}$. Furthermore, when interacting with $5 \mu\text{M}$ negatively-charged triblock peptide copolymer, it is also blue-shifted, but now less, from 618 nm to 605 nm . These results indicate that the co-assembly of charged triblock peptide copolymers with PTT forces PTT to adopt a more twisted conformation. It is noteworthy that the fluorescence intensity of PTT increases while interacting with both positively and negatively charged triblock peptide copolymers, as shown in Figure 6.7. Upon addition of the charged triblock peptide copolymers, the PTT molecules adapt themselves to the conformation of the triblock peptide copolymer, and as a result a less aggregated PTT molecular conformation is formed, thus the fluorescence intensity increases correspondingly.[19]

The presence of specific interactions between PTT and the triblock peptide copolymers is confirmed by the fluorescence emission decay measurements. The fluorescent decay profile of PTT in the presence of positively charged triblock peptide copolymer is shown in Figure 6.8a. In the absence of positively charged triblock peptide copolymer, PTT exhibits a bi-exponential decay with time constants $\tau_1 = 0.107 \text{ ns}$ (51 %) and $\tau_2 = 0.338 \text{ ns}$ (49 %), whereas the emission decay of PTT becomes much slower when it interacts with positively charged tri-

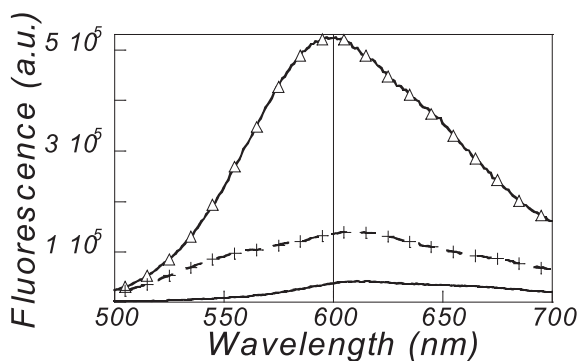


Figure 6.7: Fluorescence emission spectra of 10 μM PTT (on a monomer basis) in 10 mM phosphate buffer. (Δ) with 5 μM $\text{CS}^{\text{H}}\text{S}^{\text{H}}\text{C}$; (+) with 5 μM $\text{CS}^{\text{E}}\text{S}^{\text{E}}\text{C}$; (-) without peptide.

block peptide copolymer. A bi-exponential decay with time constants $\tau_1 = 0.261$ ns (38 %) and $\tau_2 = 0.752$ ns (62 %) is now found. A similar, but less pronounced result is found when PTT interacts with the negatively charged triblock peptide copolymer. The fluorescent decay profile of PTT in the presence of the negatively charged triblock peptide copolymer is shown in Figure 6.8b. In the presence of negatively charged triblock peptide copolymer, the PTT exhibited a bi-exponential decay with time constants $\tau_1 = 0.117$ ns (46 %) and $\tau_2 = 0.471$ ns (54 %), which is clearly longer than for the PTT itself, but not as pronounced as for the interaction with the positively-charged peptide. This might indicate that the positively charged triblock peptide copolymers tend to co-assemble relatively easily with PTT, in compared to the negatively charged triblock peptide copolymer.

The progressive increase of the emission decay times may be indicative for a stronger interaction between PTT and charged triblock peptide copolymers. Indeed, such a remarkable increase of the emission decay times strongly supports the idea that the polythiophenes co-assemble in a well-ordered and tight fashion with the charged triblock peptide copolymers.

The co-assembled nanotapes that are formed by the co-assembly of the peptide copolymers with the polythiophenes are of potential use for biosensor application.

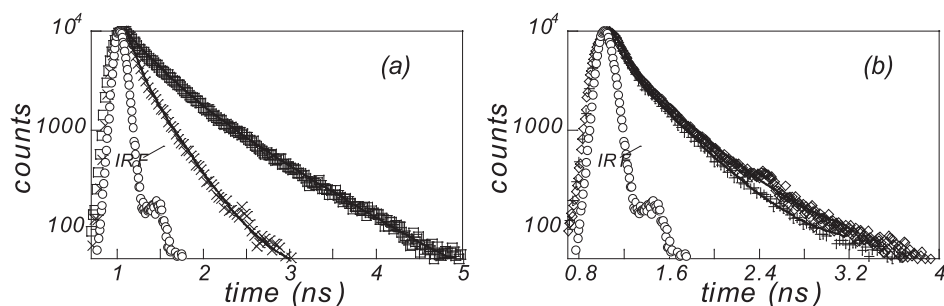


Figure 6.8: Fluorescence decay measurements of $10 \mu\text{M}$ of PTT (on a monomer basis) in 10 mM phosphate buffer 7.4 . a: (\square) with $5 \mu\text{M}$ $\text{CS}^{\text{H}}\text{S}^{\text{H}}\text{C}$; (\times) without peptide. b: (\diamond) with $5 \mu\text{M}$ $\text{CS}^{\text{E}}\text{S}^{\text{E}}\text{C}$; ($+$) without peptide. (\circ) IRF, instrument response function. The solid lines are fitted by bi-exponential decay.

6.3 Conclusions

A new type of co-assembled, highly-ordered conjugated nanotape, has been made from either positively or negatively charged triblock peptide copolymers, and a conjugated zwitterionic polythiophene derivative. The interaction of these compounds results in a change of the conformation and the electronic structure of the polythiophene. The properties of the co-assembly has been examined with AFM, CLSM, CD and time resolved as well as steady state fluorescence spectroscopy. Morphological studies have shown that the co-assembled nanotapes are longer at a higher concentration and a higher PTT / triblock peptide copolymer ratio. The fluorescent emission and emission decay studies indicate that the backbone of the PTT favors a twisted conformation when interacting with triblock peptide copolymers. The nanotapes may potentially be used as conducting filaments (nanowires) in nano-electronic device, or for bio-sensor applications.

Bibliography

- [1] H. Sakaguchi, H. Matsumura, H. Gong, A.M. Abouelwafa, *Science* **2005**, *310*, 1002-1006
- [2] A. Gesquiere, S.D. Feyter, F.C. de Schryver, F. Schoonbeek, J.H. van Esch, R.M. Kellogg, B.L. Feringa, *Nano Letters* **2001**, *4*, 201-206
- [3] A. Herland, P. Bjork, P.R. Hania, I.G. Scheblykin, O. Inganas, *Small* **2007**, *3*, 318-325
- [4] K.P.R. Nilsson, J. Rydberg, L. Baltzer, O. Inganas, *Proc. Natl. Acad. Sci. USA* **2003**, *100*, 10170-10174
- [5] A. Herland, P. Bjork, K.P.R. Nilsson, J.D.M. Olsson, P. Asberg, P. Konradsson, P. Hammarstrom, O. Inganas, *Adv. Mater.* **2005**, *17*, 1466-1471
- [6] A. Herland, K.P.R. Nilsson, J.D.M. Olsson, P. Hammarstom, P. Konradsson, O. Inganas, *J. Am. Chem. Soc.* **2005**, *127*, 2317-2323
- [7] F. Li, G. Palaniswamy, M.R. de Jong, A. Aslund, P. Konradsson, M.A. Cohen Stuart, E.J.R. Sudhölter, A.T.M. Marcelis, F.A.M. Leermakers, *submitted* (Chapter 7)
- [8] H.M. König, A.F.M. Kilbinger, *Angew. Chem. Int. Ed.* **2007**, *46*, 8334-8340
- [9] I.W. Hamley, *Angew. Chem. Int. Ed.* **2007**, *46*, 8128-8147
- [10] H. Dong, S.E. Paramonov, L. Aulisa, E.L. Bakota, H.D. Hartgerink, *J. Am. Chem. Soc.* **2007**, *129*, 12468-12472
- [11] C.W.G. Fishwick, A.J. Beevers, L.M. Carrick, C.D. Whitehouse, A. Aggeli, N. Boden, *Nano Letters* **2003**, *3*, 1475-1479

- [12] K.J. Channon, G.L. Devlin, S.W. Magennis, C.E. Finlayson, A.K. Tickler, C. Silva, C.E. MacPhee, *J. Am. Chem. Soc.* **2008**, *130*, 5487-5491
- [13] D.N. Woolfson, M.G. Ryadnov, *Curr. Opin. Chem. Biol* **2006**, *10*, 559-567
- [14] M.T. Krejchi, E.D. Atkins, A.J. Waddon, M.J. Fournier, T.L. Mason, D.A. Tirrell, *Science* **1994**, *265*, 1427-1432
- [15] W.T. Wertén, F.A. de Wolf, *Appl. Env. Microbiol.* **2005**, *71*, 2310-2317.
- [16] A.A. Martens, M. Neeleman, M.W.T. Wertén, G. Eggink, M.A. Cohen Stuart, F.A. de Wolf, *Macromolecules*, **2009**, *42*, 1002-1009
- [17] Y. Yun, A.A. Martens, N.A.M. Besseling, F.A. de Wolf, A. de Keizer, M. Drechsler, M.A. Cohen Stuart, *Angew. Chem. Int. Ed.* **2008**, *47*, 4192-4195
- [18] A. Åslund, A. Herland, P. Hammarström, K.P. Nilsson, B.H. Jonsson, O. Inganäs, P. Konradsson, *Bioconjug. Chem.* **2007**, *18*, 1860-1868
- [19] K.P.R. Nilsson, M.R. Andersson, O. Inganäs, *J. Phys.: Condensed Matter* **2002**, *14*, 10011-10020

Chapter 7

Nanowires formed by the co-assembly of gelator and polythiophene

Conjugated organic nanowires have been prepared by co-assembling a carboxylate containing low molecular weight gelator (LMWG) and an amino acid substituted polythiophene derivative (PTT). Upon introducing the zwitterionic polyelectrolyte PTT to a basic molecular solution of the organogelator, the negative charges on the LMWG are compensated by the positive charges of the PTT. As a result, nanowires form through co-assembly. These nanowires were visualized by both transmission electron microscopy (TEM) and atomic force microscopy (AFM). Depending on the concentration and ratio of the components these nanowires can be micrometers long. These measurements further suggest that the aggregates adopt a helical conformation. The morphology of these nanowires were studied with fluorescent confocal laser scanning microscopy (CLSM). The interactions between LMWG and PTT were characterized by steady state and time resolved fluorescence spectroscopy studies. The steady state spectra indicate that

In slightly modified form submitted as: F. Li, G. Palaniswamy, M.R. de Jong, A. Åslund, P. Konradsson, M.A. Cohen Stuart, E.J.R. Sudhölter, A.T.M. Marcelis, F.A.M. Leermakers. **2009**

the backbone of the PTT adopts a more planar and more aggregated conformation when interacting with LMWG. The time-resolved fluorescence decay studies confirm this interpretation.

7.1 Introduction

Co-assembly of more than one type of molecules into large objects with fixed stoichiometry is one of the main approaches in bottom-up nanotechnologies. In these large objects, one can combine functionalities of its constituents in a controlled way. In particular, conjugated polymers like polythiophenes (PTs) with various side chains and with a well-defined structure may have useful conductive properties.[1-6] PTs containing zwitterionic amino acid side chains are remarkably water-soluble and due to their zwitterionic groups, they can aggregate with protein fibers or DNA strands.[4-7] However, these aggregates are not well-organized due to the random binding of the PTs to the biomolecules.

Polythiophene derivatives with zwitterionic amino acid side chains have been studied for many years in the group of Inganas.[3-7] They are readily soluble in water in a wide pH range. The conformation of these PTs is very sensitive to pH. When the side-groups are charged, i.e at high or low pH, they adopt a planar conformation. In the uncharged state (around pH 5.7) the PT adopts a non-planar conformation. These conformational features are reflected in changes in both the UV and fluorescence spectra. Furthermore, aggregation of the fibers also influences the conformation and thus the UV and fluorescence spectra.[8] Therefore, aggregates of these PTs with peptides were initially used as an optical probe to detect amyloid fibril formation or variations in polypeptide conformations. In this study, we describe the co-assembly of PTs with a pH-reversible low molecular weight gelator (LMWG) as a template, leading to highly organized organic nanowires with fluorescent properties.

LMWGs have attracted considerable attention in recent years due to their striking self-assembling behavior and potential applications.[9-12] The highly organized 1-dimensional structures formed by many low molecular weight gelators have suggested their use as templates for the preparation of nanostructured materials.[13] In organic solution, low molecular weight gelators have been used to template the formation of polyaniline nanowires via electrostatic interactions,[14] and the formation of polydiacetylene nanowires via post-polymerization.[15]

C₃-symmetric, amino-acid based gelators with a cyclohexane core have been shown to easily and reversibly assemble into well-organized organic nanowires in an aqueous solution.[16-18] The rapid and reversible self-assembling properties often depend on external stimuli, such as pH and temperature. For instance, gelators with a carboxylate side groups, will only form nanowires at low pH, and the fiber formation is suppressed when the charges are not neutralized, i.e. at higher pH. Interestingly, these nanowires could be aligned by an external electric field,[18] and some LMWGs with fluorescent groups have been used in Fluorescence Resonance Energy Transfer (FRET) experiments.[19] All the above-mentioned properties make these LMWGs an ideal species to fabricate conductive nanowires in aqueous solution.

The structures of the PTT and LMWG used in this study are depicted in Figure 7.1. The carboxylate group containing LMWG is molecularly dissolved in water at high pH, where the acidic groups are partly deprotonated and no self-assembly occurs. The amino groups of PTT interact with the carboxylate groups of the LMWG, thus shielding the negative charges. Under these conditions, the gelator molecules form molecular nanowires, together with the PTT oligomers, which aggregate with the gelator fibers, thus reinforcing the hydrogen bonds and hydrophobic interactions. As a result, the PTT oligomers are well-aligned along the LMWG fibers. Recently, the successful formation of virus-templated conductive nanowires in aqueous solution was reported,[20] where the conjugated polymer randomly attached to the virus, based on electrostatic interactions.

In the present study, the morphologies of the formed nanowires were visualized with TEM, AFM and CLSM. Time resolved and steady state fluorescence spectroscopy were used to probe the interactions between the LMWG and PTT.

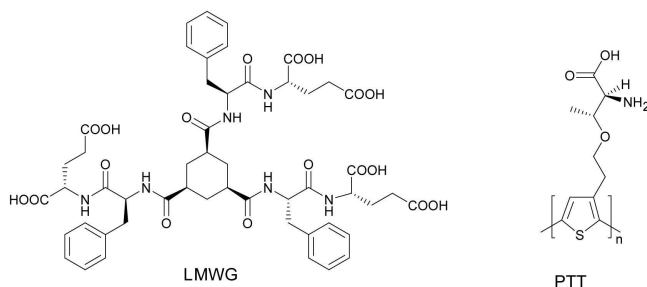


Figure 7.1: Structures of the compounds used in this study

7.1.1 Materials

The synthesis of PTT, with threonine amino acid side groups, has been reported previously.[21] The polythiophenes contain about 10-15 monomeric units. The synthesis of the LMWG based on *cis,cis*-cyclohexane 1,3,5-triscarboxamide has been reported elsewhere.[16] Phosphate buffer solutions (pH 7.4; 10 mM) were prepared from tablets purchased from Sigma. For TEM, AFM and time resolved and steady state fluorescence spectroscopy measurements, about 2 mg/ml LMWG solutions (2 mM) were prepared in a 5 mM NaOH solution. Under these conditions about half the acid groups of the LMGW will be deprotonated. The nanowire solutions were prepared by gradually adding aliquots of a concentrated solution of PTT to the above-mentioned LMWG solution while stirring until a maximum concentration of up to 5 $\mu\text{g}/\text{ml}$ PTT (0.025 mM in thiophene units) in water was reached. The initial concentration of the LMWG hardly changed during this addition. For CLSM measurement, about 2 mg/ml LMWG solutions (2 mM) were prepared in a 12 mM NaOH solution. Under these conditions all the acid groups of the LMGW will be deprotonated. The nanowire solutions were then prepared by gradually adding up to 10 $\mu\text{g}/\text{ml}$ PTT (0.05 mM in thiophene units). After preparation these mixtures were used immediately for the various experiments.

7.1.2 Transmission Electron Microscopy

TEM measurements were performed on a JEOL 1011 EX electron microscope operating at 80 kV. Images were recorded with a 1k CCD camera. Co-assembled nanowires were engrossed on CuH and 1 % formvar-coated copper grids. The grids were submerged for 1 min into the sample solution, and subsequently stained with an aqueous 1 wt % uranyl acetate solution.

7.1.3 Atomic force microscopy

Tapping-mode atomic force microscopy (AFM) experiments were carried out with a JSPM-5400 scanning probe microscope (JEOL Europe). Height images were obtained in AC mode in air using NSC35/AIBS ultra sharp cantilevers (MikroMasch Europe). 10 μl of the nanowire containing solution were deposited on a freshly cleaved mica surface at room temperature and dried in air overnight before imaging.

7.1.4 Confocal laser scanning microscopy (CLSM)

The co-assembled nanowires were aligned through molecular combing on hydrophobic surfaces. The substrates used in this study were cover slips for fluorescence microscopy. In order to get a lower surface energy of the substrates to enable the alignment of the fibrils, a PDMS stamping procedure was undertaken.[3, 7] A PDMS stamp was placed onto the substrate for 60 min, which resulted in the transfer of PDMS oligomers from the stamp and a hydrophobic pattern on the substrate. On the PDMS-modified surface, a droplet (30 μL) of the co-assembled nanowires solution was incubated for 30 min and gently blown off in one direction with nitrogen gas. The surface was carefully rinsed in deionizer water. The confocal fluorescence images of the co-assembled nanowires were then recorded with a confocal laser scanning microscope (Zeiss LSM 510 Meta), with excitation wavelength of 458 nm and long band pass of 560 nm.

7.1.5 Steady state and time-resolved fluorescence spectroscopy

For the fluorescence spectroscopy measurements, the co-assembled nanowires were diluted five times with a 10 mM phosphate buffer of pH 7.4, to get a LMWG concentration of 0.4 mM and 5 μM of PTT (in thiophene units). Steady state and time-resolved emission measurements were done using a FLS 920 spectrophotometer (Edinburgh Instruments, UK) fitted with a cooled MCP-PMT detector (R3809U-50, Hamamatsu, Japan). For the steady state measurements the samples were excited with a pulsed xenon lamp ($\lambda_{exc} = 400$ nm). For the time-resolved measurements the samples were excited ($\lambda_{exc} = 372$ nm) with a pulsed diode laser (LDH-PC-375; Pico-Quant GmbH, Germany; fwhm = 39 ps), controlled with a pulse controller (PDL 800-B; Pico-Quant GmbH, Germany). The instrument response function (fwhm of IRF = 87 ps) was determined from scattering experiments using colloidal silica (Ludox, Sigma-Aldrich). The decay curves were analyzed using “Fast” software (Edinburgh Instruments, UK).

7.2 Results and Discussion

The LMWG molecules that are initially negatively charged, are molecularly dissolved under the initial basic conditions. The charges are gradually compensated by the addition of the zwitterionic polymer PTT. At a certain degree of neutra-

lization, the gradually decreasing electrostatic repulsion is overcome by hydrogen bonding and hydrophobic interaction, and the LMWG and PTT co-assemble into nanowires. The proposed mechanism for the co-assembly of the nanowires is shown in Figure 7.2. The degree of co-assembly depends on the ratio of LMWG to PTT. Within certain limits, the more PTT, the longer the nanowires become.[22] The self-assembly is also pH dependent. When more than 6 equivalents of NaOH per LMWG are added, i.e. more than is required for the complete deprotonation of all carboxylic acid groups of the gelator molecule, the nanowires disintegrate and fall apart into their constituents.

Figure 7.3 gives an overview of images of the nanowires obtained by TEM and AFM. TEM images of negatively stained material, Figures 7.3a and 7.3b, show nanowires that are up to μm long, with a uniform diameter of about 10 nm. Very similar results have been obtained from tapping mode AFM as shown in Figures 7.3c and 7.3d. The images reveal a height that varies from 1.5 to 5.6 nm above the mica surface with regular features having a spacing of 20-30 nm along their length. Similar structures have been found before in polypeptide and supermolecular fibers and are indicative for a helical arrangement.[23-25] Upon closer inspection, one finds that sometimes thicker nanowires are present, indicating that some of the primary nanowires further assemble into higher order organized bundles.

The diameter of the gelator fibers itself is around 3 nm,[16] which corresponds to the calculated diameter of the LMWG molecule. The distance between stacked LMWG molecules in the fibers is approximately 0.5 nm.[16] This is slightly longer than the distance of about 0.38 nm between two neighboring thiophene units of the PTT.[1] We therefore propose that the PTT oligomers are not laying exactly parallel along the LMWG nanowires, but do so with a certain angle between the backbone of the PTT and the long axis of the LMWG wire. We could assume that three thiophene units of the same PTT chain interact with two carboxylate groups of coherent LMWGs. As a result the PTT molecules will be wrapped around the chiral LMWG fibers in a helical sense, indicated in Figure 7.2. These helical aggregates will be significantly different from the reported pH-sensitive self-assembled nanowires from pristine LMWG.[16] Because of the presence of the PTT the diameter will be significantly broader.

A magnified AFM image is shown in Figure 7.3d. In this image, nanowires with various widths are seen. Some highly ordered bundles of nanowires with

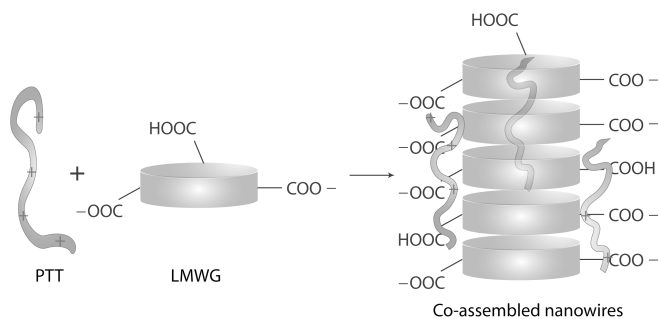


Figure 7.2: Schematic representation of the nanowire formation and structure. Note both the LMWG and the PTT are molecular solutions in their pristine solutions and only when they are mixed together, they form the linear objects through co-assembly.

clear secondary structures are also visible. The presence of higher order bundled structures depends on the ratio of PTT and LMWG in the system and the sample preparation method. Briefly, a higher PTT to LMWG ratio gives more bundles; ratios higher than those used in this work cause precipitation of the material.

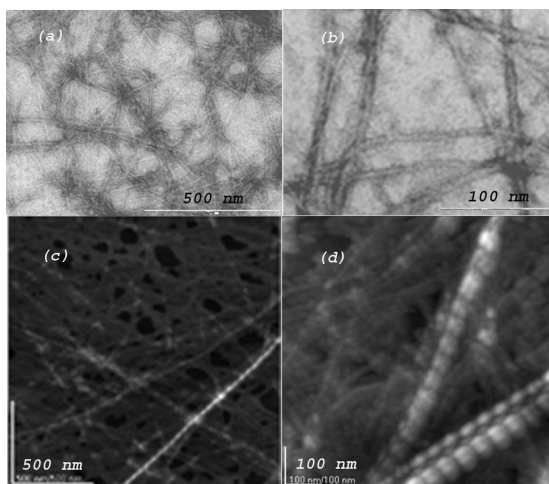


Figure 7.3: Images of co-assembled nanowires. (a) TEM image, stained with 2 % uranyl acetate (b) Magnified TEM image (c) Tapping mode AFM image (d) Magnified tapping mode AFM image.

These nanowires co-assemble also in the presence of 12 mM NaOH, where all the acid groups of LMWG are deprotonated, this makes it possible to have more PTT co-assembled in the system before precipitation takes place.

Since PTT contains fluorescent residues, the presence of the PTT in the fibers can be visualized. Therefore, the fibers were deposited on a PDMS-modified glass surface and investigated with CLSM. A detailed picture of the nanowires is shown in Figure 7.4. In this case, the nanowires were partially stretched by gently blowing the drying droplets over the surface with nitrogen gas. Clearly, up to few tens of micrometer long fluorescent nanowires were detected, which is in good agreement with previous work on the interactions between PTT and proteins.[3, 7] An important difference between these investigations and the present work is that our nanowires are obligatory co-assembled from PTT and LMWG; indeed the LMWG would remain molecularly dissolved in solution in the absence of the PTT, simply due to its complete deprotonation under the experimental conditions. Thus, in our case the PTT is well-organized along the self-assembled LMWG fiber. Possibly this could result in good electron conductivity along these nanowires.

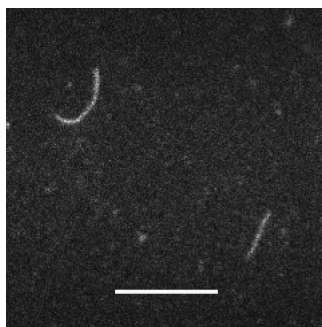


Figure 7.4: CLSM image of co-assembled nanowires on a PDMS-coated glass surface, scale bar 10 μm

From the presented microscopy images, we conclude that these molecules co-assemble into nanowires with a well-organized structure. It is however still unclear what exactly happens on the molecular level. Information about aggregation and conformational changes of the PTT molecules can be obtained from steady state fluorescence spectroscopy. Figure 7.5 shows the emission spectrum of the conjugated nanowires in comparison with the spectrum of pristine PTT molecules at pH 7.4. The maximum emission of PTT upon excitation at 400 nm is red-shifted from 589 nm to 605 nm upon interacting with LMWG. This result indicates that the co-assembly of LMWG with PTT forces PTT to adopt a more planar conformation. Furthermore, the lower fluorescence intensity, as shown in Figure 7.5

indicates that some aggregation of the PTT molecules occurs. Earlier studies of PTT showed that deprotonation of the amino groups is important for the polymer chains to form aggregates.[8] While interacting with LMWG, the negative charges on the PTT polymer are compensated, and the PTT molecules become more aggregated and the fluorescence intensity decreases correspondingly. These trends are opposite to the results of Chapter 6, where we found that PTT appeared less aggregated when interacting with both negatively and positively charged polypeptides. We note that the chemical compositions of the LMWG and the polypeptides used in previous study are very different, and it is reasonable to assume differences in forces acting on the PTT. The charge density between LMWG and polypeptides is also different. A mismatch of charge density between PTT and the complexing agent (LMWG or polypeptides) can lead to both a compressed or expanded conformation of PTT. This explains these opposite trends.

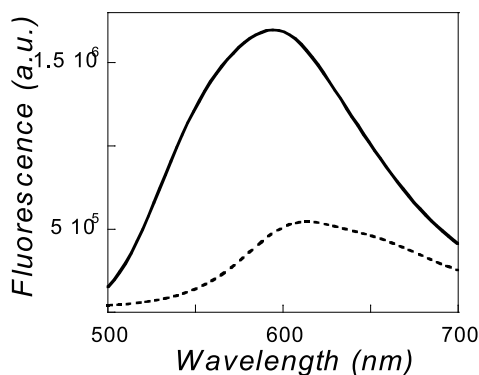


Figure 7.5: Fluorescence emission spectra of $5 \mu\text{M}$ of PTT (on a monomer basis) in 10 mM phosphate buffer pH 7.4 (solid line) and of $5 \mu\text{M}$ of PTT in the presence of $400 \mu\text{M}$ LMWG (dashed line).

The presence of specific interactions between PTT and the LMWG was also deduced from time-resolved fluorescence decay measurements. The fluorescence decay curves of PTT in the presence of LMWG at pH 7.4 in a phosphate buffer are shown in Figure 7.6. In the absence of LMWG, PTT exhibits a bi-exponential decay with time constants $\tau_1 = 0.312 \text{ ns}$ (57 %) and $\tau_2 = 0.792 \text{ ns}$ (43 %) at pH 7.4, whereas the emission decay of PTT becomes faster when it interacts with LMWG. With excess LMWG, a bi-exponential decay with time constants $\tau_1 = 0.226 \text{ ns}$ (81 %) and $\tau_2 = 0.564 \text{ ns}$ (19 %) was found. The progressive decrease of the emission

decay times are significantly different from previous time-resolved fluorescence studies of mixtures of POWT and peptides, where the emission decay times show no obvious difference between the mixtures and the POWT reference.[26] This may be caused by a stronger interaction between PTT and LMWG in comparison to the interaction between POWT and peptides. Indeed, such a clear decrease of the emission decay times strongly supports the idea that the polythiophenes co-assemble in a well-ordered and tight fashion with LMWG.

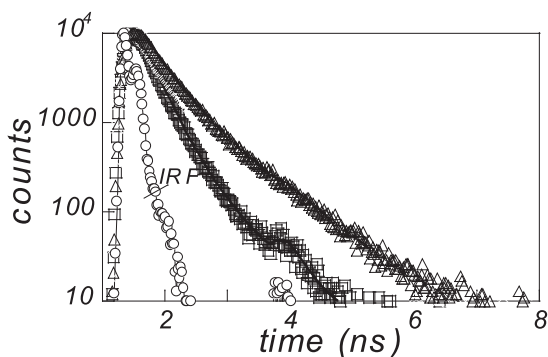


Figure 7.6: Fluorescence decay measurements of $5 \mu\text{M}$ of PTT (on a monomer basis) in 10 mM phosphate buffer pH 7.4 (Δ), of $5 \mu\text{M}$ of PTT in the presence of $400 \mu\text{M}$ LMWG (\square) and the instrument response function IRF (O). The solid lines are fitted by bi-exponential decay.

These nanowires can be reversibly formed and broken down by changing the pH. Other external stimuli such as mechanical force, and temperature can also influence the co-assembly of these nanowires.[16] Besides the presently investigated LMWG, other wire forming initiators, like pH-sensitive proteins, can potentially be used to obtain conjugated bio-nanowires which have the potential for use in biosensor applications.

7.3 Conclusions

A new type of co-assembled highly ordered organic nanowire has been prepared from a low molecular weight gelator and a conjugated zwitterionic polythiophene derivative. The interaction of these compounds results in helical nanowires where the polythiophenes adopt a more planar conformation. Morphologic studies have shown that the co-assembled nanowires adopt a helical structure that forms well-

defined nanowires with lengths up to several μm long. The steady state and time-resolved fluorescence emission measurements confirm that the backbone of the PTT adopts a more planar conformation and the PTT chains are more aggregated than in the absence of the organic gelator. These nanowires can be rather simply and reversibly manipulated by external stimuli, such as pH. The reversibility of this co-assembly makes it a promising candidate for use in bio-sensor applications.

Bibliography

- [1] H. Sakaguchi, H. Matsumura, H. Gong, A.M. Abouelwafa, *Science* **2005**, *310*, 1002-1006
- [2] A. Gesquiere, S.D. Feyter, F.C.D. Schryver, F. Schoonbeek, J.H. van Esch, R.M. Kellogg, B.L. Feringa, *Nano Letters* **2001**, *1*, 201-206
- [3] A. Herland, P. Bjork, P.R. Hania, I.G. Scheblykin, O. Inganas, *Small* **2007**, *2*, 318-325
- [4] K.P.R. Nilsson, J. Rydberg, L. Baltzer, O. Inganas, *Proc Natl. Acad. Sci. USA* **2003**, *100*, 10170-10174
- [5] A. Herland, P. Bjork, K.P.R. Nilsson, J.D.M. Olsson, P. Asberg, P. Konradsson, P. Hammarstrom, O. Inganas, *Adv. Mater.* **2005**, *17*, 1466-1471
- [6] A. Herland, K.P.R. Nilsson, J.D.M. Olsson, P. Hammarstrom, P. Konradsson, O. Inganas, *J. Am. Chem. Soc.* **2005**, *127*, 2317-2323
- [7] Bjork, P.; Herlands, A.; Scheblykin, I. G.; Inganas, O. *Nano Letters* **2005**, *5*, 1948-1953
- [8] K.P.R. Nilsson, M.R. Andersson, O. Inganas, *J. Phys. Condens. Matter* **2002**, *14*, 10011-10020
- [9] D.J. Abdallah, R.G. Weiss, *Adv. Mater.* **2002**, *12*, 1237-1247
- [10] J.H. van Esch, B.L. Feringa, *Angew. Chem. Int. Ed.* **2000**, *39*, 2263-2266
- [11] O. Gronwald, E. Snip, S. Shinkai, *Curr. Opin. Colloid Interface Sci.* **2002**, *7*, 148-156

- [12] L. Estroff, A.D. Hamilton, *Chem. Rev.* **2004**, *104*, 1201-1217
- [13] M. Liusar, C. Sanchez, *Chem. Mater.* **2008**, *20*, 782-820
- [14] C. Li, T. Hatano, M. Takeuchi, S. Shinkai, *Chem. Commun.* **2004**, *20*, 2350-2351
- [15] M. Shirakawa, N. Fujita, S. Shinkai, *J. Am. Chem. Soc.* **2005**, *127*, 4164-4165
- [16] K.J.C.V. Bommel, C.V.D. Pol, I. Muizebelt, A. Friggeri, A. Heeres, A. Meetsma, B.L. Feringa, J.H. van Esch, *Angew. Chem. Int. Ed.* **2004**, *43*, 1663-1667
- [17] A. Heeres, C.V.D. Pol, I. Muizebelt, M. Stuart, A. Friggeri, B.L. Feringa, J.H. van Esch, *J. Am. Chem. Soc.* **2003**, *125*, 14252-14253
- [18] L. Sardone, V. Palermo, E. Devaux, D. Credgington, M.D. Loos, G. Marletta, F. Cacialli, J.H. van Esch, P. Samori, *Adv. Mater.* **2006**, *18*, 1276-1280
- [19] M. Montalti, L.S. Dolci, L. Prodi, N. Zaccheroni, M.C.A. Stuart, K.J.C.V. Bommel, A. Friggeri, *Langmuir* **2006**, *22*, 2299-2303
- [20] Z.W. Niu, J. Liu, A. Lee, M.A. Bruckman, D.G. Zhao, G. Koley, Q. Wang, *Nano Letters* **2007**, *7*, 3729-3733
- [21] a. Åslund, A. Herland, P. Hammarström, K.P. Nilsson, B.H. Jonsson, O. Inganäs, P. Konradsson, *Bioconjug. Chem.* **2007**, *18*, 1860-1868
- [22] F. Li, A.A. Martens, A. Åslund, P. Konradsson, F.A. de Wolf, M.A. Cohen Stuart, E.J.R. Sudhölter, A.T.M. Marcelis, F.A.M. Leermakers. *Soft Matter*, **2009**, *5*, 1668-1673
- [23] K.L.D. Jong, B. Incledon, C.M. Yip, M.R. Defelippis, *Biophys. J* **2006**, *91*, 1905-1914
- [24] B.W. Messmore, P.A. Sukerkar, S.I. Stupp, *J. Am. Chem. Soc.* **2005**, *127*, 7992-7993
- [25] E. Jahnke, I. Lieberwirth, N. Severin, J.P. Rabe, H. Fraurenrath, *Angew. Chem. Int. Ed.* **2006**, *45*, 5383-5386
- [26] K.P.R. Nilsson, J.D.M. Olsson, F. Stabo-Eeg, M. Lindgren, P. Konradsson, O. Inganäs, *Macromolecules* **2005**, *38*, 6813-6821

Part III

Applications

Chapter 8

Pluronic polymersomes stabilized by core cross-linked polymer micelles

Vesicles from Pluronic L121 (PEO₅-PPO₆₈-PEO₅) triblock copolymers were stabilized against aggregation by Pluronic P85 (PEO₂₆-PPO₄₀-PEO₂₆) micelles. Both the vesicles and the micelles were reinforced by an interpenetrating polymer network from pentaerythritol tetraacrylate (PETA). AFM, electron microscopy and fluorescence labeling studies are used to investigate the morphology of the capsules. The P85 micelles are integrated into the L121 polymersome walls, while both types of Pluronic block copolymer are also non-covalently trapped in their respective interpenetrating acrylate networks. The micelle-containing vesicles retain their size upon heating until at least 33 °C. Upon cooling below room temperature the vesicles reversibly lose block copolymers. It is shown that the double-stabilized vesicles are readily internalized in HeLa and Caco-2 cells.

In slightly modified form published as: F. Li, L.H.J. de Haan, M.A. Cohen Stuart, E.J.R. Sudhölter, A.T.M. Marcelis, F.A.M. Leermakers. *Soft Matter* **2009**

8.1 Introduction

Polymersomes have been studied extensively in the past few years because they have, compared to the lipid counterparts, the clear benefits of stimuli responsiveness and chemical diversity.[1] Moreover, the polymersomes often are less fragile. Many amphiphilic block copolymers, especially those with large hydrophobic and relatively small hydrophilic blocks can self-assemble into vesicles[1-5] at low concentrations. To obtain functional polymersomes, normally block copolymers with stimuli-responsive groups are required.[6] A major drawback then is that proper interesting block copolymers are usually not commercially available and the design synthesis of block copolymers with functional groups is rather time-consuming. In this respect the Pluronic, poly(ethyleneoxide) *b* poly(propyleneoxide)-*b*-poly(ethyleneoxide), triblock copolymer family is an exception to the rule of being available while being relevant for the purpose of polymersome formation. Indeed, Pluronic L121 is known to spontaneously form unilamellar vesicles when dissolved in water. Moreover, Pluronics allow for further functionalization though post-chemical modification on their end groups.[7]

Pluronics are considered non-toxic and are widely used in drug delivery systems and provide exciting opportunities for gene therapy. Upon using standard vesicle preparation procedures, Pluronic L121 (PEO₅-PPO₆₈-PEO₅) forms small unilamellar vesicles with a size of approximately 100 nm,[8, 9] which revert to flat lamellar structures within a few hours after preparation, indicating that the vesicle state is metastable. Furthermore, aqueous solutions of these block copolymers are rather temperature sensitive.[10-12] At low temperatures, $T < \text{CMT}$ (critical micellization temperature), they dissolve as unimers in water, whereas at higher temperatures, $T > \text{CPT}$ (cloud point temperature), they very quickly form larger aggregates. The working window of the vesicles is small, i.e., the CMT is approximately 15 °C and the CPT is approximately at room temperature, which limits their potential use in novel polymer-based controlled-release systems.

In this work we consider strategies to enlarge the working window for Pluronic L121 vesicles. Recently, a method for stabilizing Pluronic micelles was reported in the literature. Pluronic P85 (PEO₂₆-PPO₄₀-PEO₂₆) micelles were stabilized by a permanent interpenetrating network (IPN) of polymerized pentaerythritol tetraacrylate (PETA).[13, 14] The polymerization of PETA took place mostly in the core of the micelles. A similar approach for stabilizing Pluronic L121 vesicles

was applied by us, Chapter 2.[15] Although these reinforced vesicles can retain their size and shape for rather long times, up to one month, the very short PEO groups in the L121 molecules can not prevent the aggregation of the polymersomes at elevated temperatures, i.e. we still observed phase separation above the CPT of 25 °C.

We realized that to prevent aggregation, we needed to introduce longer hydrophilic moieties into the L121 vesicles. Here, we report on the incorporation of IPN-stabilized P85 micelles into L121 vesicles. The longer PEO moieties of the P85 micelles, sticking out of the vesicle membranes, prevents them from reverting into flat bilayers. The polymersomes stabilized by the core cross-linked micelles were subsequently stabilized by a similar cross-linking by formation of an IPN from PETA in the vesicle walls. This second IPN gives stability to the L121 vesicle wall and simultaneously ensures the more permanent presence of the P85 micelles in the composite capsule. Again, the protection by the Pluronic P85 micelles is attributed to the steric stabilization that is provided by the hydrophilic coronas of the incorporated micelles. Importantly, these micelles improve the temperature stability of the capsules, i.e., the long time stability is excellent up to at least 33 °C.

The morphology of the resulting double-stabilized vesicles was studied by AFM, TEM and CLSM. Their stability as a function of temperature was studied by dynamic light scattering (DLS). Fluorescent-labeled P85 micelles were prepared and taken up in the polymersome vesicles and covalently cross-linked in the interpenetrating network (IPN), and the uptake of these double-stabilized vesicles containing the fluorescent labeled micelles in HeLa and Caco-2 cells was studied.

8.1.1 Materials

Poly(ethyleneoxide)-*b*-poly(propyleneoxide)-*b*-poly(ethyleneoxide) (PEO₅-PPO₆₈-PEO₅) (Pluronic L121) was obtained as a kind gift from BASF Corp. Pentaerythritol tetraacrylate (PETA), and hydrophobic probe Nile red were purchased from Sigma. The thermal initiator 2,2'-azobis(4-methoxy-2,4-dimethyl valeronitrile) (V-70) was obtained from Wako. The yellow-green fluorescent dye, hostasol methacrylate (HMA), was synthesized from chloronaphthalic anhydride according to US patent 2004/0016370. The extruder and the extrusion membranes

were purchased from Avanti Polar Lipids.

8.1.2 Preparation of vesicles from PEO₅-PPO₆₈-PEO₅ copolymers

The stabilization of Pluronic P85 micelles with PETA was described previously in literature.[13, 14] In short, an aqueous solution of a mixture containing 1 wt% Pluronic P85 and 0.04 wt% PETA was used. After UV-polymerization at 60 °C and extensive dialysis with a 12.4 kDa membrane against water at room temperature, the remaining solution containing the polymerized Pluronic P85 micelles was used for the preparation of the vesicles. Pluronic L121 and PETA were intimately mixed by dissolving them in a few milliliters of chloroform, which was then evaporated under a nitrogen stream and the remaining mixture was dried under vacuum overnight. A solution of the mixture containing 0.1% P85 micelles, 0.2 wt% Pluronic L121 and 0.006 wt% PETA was prepared and frozen in liquid nitrogen and subsequently thawed in a 25 °C water bath while stirring. Then the mixture was extruded 25 times through a membrane with 100 nm pores. Larger vesicles for fluorescent studies were made by extrusion through a membrane with 800 nm pores. PETA-loaded vesicle solutions were put in a quartz cuvette, and photo-polymerization was performed with UV irradiation (Heraeus TQ150 UV lamp, 150 W) for 40 min. Alternatively, 5 μ l of a stock solution of thermal radical initiator (V-70; 0.6 mg/ml) in ethanol, was added to 1 ml of freshly prepared vesicle solution, and the mixture was incubated at 25 °C for 40 min to produce vesicles stabilized by thermally induced polymerization of PETA. The latter method was used in combination with fluorescent probes to avoid photo-bleaching.

Hydrophobic Nile red containing vesicle solutions were prepared by adding 5 μ l of a stock solution of Nile red (2 mg/ml) to 1 ml of a vesicle solution containing PETA before the extrusion step. For fluorescent labeling of P85 micelles, 0.0025 wt% HMA was introduced in the micelle mixture. Immediately after polymerization and purification, the labeled micelles were applied in the Pluronic L121 solution. With extrusion the polymer network was formed by thermally induced polymerization. HMA was then covalently cross linked in the IPN, and as a result Pluronic L121 vesicles were fluorescently labeled by HMA present in the P85 micelles.

8.1.3 Confocal laser scanning microscopy

The solutions with double-stabilized vesicles containing Nile red or Nile red and HMA as fluorescent probe were deposited on a glass surface, covered with a glass slide, and then visualized directly using a confocal laser scanning microscope (Zeiss LSM 510 Meta). The cells containing HMA-labeled double-stabilized vesicles were visualized directly in a 8 well chamber after proper incubation.

8.1.4 Electron Microscopy

Samples for electron microscopy were dried on a copper grid overnight before doing the measurements. Transmission electron microscopy (TEM) measurements were performed on a TEM microscope (JEOL 1200 EX) operating at 120 kV. All images were recorded digitally (Orion, 6 E. L. I. sprl., Belgium) at a scan rate of 100 seconds (full frame) at a size of 2528 x 2030, 8 bit.

8.1.5 Atomic force microscopy

Tapping mode atomic force microscopy (AFM) experiments were carried out on a MFP-3D atomic force microscope from Asylum Research (Santa Barbara, CA). Height imaging was done in AC mode in air using OMCL-AC240 silicon cantilevers (Olympus Corporation, Japan). One drop of the vesicle solution was deposited on a freshly cleaved mica surface at room temperature and dried overnight before measurements.

8.1.6 Dynamic light scattering

DLS was carried out on an ALV/ DLS-5000 light-scattering apparatus (ALV, Langen, Germany), equipped with an argon ion laser (LEXEL, Palo Alto, CA) operating at a wavelength of 514.5 nm. All experiments were performed at a scattering angle of 90°. Temperature was controlled by using a Haake C35 thermostat. The hydrodynamic radius was calculated from cumulant fits or a CONTIN multi-exponential fit.

8.1.7 Incubation of cells with the stabilized vesicles

HeLa cells were cultured in DMEM supplemented with 10% FCS, L-glutamine (1 mM) and gentamycine (5 µg/ml) and Caco-2 cells in DMEM/F12 cell supplement-

ted with 10% FCS, gentamycine ($5 \mu\text{g}/\text{ml}$) and non essential amino acids. Media and supplements were obtained from Invitrogen (The Netherlands). Cells of both cell lines were seeded in a 8-well chamber (Sigma, The Netherlands). After adding cell culture medium cells were incubated for 24 h at 37°C in a humidified atmosphere with 5% CO_2 . Then, $2 \mu\text{l}$ of the stabilized vesicles (100 nm) were added to the HeLa or Caco-2 cells in $40 \mu\text{l}$ of growth medium. The cells were subsequently incubated for 3 h.

8.2 Results and Discussion

Pluronic L121, containing PETA, was well mixed with IPN-stabilized P85 micelles during the freeze-thaw cycling; then the mixture was extruded and the resulting vesicles were stabilized by IPN formation using either UV-induced or thermally-induced free radical polymerization. Upon addition of the IPN-P85 micelles to the L121 system, the micelles associate within the polymersome wall. We expect that only a small fraction of the Pluronic P85 micelles remain present in the aqueous solution. In principle, the possibility exists that freely dissolved P85 molecules and IPN-free P85 micelles are present, which could extract L121 molecules from the polymersome.[16] Experiments show however that such scenarios are of minor importance.

AFM images of the stabilized vesicles obtained after extrusion through a 100 nm membrane and deposited onto mica are shown in Figure 8.1. It is important to realize that before measuring the samples were dried, and the sole fact that we can find structures on the mica that result from the deformed capsules, proves that the IPN has a major impact on the integrity of the vesicles. Indeed, in the absence of an IPN it is impossible to find any vesicular structures on the mica surface using a similar drying procedure. The 3D image (Figure 8.1b) as well as the height image (Figure 8.1a) clearly show rather monodisperse small vesicles that have a different response to the force of the AFM probe for the edge than for the center of the deformed vesicles. These differences in the force response are caused by collapse of the vesicles upon drying and are well-known for vesicles and have been observed and discussed in the literature at length.[17] The height of the vesicle is rather homogeneous and is found to be about 1 nm (Figure 8.1c). This is less than found for the PETA-stabilized polymersomes reported in Chapter 2.[15] This suggests that the presence of the P85 micelles in the vesicle walls influences

the formation of the PETA network in the remainder of the L121 vesicles and makes the network less rigid. In the present case the PETA network appears more homogeneously dispersed in the P85 enriched polymersome membranes compared to the polymersome stabilized by PETA alone, and the vesicles are more flexible than the vesicles in the absence of Pluronic P85.

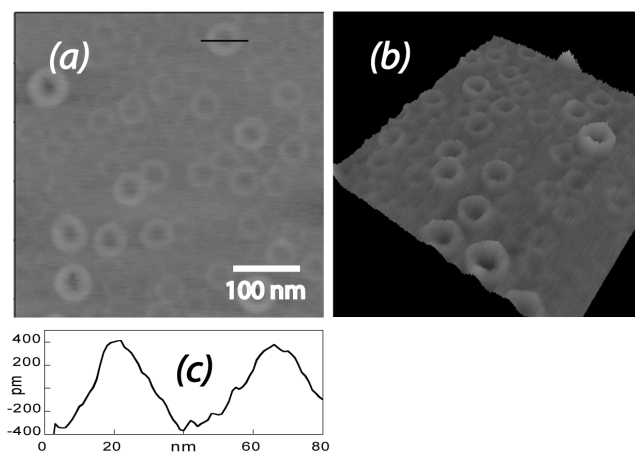


Figure 8.1: AFM images of double-stabilized vesicles obtained by extrusion through an 100 nm membrane. (a) height image, (b) 3D height image of the same area, (c) height section analysis

Interestingly, due to the presence of a homogeneous densely cross-linked PETA network, the contrast of these double-stabilized L121 vesicles under a TEM microscope is so high that it is possible to study their morphology without using a negative staining agent. Typical examples are shown in Figure 8.2. The vesicles were again prepared with a 100 nm extrusion membrane. The two TEM images show vesicles having an average diameter of approximately 160 nm.

To prove that the PETA-crosslinked P85 micelles are really taken up in the walls of the L121 vesicles, fluorescent labeling experiments were performed. For this purpose, larger vesicles were prepared, because they can be directly visualized by fluorescent microscopy. Both the hydrophobic probe Nile red and HMA fluorescent-labeled P85 micelles were used. Figure 8.3 shows the CLSM images of vesicles prepared by extrusion through a 800 nm membrane. Vesicles are seen with a size of around 1 μm , which is comparable to the pore size of the membrane used for the preparation. The hydrophobic dye, Nile red, has a very low fluorescence in aqueous solution, but an enhanced fluorescence in a hydrophobic

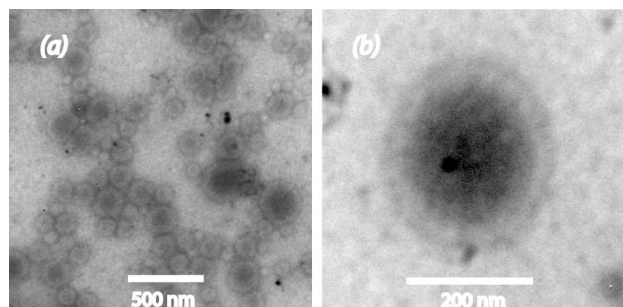


Figure 8.2: TEM images of vesicles prepared by extrusion through an 100 nm membrane at two different magnifications.

environment,[18] so only the hydrophobic shells of the vesicles are visualized in Figure 8.3a. HMA is a methacrylate based probe with green fluorescence, which is covalently taken up in the PETA network upon polymerization. The green fluorescence from vesicles containing HMA-labelled micelles is shown in Figure 8.3b. The overlap of the red and green fluorescence images in the stabilized polymersomes is direct evidence that the polymerized P85 micelles, which contain the covalently attached HMA label in their IPN, are present in the vesicle walls. The insertion of cross-linked micelles can potentially be used as a strategy to introduce fluorescent probes in vesicle walls to study intercellular vesicle delivery in vivo.[19] Indeed, the idea of using micelles as a method to covalently load fluorescent probes into the polymersome leaves us with a large range of opportunities to modify the vesicles with different fluorescent labels. The flexible way of sample preparation provides us also with a relatively simple method to tune the polymersome size and functionality with relatively little synthetic effort.[6, 9]

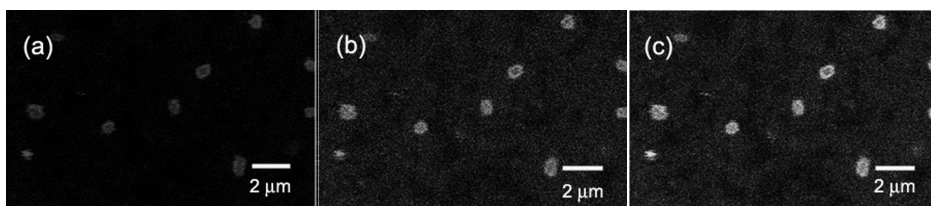


Figure 8.3: CLSM images of vesicles extruded through a 800 nm membrane (a) showing Nile red present in the vesicle walls (b) showing HMA-labeled core cross-linked P85 micelles (c) overlap of the two images.

The combination of AFM, TEM and CSLM data confirm that the vesicles are detectable and nicely retain their spherical shape in the dry state as well as in aqueous solution. It is reasonable to assume that these vesicles are stabilized because of their extra protection by the longer hydrophilic chains of Pluronic P85 and more densely packed PETA network. Therefore a more detailed study was performed on their stability as a function of temperature using dynamic light scattering (DLS).

A sample of stabilized vesicles prepared by extrusion through a 100 nm membrane was analyzed by DLS over a temperature range from 20 °C to 33 °C. The relative scattering intensity and radius as a function of temperature obtained from the cumulant fits are shown in Figure 8.4a. It is seen that the size of the polymerized vesicles changes reversibly in this temperature range without aggregation taking place, whereas aggregation already took place at 25 °C when only a PETA network is present without P85 micelles.[15] When the vesicle solution is slowly heated from 20 °C to 33 °C at a rate of about 2 °C per hour, the scattering intensity and the hydrodynamic radius of the particles increases. The solubility of Pluronic (and also Pluronic L121) in water decreases at high temperatures. Since the Pluronic are not covalently attached to the IPN, some molecules can slowly associate to the network upon heating to 33 °C. Upon decreasing the temperature they dissociate again from the vesicles, and the radius and scattering intensity return again to their original values. After polymerization of the PETA molecules in the polymersome walls, the double-stabilized polymersomes remained stable to at least 33 °C. Depending on the number density of the P85 micelles in the vesicles the system can survive an exposure to higher temperatures for a limited time, e.g. a few hours at 37 °C hardly decreases the vesicle integrity. However, storing the vesicles for longer times above 33 °C still leads to aggregation and phase separation. Even though the operating window opened up with less than 10 degrees, we believe that it is a promising step towards the development of this system for applications. The CONTIN analyses of the measurements, done at 20 °C and 33 °C and shown in Figure 8.4b, reveal that rather monodisperse vesicles are present in solution. Therefore, the average size of the vesicles and their size distribution do not change dramatically within this temperature range, and there is also no apparent aggregation taking place within this temperature range. So, the stability of the P85 micelle-assisted L121 vesicles is definitely increased as compared to the PETA-polymerized L121 vesicles, Chapter 2. The latter were

only stable up to 25 °C, whereas the polymerized L121 vesicles remain stable till at least 33 °C.

Again, the light scattering measurements indicate that the copolymers can dissociate and re-associate again with the PETA capsules as a function of temperature. This temperature dependent behavior may have the consequence that the permeability and thus release of entrapped species through the vesicle walls may be changed systematically.

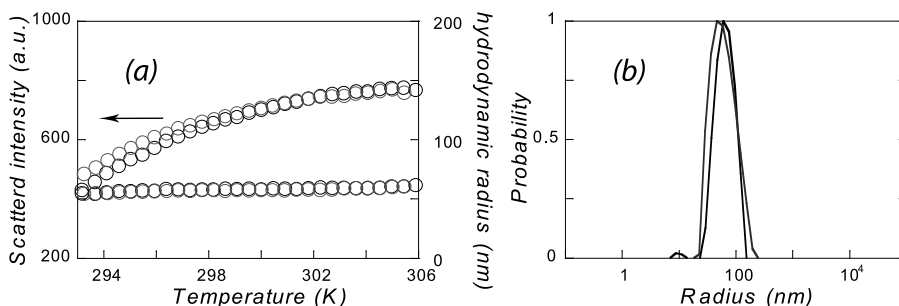


Figure 8.4: DLS measurements of double-stabilized vesicles obtained by extrusion through a 100 nm membrane as a function of temperature (a) scattered light intensity (arbitrary units) (dark circle) upon increasing temperature (light circle) upon decreasing temperature; (b) CONTIN analysis of the sample measured at (light circle) 20 °C and (dark circle) 33 °C.

To get an indication of the biocompatibility of these 100 nm doubled-stabilized vesicles, and to see if cell uptake of these vesicles occurs, the interactions with two types of cell models (Hela cell[20] and Caco-2 cell) were investigated. Within a few hours of incubation, vesicles are efficiently taken up by Hela cells and accumulate in the cytoplasm of the cells (Figure 8.5a). A much lower uptake efficiency was found for Caco-2 cells (Figure 8.5b). No significant cell death was observed under the experimental conditions. This suggests that drugs or biomolecules encapsulated in these vesicles can easily be delivered in vivo.

8.3 Conclusions

Starting from inexpensive, readily available materials we can fabricate double-stabilized Pluronic L121 vesicles that are stable to at least 33 °C and for short times (a few hours) can withstand even higher temperatures. We can routinely control the size of these vesicles by extruding them through an appropriately sized

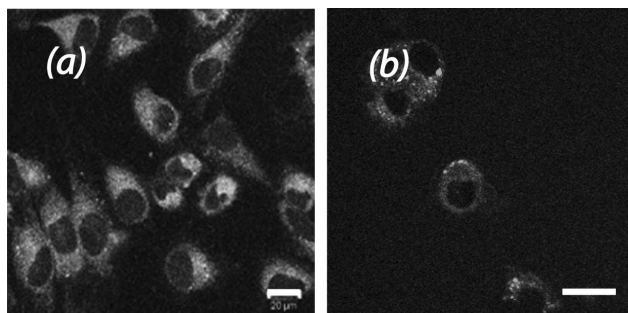


Figure 8.5: Uptake of 100 nm stabilized vesicles containing HMA-labeled core cross-linked P85 micelles after 3h of incubation at 37 °C by (a) HeLa cells (b) Caco-2 cells. Scale bar 20 μm

filter before the interpenetrating polymer network is formed. Furthermore, we can covalently polymerize fluorescent molecules in the interpenetrating network, and these stabilized fluorescent vesicles can be easily taken up by cells. Hence these vesicles are attractive for a broad range of possible applications. Clear advantages are the possibility to vary the fluorescent properties by using other methacrylate-based fluorescent probes and the possibility to modify the properties of the vesicles by using functionalized Pluronics or other micelle-forming Pluronics. This system is potentially useful for molecular imaging, biological assays, as biomarker, for cell-labeling,[21] drug delivery and food applications.

Bibliography

- [1] D.E. Discher, A. Eisenberg, *Science* **2002**, *297*, 967-973
- [2] T.A. Bronich, M. Ouyang, V.A. Kabanov, A. Eisenberg, F.C. Szoka, A.V. Kabanov, *J. Am. Chem. Soc.* **2002**, *124*, 11872-11873
- [3] B.M. Discher, Y.Y. Won, D.S. Ege, J.C.M. Lee, F.S. Bates, D.E. Discher, D.A. Hammer, *Science* **1999**, *284*, 1143-1146
- [4] H. Kukulka, H. Schlaad, M. Antonietti, S. Forster, *J. Am. Chem. Soc.* **2002**, *124*, 1658-1663
- [5] Y. Kim, P. Dalhaimer, D.A. Christian, D.E. Discher, *Nanotechnology* **2005**, *16*, S484-S491
- [6] E. Holowka, V.Z. Sun, D.T. Kamei, T.J. Deming, *Nature Materials* **2007**, *6*, 52-57
- [7] J.P.A. Custers, P. Kelemen, L.J.P. van den Broeka, M.A. Cohen Stuart, J.T. F. Keurentjes. *J. Am. Chem. Soc.* **2005**, *127*, 1594-1595
- [8] K. Schillen, K. Bryske, Y.S. Melnikova, *Macromolecules* **1999**, *32*, 6885-6888
- [9] K. Bryskhe, J. Jansson, D. Topgaard, K. Schillen, U. Olsson, *J. Phys. Chem. B* **2004**, *108*, 9710-9719
- [10] A.V. Kabanov, P. Lemieux, S. Vinogradov, V. Alakhov, *Adv. Drug Deliv. Rev.* **2002**, *54*, 223-233
- [11] J. Jansso, K. Schillen, M. Nilsson, O. Soderman, G. Fritz, A. Bergmann, O. Glatter, *J. Phys. Chem. B* **2005**, *109*, 7073-7083

- [12] P. Alexandridis, J.F. Holzwarth, T.A. Hatton, *Macromolecules* **1994**, *27*, 2414-2425
- [13] P. Petrov, M. Bozukov, C.B. Tsvetanov, *J. Mater. Chem.* **2005**, *15*, 1481-1486
- [14] P. Petrov, M. Bozukov, M. Burkhardt, S. Muthukrishnan, A.H.E. Müller, C.B. Tsvetanov, *J. Mater. Chem.* **2006**, *16*, 2192-2199.
- [15] F. Li, T. Ketelaar, A.T.M. Marcelis, F.A.M. Leermakers, M.A. Cohen Stuart, E.J.R. Sudhölter, *Macromolecules* **2007**, *40*, 329-333
- [16] V. Pata, F. Ahmed, D.E. Discher, N. Dan, *Langmuir* **2004**, *20*, 3888-3890
- [17] M. Yang, W. Wang, F. Yuan, X.W. Zhang, J.Y. Li, F.X. Liang, B.L. He, B. Minch, G. Wegner, *J. Am. Chem. Soc.* **2005**, *127*, 15107-15111
- [18] M.M.G. Krishna, *J. Phys. Chem. A* **1999**, *103*, 3589-3595
- [19] R. Savic, L. Luo, A. Eisenberg, D. Maysinger, *Science* **2003**, *300*, 615-618
- [20] X.H. Yan, Q. He, K.W. Wang, Li. Duan, Y. Cui, J.B. Li, *Angew. Chem.Int. Ed.* **2007**, *26*, 2431 -2434
- [21] H. Kawaguchi, *Prog. Polym. Sci.* **2000**, *25*, 1171-1210

Chapter 9

Triggered Templated Assembly of Protein Polymersomes

In biomedical applications there is a strong demand for robust targetable nano-sized containers. Having a general strategy to assemble functional biomolecules into stable nanostructures with desired size and shape is a challenge. Liposomes for instance are extremely fragile, having little stimuli responsiveness and chemical diversity.[1] Most polymersomes, on the other hand, lack biofunctionality, which restricts their ability to interact with cells or tissues. Here we present a versatile method to make stable biocompatible protein polymersomes through a route of triggered templated self-assembly. Pluronic vesicles, routinely made in a narrow size distribution ranging from 50-2000 nm in diameter, serve as a matrix that can take up large quantities of a biosynthetic triblock copolymers $CS^X S^X C$ in the unilamellar shell. The middle block $S^X S^X$ of the protein has silk-like repeats, where X stands for the chargeable units, glutamic acid (E) and in another case histidine (H). In response to pH change, the S-block of the protein polymer becomes hydrophobic and adopts itself to the template, which directs the formation of protein polymersome. Alternatively, by adding macromolecules, such as the negatively charged $CS^E S^E C$ or siRNA, which then co-assembles with the positively

In slightly modified form submitted as: F. Li, A.T.M. Marcelis, M.A. Cohen Stuart, F.A. de Wolf, E.J.R. Sudhölter, F.A.M. Leermakers. **2009**

charged $CS^H S^H C$ at the Pluronic membrane. In addition to their stability and biocompatibility,[2] such a templated self-assembly approach allows integration of designed polymers, which can provide multifunction materials for drug delivery and gene delivery applications in a simple manner.

9.1 Introduction

Our new method may be characterized as "triggered templated assembly" (TTA) and is schematically shown in Figure 9.1. In a first step we make medically approved Pluronic vesicles[3, 4] with tunable diameter in the range of 50 to 2000 nm in the presence of fully water-soluble protein $CS^X S^X C$ polymers (the C block which is a random collagen-like block is tested to be hypo-allergenic). In a second step we trigger the assembly by neutralizing the charge X on the S-block. The protein develops β -sheet secondary structures and inserts itself into the vesicle walls. The collagen-like C-blocks remain fully water soluble and form stabilizing corona layers. The capsules thus formed may be referred to as protein polymersomes. Protein polymersomes are a new class of self assembled vesicles, that recently enjoys systematic investigations.[5-7] From chemical synthetic polypeptide based block copolymers[2, 5] to virus capsids,[7] they all have great biocompatibility, but typically have the disadvantage that it is rather tedious and time consuming to make the functionalized starting material. Our TTA system does not share this problem.

The molecules for the TTA system have been carefully selected and are available in large amounts. The primary vesicles that form the template material are made of Pluronic L121, EO-PO-EO, which is a thermo-sensitive amphiphilic block copolymer with a large, marginally hydrophobic poly(propylene oxide) middle block and two very short oligo(ethylene oxide) outer ones.[4] This polymer forms spontaneously unilamellar vesicles in the small temperature range between the critical micellisation temperature and the cloud point temperature. This means that for $T < 15$ °C there is just a molecular solution, whereas at for $T > 25$ °C the vesicles quickly aggregate. Around room temperature the fragile membrane is composed of loosely packed polymers, ready to host the proteins.

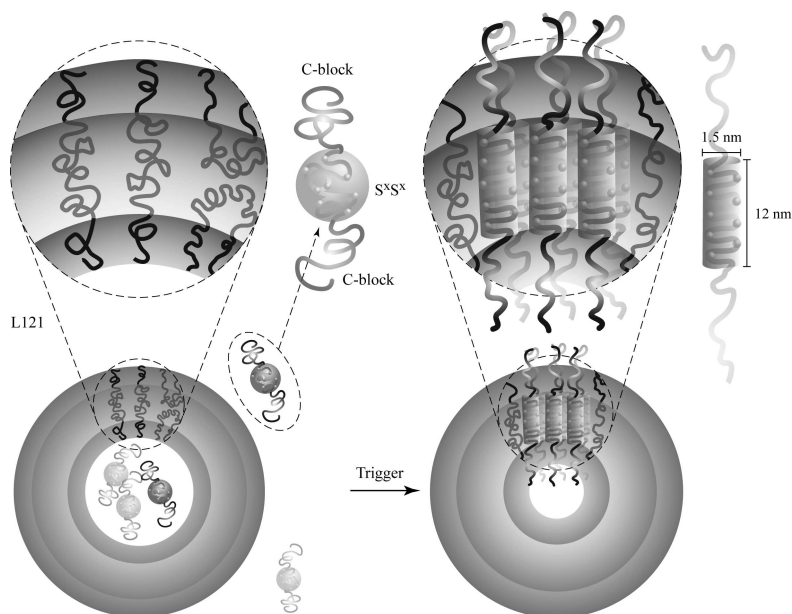


Figure 9.1: Schematic representation of the triggered templated assembly of protein polymersomes. Pluronic L121 vesicles surrounded by triblock peptide copolymer $CS^X S^X C$. After a trigger the X-groups highlighted as spherical dots become uncharged. The S-block obtain β -sheet secondary structures and drives the insertion of the protein polymers into the template. The experiments indicate that the protein polymer loading is exceptionally high that eventually they form a compact protein layer with perhaps few remaining Pluronic L121 molecules.

9.2 Results and Discussion

Next we employed the designed protein polymers route, wherein chosen amino acid sequences are expressed in an appropriate host organism. With this method one retains the absolute control over polymer length and sequence provided by a biosynthetic approach and produces biocompatible products with large quantities and unprecedented specifications. Two of such protein polymers that may be called twins, because they have an almost identical primary sequence of amino acids (see Chapter 6), have been produced. Both molecules were separately expressed in yeast. The twins have a modular $CS^X S^X C$ structure. The C block has a collagen-like amino acid sequence and carries few charges. This block is water-soluble at all pH values used. The central motive SX has a number of silk-like repeats separated by a chargeable amino acid X. These groups differ for the twins. The histidine bearing one is referred to with $X = H$, whereas the glutamic acid bearing one has a name with $X = E$. If this group is charged, i.e. around neutral pH, the S block has no secondary structure and is water soluble (see Figure 9.1). However, in the absence of the charge, folding takes place and β -rolls or in some cases β -sheets form through intra-molecular H-bonding. These secondary structure elements have hydrophobic faces and the molecules further assemble into ribbon-like aggregates in a rather slow 'nucleation and growth' process that takes several hours (depending on protein concentration). Extensive investigations of these objects were recently reported.[8, 9] A key observation is that one dimension of the ribbon, namely the distance separating the two collagen-like blocks, is approximately 12 nm. Such a relatively long dimension is still compatible with the PO block of the Pluronic (see Figure 9.1). Hence these protein polymers are expected to be membrane-active in the sense that they are candidates to insert themselves in the Pluronic vesicle in the absence of charges in the S block.

For facile imaging of the protein, we fluorescently labeled the C blocks of the protein polymers. FITC dyes were exclusively attached to the lysine amino group through isothiocyanate coupling, and the labels do not interfere with the driving force for the self-assembly of the protein polymers. In Figure 9.2 results are shown wherein we added the labeled polymer $CS^E S^E C$ while preparing the vesicles. Upon pH triggering, remarkably monodisperse capsules form smoothly. Figure (9.2a-c) presents confocal images where a hydrophobic fluorescent label, Nile red, has also been introduced to highlight hydrophobic regions, and the location of

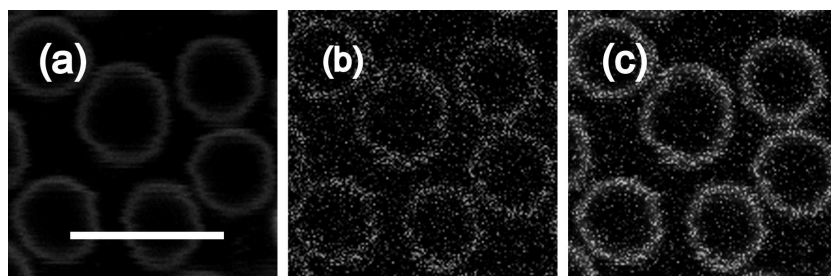


Figure 9.2: Confocal microscopic images: (a) vesicle membrane labeled with Nile red (b) CSESEC labeled with FITC; the inset only labeled with FITC with no addition of Nile red, scale bar: 5 μm . (c) overlapping of the first two images.

FITC labeled protein has been pointed. The overlay of the images shows that, on the resolution of the optical microscope, most of the protein polymers are at the same location as the Pluronic.

The fragile Pluronic vesicles can be extruded through a polycarbonate membrane which yields after the triggering step relatively monodisperse protein polymersome with controlled diameter down to 100 nm, Figure 9.7. Dynamic light scattering, shows that the size is kept constant for at least two weeks, Figure 9.3. There is a very small trend in the data that the average size increases and also the scattered light intensity grows slowly. This is consistent with a slow addition of more and more protein polymers to the capsules in the course of time. Interestingly, the Contin analysis shows that the vesicles become progressively more monodisperse in time.

We should not expect that the protein polymers are simply molecularly dissolved in the hydrophobic vesicle membrane phase. At this stage it is important to realize that all protein polymers are identical, meaning that they are chirally pure and monodisperse. This unique property gives these protein polymers the extraordinary strong capability to order themselves into inter-molecular aggregates. Such protein ordering is likely to continue to very large protein polymer to Pluronic ratios. SANS measurements confirms that the thickness of bilayer core significantly increases from 6 nm to 16 nm upon the addition of 2 mg/ml $\text{CS}^{\text{E}}\text{S}^{\text{E}}\text{C}$, which even becomes 20 nm with introducing of another 0.25 mg/ml $\text{CS}^{\text{H}}\text{S}^{\text{H}}\text{C}$, Figure 9.4. The changes in bilayer core thickness indicate that the silk-like domain is inserted into the Pluronic membrane while keeping the collagen-like domains in the aqueous phases. Indeed the build-up of these layers is kept responsible for

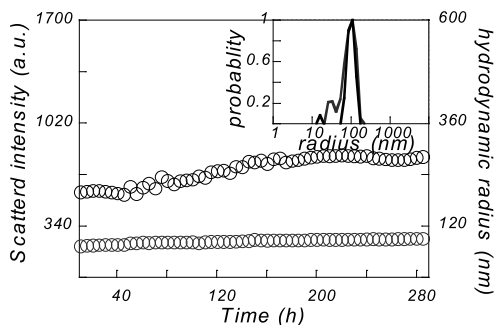


Figure 9.3: Stability study of 100 nm extruded vesicles by DLS (light circle) hydrodynamic radius of vesicles by cumulant fitting (dark circle) scattered intensity of the vesicles; the inset shows contin analysis results; For the inset, 24 hour after preparation (light curve) and 280 hour after preparation (dark curve).

the improved stability of the capsules.

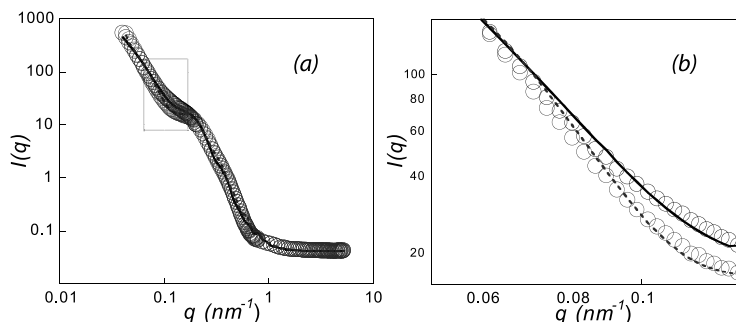


Figure 9.4: SANS measurements of 100 nm extruded vesicles with different proteins. (a) From top to bottom: 8 mg/ml L121 with 2 mg/ml $CS^E S^E C$ (dark grey), 2 mg/ml $CSESEC$ and 0.25 mg/ml $CS^H S^H C$ (light grey). (b) Magnified the marked area of Figure 9.4(a)

The time scale needed for protein polymers to be inserted into the vesicle membrane is apparently shorter than needed for protein self assembly into long rigid ribbons. The fast stabilization of Pluronic vesicles also indicates that the insertion is fast. The protein polymers adopt, through intra-molecular H-bonding, β -sheet or β -rolls secondary structures. Recent computer simulation studies of the silk-like repeats prove the extraordinary stability of these types of secondary structures.[8, 9] With FCS measurements, we quantitatively indentified the speed and the amount of protein polymer that participated in the vesicle membrane,

Figure 9.5. Pluronic vesicles are initially permeable for the protein polymer, and there is no protein detected on the vesicle membrane right after the sample preparation. However, roughly 40% of the total protein participates in the vesicle membrane within four hours, and this levels off at approximately 70% after seven hours of sample preparation.

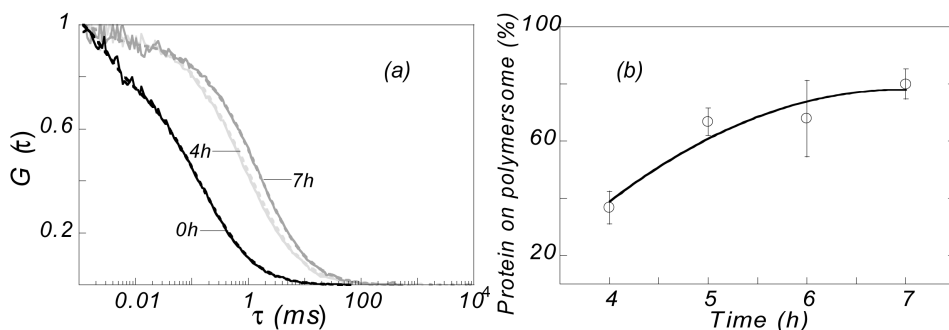


Figure 9.5: FCS measurements of 100 nm extruded vesicles with FITC labeled $CS^E S^E C$. (a) Autocorrelation curve measured at several moments after sample preparation. (b) Amount of protein on polymersome bilayer as a function of time, numbers were subtracted from two components model fitting and exponential solid curve was plotted to guide the eye.

9.3 Outlook

The new method to make stable capsules is versatile in the sense that we can incorporate various biologically active materials into the protein polymersome by a proper choice of the triggering methods. For instance, the positively charged protein polymer $CS^H S^H C$ polymer, Figure (9.6a-c), can be triggered by negatively charged polyelectrolytes, such as siRNA, Figure (9.6h-g), which then makes a stable biocompatible gene container. This opens up the interesting option that some biological active species can be made co-responsible for the stability of the capsules (possibly giving the capsules some cooperative release mechanism). This approach provide a wide possibility to assemble multifunctional biomolecules into stable nanostructures with desired size and shape. Moreover, the protein polymersome containing both $CS^E S^E C$ and $CS^H S^H C$ polymer is delivered in human cells, both protein species are taken up by the cytoplasm of the cell, Figure (9.6d-f). No significant cell death was observed under the experimental conditions. This

suggests that biomolecules incorporated in these vesicles can easily be transported *in vivo*. And siRNA is noticed to be able to create novel therapeutic approaches if it can be effectively applied *in vivo*. [8] It is in the progress of delivering our siRNA containing protein polymersome.

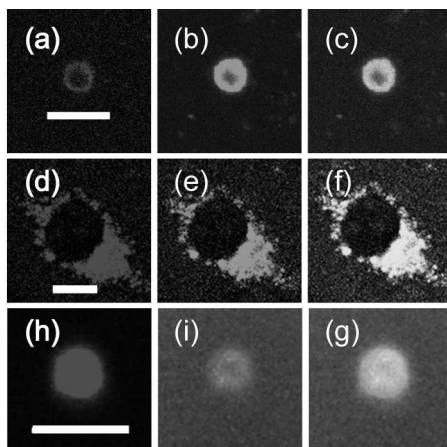


Figure 9.6: Co-assembly of protein polymersome and delivery in living cell (a-c) Pluronic and both negatively and positively charged triblock peptide block copolymer (a) $CS^H S^H C$ labeled with FluorTM647; scale bar: 5 μm . (b) $CS^E S^E C$ labeled with FITC (c) merge of the first two images. ($CS^H S^H C$ inside, $CS^E S^E C$ outside) (d-f) deliver of 100 nm extruded Pluronic with both $CS^H S^H C$ and $CS^E S^E C$ co-assembled vesicles in caco-2 cell. (d) color from FluorTM 647 labeled $CS^H S^H C$; scale bar: 10 μm . (e) color from FITC labeled $CS^E S^E C$ (f) merge of the image d and e. (h-g) co-assembly of Pluronic with $CS^H S^H C$ and siRNA (h) $CS^H S^H C$ labeled with FluorTM 647; scale bar: 2 μm (i) FITC labeled siRNA (g) merge of the image h and i.

Another remarkable feature of the protein polymer $CS^X S^X C$ is that it is designed and expressed in yeast. It means that extremely identical protein can be produced in large quantities, which is a significant improvement over synthetic polypeptides. In addition, other functional groups can be designed and incorporated into the protein polymer. For example, appropriate targeting sequences can be inserted in the C-block of the protein polymers which allows the capsules to deliver its contents in a very controlled way. Our TTA method provide a intelligent approach to incorporate multifunctional materials for drug delivery and gene delivery applications.

Appendix

Materials

Poly(ethyleneoxide)-b-poly(propyleneoxide)-b-poly(ethyleneoxide) (PEO₅-PPO₆₈-PEO₅) (Pluronic L121) was obtained as a kind gift from BASF Corp. Protein fluorescent labeling reagent, HiLyte FluorTM 647 is purchased from Thermo Scientific, and NHS-fluorescein is purchased from Molecular Probes. Nile red was purchased from Sigma. Labeled fluorescein labeled siRNA is obtained from Dharmacon. The synthesis of the triblock peptide copolymers (CS^{ESE}C / CS^{HSH}C, E and H stands for glutamate and histidine, respectively, with molecular weight of 65 kDa, and 49 chargeable amino acids per polymer) has been reported elsewhere.[9, 10] Details of the exact amino acid sequences are available in Chapter 6. Triblock peptide copolymer solutions, 1 mg/mL (15 μM, equal to 750 μM in chargeable amino acids units), were prepared in a 10 mM NaOH or HCl solution. 40 mg/ml Pluronic L121 were made with the above mentioned protein polymer solutions. Giant capsules were made without an extruder step. After freezing with liquid nitrogen, the temperature of the mixture was gently increased while stirring, once equilibrium conditions at room temperature was reached, the mixture was four times diluted in water. During this dilution step the trigger is implemented. For example in the case of the CS^{ESE}C containing mixtures, the pH was adjusted to be in the range pH = 2.4 - 3. Alternatively, for the CS^{HSH}C containing mixtures, the pH was adjusted to pH = 12 - 12.5. Slowly the vesicles matured and became progressively more stable. This can take up to tens of hours depends on the polymer concentrations applied. Smaller vesicles were made similarly as giant vesicles, however after thawing the vesicle solution is extruded through a filter. The extrusion membranes were purchased from Avanti Polar Lipids. Samples applied for DLS, TEM and SANS were extruded through a 100 nm carbohydrate membrane.

Confocal laser scanning microscopy (CLSM)

Confocal fluorescence images were recorded with an confocal laser scanning microscope (Zeiss LSM 5 EXCITER). Those protein polymersomes labeled with a hydrophobic probe, Nile red, was excited with the wavelength of 543 nm and collected with a long band pass of 630 nm. To identify the location of the triblock

peptide copolymers, $CS^{E}S^{E}C$ and $CS^{H}S^{H}C$ were labeled with NHS-fluorescein and FluorTM 647, respectively, and purified according to the protocol. One fifth of them are added to the indicated solution as fluorescent probes. The free amine groups on the peptide copolymers allow facile attachment of fluorescent dyes through isothiocyanate coupling to the triblock peptide copolymers, and they were found to have same properties as those unlabeled ones. FluorTM 647 labeled $CS^{E}S^{E}C$ was excited with the wavelength of 633 nm and collected with a long band pass of 650 nm. NHS-fluorescein labeled $CS^{H}S^{H}C$ was excited with the wavelength of 488 nm and collected with a band pass of 505-530 nm. We have added 2 μ M of the anti bleaching reagent dabaco was in both cases. Samples were equilibrated at least two hours at room temperature before measurements. The CLSM measurements for cells containing FITC labeled $CS^{E}S^{E}C$ and FluorTM 647 $CS^{H}S^{H}C$ polymersomes were performed directly in a 8 well chamber after proper incubation.

Dynamic light scattering

DLS was carried out on an ALV/ DLS-5000 light-scattering apparatus (ALV, Langen, Germany), equipped with an argon ion laser (LEXEL, Palo Alto, CA) operating at a wavelength of 514.5 nm. All experiments were performed at a scattering angle of 90°. Temperature was set to 20 °C, and it was controlled by using a Haake C35 thermostat. The hydrodynamic radius was calculated from cumulant fits or a CONTIN multi-exponential fit.

Small Angle Neutron Scattering (SANS)

Small angle neutron scattering experiments were performed at the Institut Max von Laue-Paul Langevin (ILL), Grenoble, France, on the D11 instrument. Three sample-to-detector distances were chosen to cover a wide q -range of 0.019-5.220 nm^{-1} , with an incident wavelength of 0.6 nm and a wave-vector resolution $\Delta q/q$ of 10%. Samples were contained in quartz cuvettes with a neutron pathway of 1 mm, placed in a thermostated sample-holder at 20 °C with a precision of 0.1 °C. Data were accumulated on a two dimensional detector with an active counting area of 100 x 100 cm^2 with a pixel size of 0.75 x 0.75 cm^2 . Scattering patterns were isotropic and subsequently radial-averaged. The spectra were treated according to standard ILL procedures, and the scattering cross-sections are expressed

in cm^{-1} . Normalisation was achieved by measuring H_2O as secondary calibration standard. The SANS data are modeled using the SASfit software written by Joachim Kohlbrecher, which is available from ETH.[11] The mathematical background for the fitting is also described at this website. The sample used for SANS measurement contains 8 mg/ml Pluronic L121 and 1 to 2 mg/ml peptide block copolymers to increase the scattering contrast for the peptides.

Fluorescence correlation spectroscopy

The solutions containing $\text{CS}^E\text{S}^E\text{C}$ polymersomes were deposited on a 8 well chamber, and then studied directly using a confocal laser scanning microscope (Zeiss LSM 510 Meta) to obtain FCS data. The laser beam was focused on a 40X water immersion objective and the sensitivity of detectors and filters were adjusted accordingly in order to obtain maximum signal to noise ratio.

Cryo-Transmission Electron Microscopy (cryo-TEM)

A few microliters of sample were placed on a holey carbon film supported on a TEM grid. A filter paper was then used to blot the drop so as to create a thin film. This sample was cryo-fixed by rapidly immersing into liquid ethane cooled to -170 to -180 °C. The specimen was inserted into a cryo-transfer holder and then transferred to a JEOL JEM 2100 TEM. Examinations were carried out at temperatures around -170 °C. The TEM was operated at an acceleration voltage of 200 kV. Zero-loss filtered images were taken under low dose conditions (1000 - 2000 nm^2).

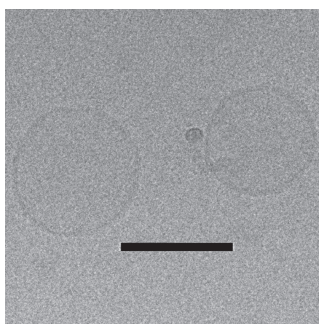


Figure 9.7: *cryo-TEM image of 100 nm extruded vesicles, scale bar 100 nm.*

Bibliography

- [1] D.E. Discher, A. Eisenberg, *Science* **2002**, *297*, 967-973.
- [2] E. Holowka, V.Z. Sun, D.T. Kamei, T.J. Deming, *Nature Materials* **2007**, *6*, 52-57.
- [3] K. Schillen, K. Bryske, Y.S. Melnikova, *Macromolecules* **1999**, *32*, 6885-688.
- [4] J. Jansso, K. Schillen, M. Nilsson, O. Soderman, G. Fritz, A. Bergmann, O. Glatter, *J. Phys. Chem. B* **2005**, *109*, 7073-7083.
- [5] E.G. Bellomo, M.D. Wyrsta, L. Pakstis, D.J. Pochan, T.J. Deming, *Nature Materials* **2004**, *3*, 244-248.
- [6] J. Rodriguez-Hernandez, S. Lecommandoux, *J. Am. Chem. Soc.* **2005**, *127*, 2026-2027.
- [7] M.C. Aragons, H. Engelkamp, V.I. Claessen, N.A.J.M. Sommerdijk, A.E. Rowan, P.C.M. Christianen, J.C. Maan, B.J.M. Verduin, J.J.L.M. Cornelissen, R.J.M. Nolte, *Nature Nanotechnology* **2007**, *2*, 635-639.
- [8] E. Iorns, C.J. Lord, N. Turner, A. Ashworth, *Nat. Rev. Drug Discov* **2007**, *6*, 556.
- [9] A.A. Martens, M. Neeleman, M.W.T. Werten, G. Eggink, M.A. Cohen Stuart, F.A. de Wolf, *Macromolecules*, **2009**, *42*, 1002-100.
- [10] Y. Yun, A.A. Martens, N.A.M. Besseling, F.A. de Wolf, A. de Keizer, M. Drechsler, M.A. Cohen Stuart, *Angew. Chem. Int. Ed.* **2008**, *47*, 4192-4195.
- [11] <http://kur.web.psi.ch/sans1/SANSSoft/sasfit.html>

Chapter 10

Mobility of fluorescently labeled polymer micelles in living cells

Pluronic P85 (PEO₂₆-PPO₄₀-PEO₂₆) micelles were stabilized by an interpenetrating polymer network (IPN) that formed by the crosslinking action of pentaerythritol tetraacrylate (PETA). The hydrophobic fluorescent molecule, hostasol methacrylate (HMA) is covalently incorporated into this IPN. AFM, fluorescence correlation spectroscopy (FCS) and steady-state fluorescence spectroscopy are used to characterize the micelles. The fluorescently labeled P85 micelles are photostable and are easily internalized in human (HeLa) cells. The diffusion property of the micelles in cytoplasm of human cells is studied by FCS which proves the stability of the micelle and gives information on the local viscosity.

In slightly modified form submitted as: F. Li, A.H. Westphal, M.A. Cohen Stuart, E.J.R. Sudhölter, A.T.M. Marcelis, F.A.M. Leermakers. **2009**

10.1 Introduction

Polymeric micelles are a major class of nanoscopic carriers, being studied for drug solubilization, controlled drug release, and drug targeting in pharmaceutical research.[1-4] In addition to these polymer-drug conjugates, recent experiments have been carried out on polymeric micelles that carry biomolecules, like, DNA, proteins and some magnetic resonance imaging (MRI) active agents.[5-8] At this stage, much is known about the physical properties of polymeric micelles that are the key for drug delivery. In this respect Pluronic block copolymers are truly the prototype polymeric micelles. They are neutral and non-toxic and have been shown to provide exciting opportunities for gene therapy.[9] The self-assembling properties of these polymers are remarkably temperature sensitive. For instance, the CMC of Pluronic P85 decreases sharply upon a small increase of the temperature (CMT is only slightly below room temperature). Often, the small temperature window for thermodynamically stable micellisation, significantly reduces the Pluronic micelle delivery efficiency in practical situations.

In this work, we described an application of Pluronic P85 micelles that are stabilized with a permanent interpenetrating polymer network (IPN) and co-reacted with a small fraction of a hydrophobic fluorescent probes. The synthesis of the IPN and various properties of these micelles, were described before.[10, 11] The IPN stabilized fluorescent P85 micelles remain stable for several months at room temperature and are readily internalized in human cells. Little is known about the fate of such micelles in these complex environments. Understanding, e.g., the subcellular distribution and how this can be influenced is essential for potential applications. One of such applications is the targeted delivery of hydrophobic objects that can be incorporated into the IPN stabilized P85 micelles, similarly as the fluorescent probes in the current study.

Few studies on fluorescently labeled micelles were performed inside cells. An example of the cellular uptake of fluorescent labeled PCL-PEO micelles, studied by confocal microscopy was reported in reference.[12] The fluorescence from the micelles was detected in the cytoplasm, but the limited intrinsic resolution of the optical microscopy prevented a more detailed analysis, nor did it reveal potential interactions with molecular complexes or organelles, that occur on the scale of nanometers.[13] To access the information for this type of phenomena one has to turn to, e.g., fluorescence correlation spectroscopy (FCS), and for this reason FCS

has become a popular tool for studies in living cells.[14, 15]

At this stage it is important to realize that the stabilized P85 micelles keep largely in tact in living cells. This is thought to result from the presence of the IPN. This unique property allows us to study their mobility in the cytoplasm. To the best of our knowledge, this is first time that FCS measurements are performed on polymeric micelles inside living cells. FCS studies have been performed on particles on the nanometer scale, such as quantum dots or micrometer-sized gold beads.[16, 17] With respect to these solid (hard) colloids, the polymeric micelles (soft colloids) applied here provide high loading efficiencies for hydrophobic objects (drug) and offer increased flexibility in terms of sample preparation and applicability (use of other fluorescent probes or biomolecules). Our labeled Pluronic micelle can be used as a model to probe the behavior of (soft) nano-materials in vivo. Furthermore, Pluronic allow for further functionalisation through post-chemical modification on their end groups.[18] This makes it possible to study the interactions between specifically designed nanoparticles and small organelles inside cells.

10.1.1 Materials

Poly(ethyleneoxide)-*b*-poly(propyleneoxide)-*b*-poly(ethyleneoxide) triblock copolymer (PEO₂₆-PPO₄₀-PEO₂₆) (Pluronic P85) was obtained from BASF Corp. Pentaerythritol tetraacrylate (PETA) was purchased from Sigma. The thermal initiator 2,2'-azobis(4-methoxy-2,4-dimethyl valeronitrile) (V-70) was obtained from Wako. The yellow-green fluorescent dye, hostasol methacrylate (HMA), was synthesized from chloronaphthalic anhydride according to US patent 2004/0016370.

10.1.2 Preparation of PEO₂₆-PPO₄₀-PEO₂₆ micelles

The stabilization of Pluronic P85 micelles with PETA was described previously.[10, 11] In short, an aqueous solution of a mixture containing 1 wt% Pluronic P85, 0.0025 wt% HMA and 0.04 wt% PETA was used. For thermal-polymerization of the network, 5 μ l of a stock solution of thermal radical initiator (V-70; 0.6 mg/ml) in ethanol, was added to 1 ml of freshly prepared micelle solution, and the mixture was incubated at 60 °C for 40 min to produce micelles stabilized by thermally induced polymerization of PETA. HMA was then covalently cross linked in the IPN, and as a result P85 micelles was fluorescently labeled by HMA. After thermal-

polymerization at 60 °C and extensive dialysis with a 12.4 kDa membrane against water at room temperature, the remaining solution that contains the stabilized Pluronic P85 micelles, was used for all the measurement.

10.1.3 Steady state and time-resolved fluorescence spectroscopy

Steady state and time-resolved emission measurements were done using FLS 920 spectrophotometer (Edinburgh Instruments, U.K.) fitted with a cooled MCP PMT detector (Hamamatsu, R3809U-50). For the steady state measurements the samples were excited with a pulsed xenon lamp. For the time resolved measurements the samples were excited ($\lambda_{exc} = 372$ nm) with a pulsed diode laser (LDH-PC- 375; PicoQuant GmbH, Germany; fwhm = 39 ps), controlled by a pulse controller (PDL 800-B; Pico-Quant GmbH, Germany). The instrument response function (fwhm of IRF = 87 ps) was determined, calibrated from scattering experiments using colloidal silica Ludox (Sigma-Aldrich). The decay curves were analyzed using "Fast" software (Edinburgh Instruments, U.K.).

10.1.4 Fluorescence correlation spectroscopy

The solutions with stabilized P85 micelles containing HMA as a fluorescent probe were diluted 30 times and then deposited on a 8 well chamber, and then studied directly using a confocal laser scanning microscope (Zeiss LSM 510 Meta) to obtain laser scanning microscopes or FCS data. The laser beam was focused on a 40X water immersion objective and the sensitivity of detectors and filters were adjusted accordingly in order to obtain maximum signal to noise ratio. The FCS measurements for cells containing HMA-labeled P85 micelles were performed directly in a 8 well chamber after proper incubation.

10.1.5 Atomic force microscopy

Tapping mode atomic force microscopy (AFM) experiments were carried out on a MFP-3D atomic force microscope from Asylum Research (Santa Barbara, CA). Height imaging was done in AC mode in air using OMCL-AC240 silicon cantilevers (Olympus Corporation, Japan). One drop of the micellar solution was deposited on a freshly cleaved mica surface at room temperature and dried overnight before measurements.

10.1.6 Incubation of cells with the stabilized micelles

HeLa cells were cultured in DMEM supplemented with 10 % FCS, L-glutamine (1 mM) and gentamycine (5 $\mu\text{g}/\text{ml}$). Media and supplements were obtained from Invitrogen (The Netherlands). Cells were seeded in a 8-well chamber (thermal fisher, The Netherlands). After adding cell culture medium cells were incubated for 24 h at 37 °C in a humidified atmosphere with 5 % CO_2 . Then, 13 μl of the stabilized P85 micelles were added to the HeLa cells in 400 μl of growth medium for CLSM image. Once a proper CLSM image was obtained, the same sample was measured directly for FCS studies. The cells were subsequently incubated for half hour before measurements.

10.2 Results and Discussion

Pluronic P85, containing PETA, was thoroughly mixed with the hydrophobic fluorescent probe HMA at 60 °C, at which temperature, most of the Pluronics has assembled in micelles (CMC is so low that it is not detectable) and the HMA molecules were incorporated inside the micellar core. Subsequently, the micelles were stabilized by IPN formation using the thermally-induced free radical polymerization method mentioned above. HMA is a methacrylate-based probe with green fluorescence, which is covalently taken up into the PETA network upon polymerization. Subsequent dialysis and centrifugation at room temperature removed some free Pluronic polymers and still mobile HMA molecules that were not associated to the Pluronic micelles. As expected, the remaining micellare solution shows green fluorescence due to the presence HMA in the core of the micelles. Figure 10.1 shows the emission map of HMA labeled Pluronic micelles. The maximum excitation at wavelength of 470 nm corresponds to the maximum emission wavelength of 525 nm. When excited at wavelengths higher than 470 nm, the fluorescence emission intensity decreased (data not shown).

The corona of a Pluronic micelle protects the hydrophobic HMA probes from precipitation in aqueous solution. Interestingly, due to the presence of a homogeneous densely cross-linked PETA network, the micelle remain stable at room temperature for months. Furthermore, it was found that the labels have a long fluorescence life time. An example of the fluorescence decay is shown in Figure 10.2. Data analysis shows that there is a bi-exponential decay with time constants

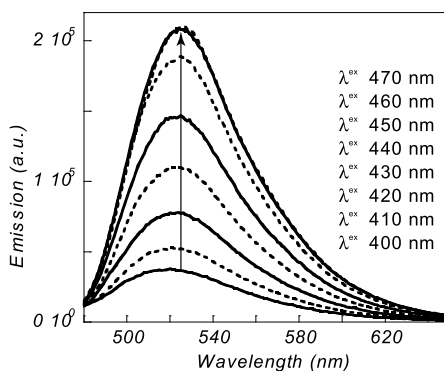


Figure 10.1: Fluorescence emission spectra of HMA labeled core cross-linked Pluronic P85 micelles, with emission wavelength gradually increased from 400 nm to 470 nm with steps of 10 nm, as indicated.

$\tau_1 = 2.379$ ns (6.5 %) and $\tau_2 = 7.995$ ns (93.5 %). These numbers are comparable to previous studies on silicon quantum dots.[19] Quantum dots are considered as photostable fluorescent nano particles and particularly interesting in bioimaging purpose.

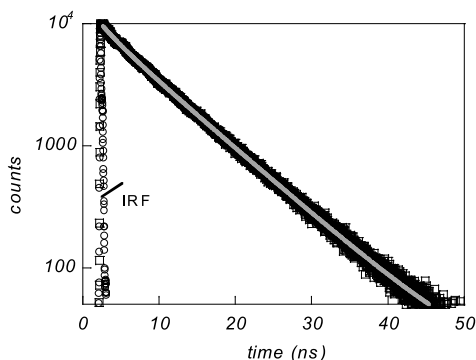


Figure 10.2: Fluorescence decay measurements of HMA labeled core cross linked Pluronic P85 micelle (\square) sample in aqueous solution. (\circ) IRF, instrument response function. The solid lines are fitted by bi-exponential decay. Data collected with excitation wavelength 444 nm and emission wavelength 525 nm.

To prove that the Pluronic micelles are correctly stabilized by IPN and have the proper size to be taken up by living cell, AFM and FCS experiments were performed. AFM images of stabilized micelles that simply have been deposit onto mica and subsequently dried, is shown in Figure 10.3. It is important to realize

that in the absence of a IPN, it is impossible to find with a similar drying procedure discrete objects in these samples. The fact that we do see small objects is thus the prove that the stabilization by the IPN has been achieved. In Figure 10.3a we show a relatively low magnifications so that it can be seen that the particles are relatively monodisperse and colloidal stable. With higher magnification, it is possible to estimate the size of these particles, Figure 10.3b. We should take note of the fact that due to the drying the average micelle radius, approximately found to be 30 nm, is slightly larger than the corresponding size obtained by dynamic light scattering or FCS measurements in solution. This is consistent with previous studies.[10, 11] From this it is reasonable to anticipate that the IPN has a major impact on the permanent integrity of the micelles and that this also contributes to the micelle stability and HMA solubility in aqueous solution.

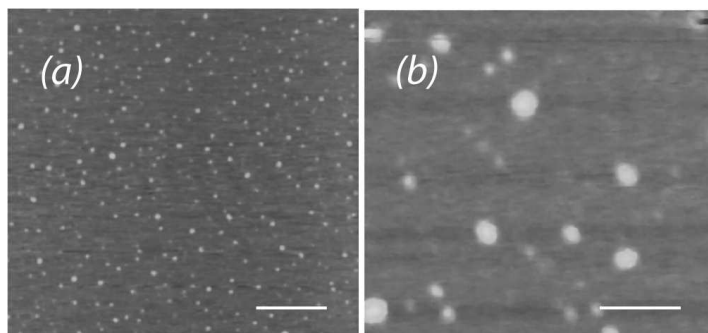


Figure 10.3: AFM image of HMA labeled core cross linked Pluronic P85 micelle, (a) scale bar 1 μm (b) 200 nm.

The combination of fluorescence spectra, and AFM data confirm that the stabilized Pluronic micelles indeed have HMA labels internalized. They retain their size in the dry state as well as in aqueous solutions. It is reasonable to assume that these micelles can be taken up by cells. Here we may draw attention to the fact that the micelles have a poly ethylene glycol (PEG) corona. The PEG brush is known to have low affinity to biological materials such as proteins. For this reason, PEG brushes provide colloidal systems with so-called stealth properties.[20] At the same time the PEG corona are held together by the presence of IPN in the micellar core. Interestingly, our micelles have a relatively narrow fluorescence emission band and a high photo-stability. All these properties make them ideal model systems to study the internalisation and subsequent mobility of

nano-particles inside living cells.

To test the cellular uptake and subcellular distribution of our labeled Pluronic micelles, HeLa cells were used. Figure 10.4a proves that within a few hours of incubation, the micelles are efficiently taken up by HeLa cells and accumulated into the cytoplasm of the cells. As a comparison, the image of cells with no addition of fluorescent P85 micelles is shown in Figure 10.4b, where the green fluorescence is hardly detectable. This confirms that the significant fluorescence in the cytoplasm of the cell indeed comes from the labeled Pluronic micelle. We also noticed that no significant cell death was observed under the experimental conditions. This suggests that drugs or biomolecules that are encapsulated in such micelles can be delivered efficiently *in vivo*.

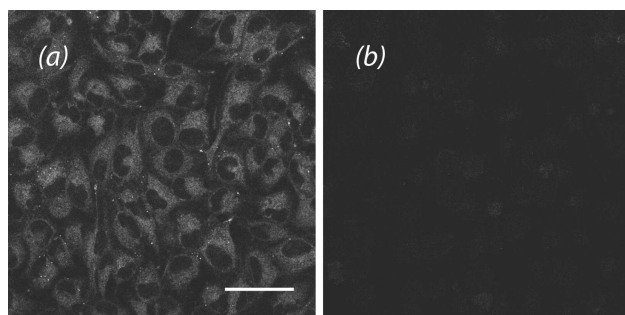


Figure 10.4: Uptake of HMA labeled core cross linked Pluronic P85 micelle by HeLa cells after few hours incubation with (a) 0.03 % fluorescent P85 micelle (b) 0 % fluorescent P85 micelle, scale bar 20 μm .

To have deep understanding of the behaviors of our micelles in living cells, we performed FCS studies in HeLa cell. By extracting information from FCS, we can access to micelle diffusion processes on a molecular scale. FCS studies also confirmed that the micelle has a proper size that is ideal for *in vivo* delivery applications.[21, 22] According to appropriate data reduction procedures,[23, 24] the hydrodynamic radius of the stabilized Pluronic micelles was deduced from the FCS autocorrelation curve to be approximately 9 nm in average (corresponding to a diffusion time of 0.604 ms), Figure 10.5. This micellar size correlates extremely well with dynamic light scattering results for Pluronic P85 micelle, which indicates that the size of P85 micelles does not change very much upon the encapsulation of the IPN loaded with HMA. The fluorescence intensity spectrum of the labeled Pluronic micelles is reasonably homogeneously distributed (data not shown). This

indicates that the micelles are stable within the nanometer range and that no larger clusters of micelles or aggregates are detected in the solution.

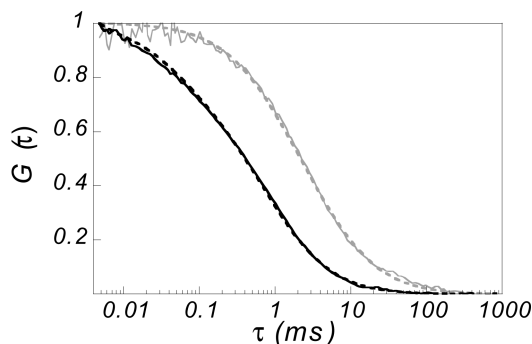


Figure 10.5: Normalized fluorescent correlation spectrum autocorrelation curve of HMA labeled core cross linked Pluronic P85 micelle in aqueous solution (black lines) and in living cell (gray curve); solid lines are from experimental data and dashed lines are from their theoretical fittings.

When the micelles are internalized in living cells. Due to the difference in viscosity between cytoplasm and the extracellular media, Pluronic micelles gave a quite different diffusion time, 5.17 ms, within the complex mixture of proteins and other small organelles in the cytoplasm, Figure 10.5. The number is approximately an order of magnitude higher than the one in aqueous solution. Therefore, based on current experiment, we can subtract information like the viscoelastic behaviour of the cytoplasm and crowdedness of the intracellular fluid. With further modification of Pluronic, binding property of the modified Pluronic micelles and organelles inside living cells can be carried out. Studies on targeted Pluronic micelle drug delivery are under investment. Binding and co-diffusion of these micelles to their acceptors are being studied with FCS.

In summary, the IPN stabilized Pluronic micelle is potentially useful for molecular imaging, biological assays, as biomarker, for cell-labeling and drug delivery.

10.3 Conclusions

Pluronic micelles are stabilized by an interpenetrating network, which keeps them stable for months. Furthermore fluorescent molecules are covalently polymerized in the interpenetrating network, and these stabilized fluorescent micelles can be

easily taken up by HeLa cells and remain integrated in the cytoplasm. FCS study of these micelles in living cell indicates the diffusion property behave significantly different from those micelles dissolved in aqueous solution. Our Pluronic micelles can be used as a model system for delivery study or single molecule experiment in living cells.

Bibliography

- [1] R. Haag, *Angew. Chem. Int. Ed.* **2004**, *43*, 278-282
- [2] A. Klaiherd, C. Nagamani, S. Thayumanavan, *J. Am. Chem. Soc.* **2009**, *131*, 4830-4838
- [3] N. Nasongkla, X.T. Shuai, H. Ai, B.D. Weinberg, J. Pink, D.A. Boothman, J.M. Gao, *Angew. Chem. Int. Ed.* **2004**, *43*, 6323-6327
- [4] D. Kim, E.S. Lee, K.T. Oh, Z.G. Gao, Y.H. Bae, *Small*, **2008**, *4*, 2043-2050
- [5] S. Takae, K. Miyata, M. Oba, T. Ishii, N. Nishiyama, K. Itaka, Y. Yamasaki, H. Koyama, K. Kataoka, *J. Am. Chem. Soc.* **2008**, *130*, 6001-6009
- [6] Y. Lee, T. Ishii, H. Cabral, H.J. Kim, J.H. Seo, N. Nisjiyama, H. Oshima, K. Osada, K. Kataoka, *Angew. Chem. Int. Ed.* **2009**, *48*, 1-5
- [7] N. Nasongkla, E. Bey, J. Ren, H. Ai, C. Khemtong, J.S. Guthi, S.F. Chin, A.D. Sherry, D.A. Boothman, J.M. Gao, *Nano Letters*, **2006**, *6*, 2427-2430
- [8] J.M. Jamjic, M. Srinivas, D.K. Kadayakkara, E.T. Ahrens, *J. Am. Chem. Soc.* **2008**, *130*, 2832-2841
- [9] E.V. Batrakova, S. Li, V.Y. Alakhov, D.W. Miller, A.V. Kabanov, *J. Pharmacol. Exp. Ther.* **2003**, *304*, 845-854
- [10] P. Petrov, M. Bozukov, C.B. Tsvetanov, *J. Mater. Chem.* **2005**, *15*, 1481-1486
- [11] P. Petrov, M. Bozukov, M. Burkhardt, S. Muthukrishnan, A.H.E. Muller, C.B. Tsvetanov, *J. Mater. Chem.* **2006**, *16*, 2192-2199.

- [12] R. Savic, L. Luo, A. Eisenberg, D. Maysinger, *Science* **2003**, *300*, 615 – 618.
- [13] K. Bacia, S.A. Kim, P. Schwille, *Nat. Methods* **2006**, *13*, 83-89
- [14] O. Stoevesandt, K. Köhler, R. Fischer, I.C.D. Johnston, R. Brock, *Nat. Methods* **2005**, *2*, 833-835
- [15] S.J. Briddon, R.J. Middleton, Y. Cordeaux, F.M. Flavin, J.A. Weinstein, M.W. George, B. Kellam, S.J. Hill, *Proc. Natl. Acad. Sci. USA* **2004**, *101*, 4673–4678
- [16] D.R. Larson, W.R. Zipfei, R.M. Williams, S.W. Clark, M.P. Bruchez, F.W. Wise, W.W. Webb, *Science* **2003**, *300*, 1434-1436
- [17] G. Guigas, C. Kalla, M. Weiss, *Biophys. J.* **2007**, *93*, 316-323
- [18] J.P.A. Custers, P. Kelemen, L.J.P. van den Broek, M.A. Cohen Stuart, J.T.F. Keurentjes. *J. Am. Chem. Soc.* **2005**, *127*, 1594-1595
- [19] J. H. Warner, A. Hashino, K. Yamamoto, R.D.Tilley, *Angew. Chem. Int. Ed.* **2005**, *44*, 4550 –4554
- [20] R. Duncan, *Nature Reviews.* **2006**, *6*, 688-701
- [21] N. shiyama, *Nature Nanotechnology* **2007**, *2*, 203-204
- [22] W. Jiang, B.Y.S. Kim, J.T. Rutka, W.C.W. Chan, *Nature Nanotechnology* **2008**, *3*, 145-150
- [23] P. Rigler, W. Meier, *J. Am. Chem. Soc.* **2006**, *128*, 367-373
- [24] R. Rigler, A. Pramanik, P. Jonasson, G. Kratz, O.T. Jansson, P.Å. Nygren, S. Ståhl, K. Ekberg, B.L. Johansson, S. Uhlén, M. Uhlén, H. Jörnvall, J. Wahren, *Proc. Natl. Acad. Sci. USA* **1999**, *96*, 13318–13323

Chapter 11

Fluorescent micelle thermometer with a potential use in biological cells

Pluronic P85 (PEO₂₆-PPO₄₀-PEO₂₆) micelles were stabilized by an interpenetrating polymer network (IPN) that formed by the crosslinking action of pentaerythritol tetraacrylate (PETA). The hydrophobic fluorescent molecule, hostasol methacrylate (HMA) is covalently incorporated into this IPN. CLSM, fluorescence correlation spectroscopy (FCS) and steady-state fluorescence spectroscopy are used to characterize the micelles. The Pluronic micelles are rather temperature sensitive. The changes in hydrophobicity of the microenvironment of the micelle core results in a high thermosensitivity of the fluorescent hydrophobic probe. We foresee that it is possible to use these micelles as a biosensor to measure temperature in living cells. To date we have shown that the micelles are easily incorporated in Hela cells and that the fluorescent properties can be investigated in a FCS setup. Work to calibrate the micellar thermometer in cells is in progress.

In slightly modified form submitted as: F. Li, M.A. Cohen Stuart, E.J.R. Sudhölter, A.T.M. Marcelis, F.A.M. Leermakers. **2009**

11.1 Introduction

Temperature is one of the most important parameter that determines physical and chemical processes in living cells. For instance, cell division, gene expression, and metabolism can induce cellular temperature change. A temperature change shifts the electrochemical equilibrium of ions,[1] and a temperature gradient generates directional motion of particles.[2] Therefore, measuring cellular temperature can contribute to the explanation of cellular thermophysiology, the development of novel diagnoses and the treatment of tumors.[3-6]

The temperature in cells, however, has been frequently treated as being constant or slowly changing. In fact, only a few experimental methods have been developed to measure temperature at the single-cell level, although it is theoretically possible to define local temperature down to the submicrometer level in water.[7] Very recently, a fluorescent nanogel, microinjected in living cells, was applied for the first time as thermometer for intracellular thermometry. Due to the sensitivity of the fluorescence to temperature changes, intracellular temperature was deduced.[8]

In this work, we describe an application of fluorescent micelles as a potential thermometer. These micelles are stabilized with a permanent interpenetrating polymer network (IPN) and co-reacted with a small fraction of a hydrophobic fluorescent probe. The synthesis of the IPN and various properties of these micelles, were described before.[9, 10] The IPN-stabilized fluorescent micelles remain stable for several months at room temperature and are readily internalized in cells.

The micelle forming block copolymer studied in this work is Pluronic P85. This polymer is neutral and non-toxic and have been shown to provide exciting opportunities for gene therapy.[11] The self-assembling properties of these polymers are known to be remarkably temperature sensitive. For instance, the CMC of Pluronic P85 sharply decreases upon a small increase of the temperature. The inclusion of hydrophobic probes in the micelle core, however, is expected to prevent the interaction between the fluorophore and virtually all cellular components, like the small organelles inside cells. As a result, the fluorescence of the micelle is argued to respond to the microenvironmental changes of the micelle core. Hence, the micelle can work as a sensitive intracellular thermometer. Furthermore, Pluronics allow for further functionalisation though post-chemical modification on their end groups.[12] This makes it possible to study for example the organelle-specific

thermometry within living cells.

11.1.1 Materials

Poly(ethyleneoxide)-poly(propyleneoxide)-poly(ethyleneoxide) block copolymer (PEO₂₆-PPO₄₀-PEO₂₆) (Pluronic P85) was obtained from BASF Corp. Pentaerythritol tetraacrylate (PETA) was purchased from Sigma. The thermal initiator 2,2'-azobis(4-methoxy-2,4-dimethyl valeronitrile) (V-70) was obtained from Wako. The yellow-green fluorescent dye, hostasol methacrylate (HMA), was synthesized from chloronaphthalic anhydride according to US patent 2004/0016370.

11.1.2 HMA labeled IPN stabilized PEO₂₆-PPO₄₀-PEO₂₆ micelles

The stabilization of Pluronic P85 micelles with PETA was described previously.[9-10] In short, an aqueous solution of a mixture containing 12 wt% Pluronic P85, 0.03 wt% HMA and 0.48 wt% PETA was used. For thermal-polymerization of the network, 5 μ l of a stock solution of thermal radical initiator (V-70; 0.6 mg/ml) in ethanol, was added to 1 ml of freshly prepared micelle solution, and the mixture was incubated at 60 °C for 40 min to produce micelles stabilized by thermally induced polymerization of PETA. HMA was also covalently cross linked in the IPN, and as a result P85 micelles were fluorescently labeled by HMA. After thermal polymerization at 60 °C and one hour centrifugation at 20000 rpm at room temperature, the remaining solution that contained the stabilized Pluronic P85 micelles, was used for all the measurement.

11.1.3 Steady state and time-resolved fluorescence spectroscopy

Steady state and time-resolved emission measurements were done using FLS 920 spectrophotometer (Edinburgh Instruments, U.K.) fitted with a cooled MCP PMT detector (Hamamatsu, R3809U-50). For the steady state measurements the samples were excited with a pulsed xenon lamp. For the time resolved measurements the samples were excited ($\lambda_{exc} = 372$ nm) with a pulsed diode laser (LDH-PC- 375; PicoQuant GmbH, Germany; fwhm = 39 ps), controlled by a pulse controller (PDL 800-B; Pico-Quant GmbH, Germany). The instrument response function (fwhm of IRF = 87 ps) was determined, calibrated from scattering experiments using colloidal silica Ludox (Sigma-Aldrich). The decay curves were analyzed using "Fast" software (Edinburgh Instruments, U.K.).

11.1.4 Fluorescence correlation spectroscopy

The solutions with stabilized P85 micelles containing HMA as a fluorescent probe were diluted 400 times and then deposited on a 8 well chamber, and then studied directly using a confocal laser scanning microscope (Zeiss LSM 510 Meta) to obtain laser scanning microscopes or fluorescence correlation spectroscopy (FCS) data. The laser beam was focused on a 40X water immersion objective and the sensitivity of detectors and filters was adjusted accordingly in order to obtain a maximum signal to noise ratio. The FCS measurements for cells containing HMA-labeled P85 micelles were performed directly in a 8 well chamber after proper incubation.

11.1.5 Confocal laser scanning microscopy

The solutions with stabilized micelles with HMA covalently incorporated as fluorescent probes were deposited on a glass surface, covered with a glass slide, and then visualized directly using a confocal laser scanning microscope (Zeiss LSM 510 Meta).

11.2 Results and Discussion

The configuration of the Pluronic fluorescent micelle is schematically shown in Figure 11.1. Pluronic P85, containing PETA, was thoroughly mixed with the hydrophobic fluorescent probe HMA at 60 °C, at which temperature most of the Pluronic has assembled in micelles (CMC is so low that it is not detectable) and the HMA and PETA molecules are incorporated inside the micellar core. Subsequently, IPN formation was induced by free radical polymerization. HMA is a methacrylate-based probe with green fluorescence, which is covalently taken up into the PETA network upon polymerization. Subsequent centrifugation at room temperature removed insoluble PETA and still mobile HMA molecules that were not associated to the Pluronic micelles. The fluorescent probe is hydrophobic, and hardly dissolves in water. It is only soluble in the hydrophobic core of the micelle, similar to the IPN former, PETA. After purification, the remaining micelle solution shows green fluorescence due to the presence of HMA that is covalently linked in the IPN in the core of the micelles. One very well known feature of the Pluronic micelles is that they are very sensitive to temperature

change. In the absence of the IPN stable micelles are found above the CMT (critical micellisation temperature) and below the CPT (cloud point temperature). More specifically, P85 has a convenient micellisation window extending from well below room temperature (CMT < room temperature) to well-above body temperatures (CPT > body temperature). In the presence of IPN the micellisation performance is changed, however the CPT is expected to remain relevant. The sharp increase in hydrophobicity of the micelle core upon heating results in a high sensitivity towards small temperature changes around ambient conditions. This is consequently expressed in changes in fluorescent intensity.

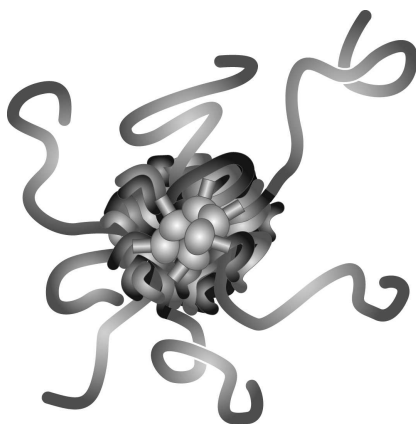


Figure 11.1: *Schematic drawing of core cross linked Pluronic micelles loaded with green fluorescent probes. The dark lines represent the poly-propylene oxide block and the poly-ethylene oxide ones. The light lines represent the interpenetrating polymer network and the molecules in the center are where HMA located. It is expected that the Pluronic polymers are not attached to the IPN, whereas the fluorescent probes are covalently linked to it.*

To investigate the temperature sensitivity, the emission spectrum of the sample was measured. Figure 11.2a shows the emission spectra of HMA labeled Pluronic micelles at different temperatures. Upon heating from 27 °C to 32 °C, the maximum emission intensity increase about eight times. In the same time, the maximum emission wavelength shifts from 535 nm to 518 nm, which implies that the hydrophobicity of the microenvironment for the fluorescent probe increases.[13] On a whole, this is a strong indication that the incorporated HMA does respond strongly to microenvironmental changes of the micelle core and thus the micelle can in principle be used as a nanometer sized thermometer.

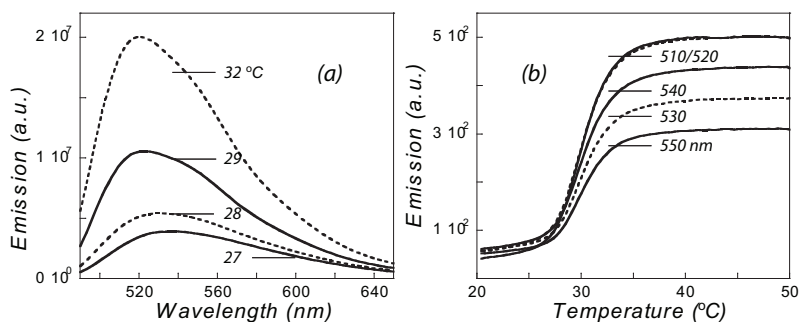


Figure 11.2: Fluorescent emission intensity of HMA labeled core cross-linked Pluronic P85 micelles as a function of temperature (a) emission spectra at different temperatures, temperature increases from bottom curve to the top one (b) emission change for different wavelengths as a function of temperature, emission wavelength decreases from bottom curve to the top one.

To further confirm the temperature sensitivity and to identify the transition temperature, a temperature scan was performed from 20 °C to 50 °C, as shown in Figure 11.2b. For all the measurements, an excitation wavelength of 470 nm was applied, and the temperature emission scan at several emission wavelengths between 510 nm and 550 nm was collected. Under these conditions, the highest fluorescence intensity always appeared around the 520 nm. Moreover, a sharp increase in fluorescence intensity was found for all emission wavelengths upon increasing the temperature. The temperature at which this sharp increase occurs is around 30 °C and is slightly affected by the sample concentration, the higher the polymer concentration, the lower the transition temperature. This closely relates to the fact that the microenvironmental polarity of polymeric micelle increases upon increasing temperature. This process is actually reversible, so upon cooling, the emission intensity goes down, and the procedure can be repeated many times (data not shown).

The corona of a Pluronic micelle protects the hydrophobic HMA probes from precipitation in aqueous solution. Interestingly, due to the presence of a homogeneous densely cross-linked PETA network, the micelle solution remains stable at room temperature for months. Furthermore, even upon dilution, the micelles remain intact and work efficiently as a nano-sized thermometer. The process occurs on the scale of nanometers. To investigate the properties of these labeled nanoparticles in a more quantitative way, we performed fluorescence correlation

spectroscopy (FCS) measurement on these particles. The technique is a popular tool for studies of dynamics or interactions in living cells in recent years.[14, 15] Samples were first diluted 400 times before the measurements. Very good auto-correlation curves were obtained as shown in Figure 11.3. This indicates that the micelles remain intact under such a dilution, 0.03% w/v, which is far below the CMC of P85 (4% w/v at 25 °C). Upon heating from 20 °C to 37 °C, the diffusion time of the micelles changed from 0.86 ms to 1.29 ms, which corresponds to a change of the hydrodynamic radius of the micelles from 13 nm to 20 nm. This is a strong indication that the micelles respond significantly to the temperature change. From this it is reasonable to assure that the IPN strongly contributes to the permanent integrity and stability of the micelles and the solubility of HMA in aqueous solution.

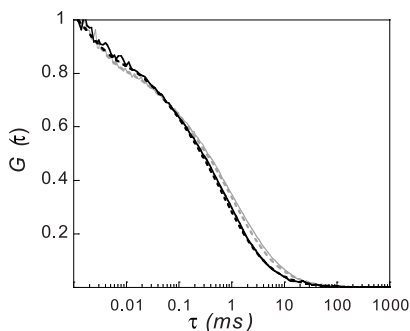


Figure 11.3: Normalized fluorescent correlation spectrum autocorrelation curve of HMA labeled core cross linked Pluronic P85 micelle in aqueous solution at 20 °C (blank lines) and at 37 °C (gray curve); solid lines are from experimental data and dashed lines are from their theoretical fittings.

The combination of fluorescence spectra and FCS data confirm that the stabilized Pluronic micelles indeed have HMA labels internalized, and that the fluorescence responds quickly to temperature changes. Interestingly, at elevated temperatures cylindrically shaped aggregates were observed, indicating the approach of the micellar solution towards its cloud point. This temperature effect can also be confirmed by CLSM, as shown in Figure 11.4. Images were obtained at two different temperatures. At room temperature, only a few cylindrically shaped aggregates were detected with confocal microscopy, as shown in Figures 11.4a and 11.4b. However, upon heating to 50 °C, the whole image was covered by cylindrical micelles as shown in Figures 11.4c and 11.4d. Clearly an aggre-

gate is formed by many primary IPN stabilized micelles. The formation of these aggregates highlights the micelle temperature sensitivity and the corresponding changes in fluorescence also indicates the hydrophobicity of the micelle core is strongly influenced by environmental temperature.

In the literature, cylindrical micelles, also known as filomicelles, were found persisted in the blood circulation up to one week after intravenous injection. This is about ten times longer than their spherical counterparts and is more persistent than any known synthetic nanoparticles.[16] the micellar particles used in this study consist of Pluronic P85 copolymers. P85 possess two hydrophilic chains of polyethyleneglycol (PEG), which are widely used to prolong circulation in vivo.[17-19] The PEG brush is known to have a low affinity to biological materials such as proteins. At the same time the PEG coronas of the present particles are held together by the IPN in the micellar core.

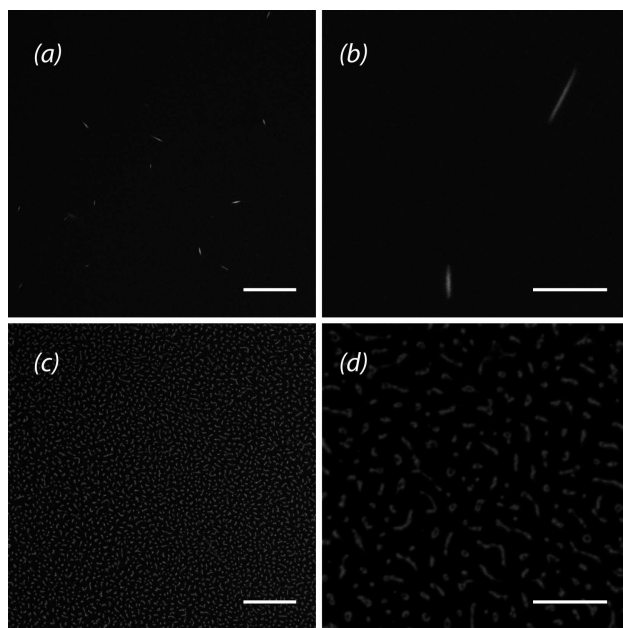


Figure 11.4: CLSM image of highly concentrated fluorescent micelle under temperature (a,b)20 °C (c,d)50 °C; (a) scale bar 20 μm (b) scale bar 5 μm (c) scale bar 20 μm (d) scale bar 5 μm. Note that the lateral resolution of of the CLSM is limited. In reality the cross-section dimension of the worm-like micelles as shown in panel d is much less this optical resolution.

Recently, it was shown that similar IPN stabilized micelles are efficiently taken

up by HeLa cells and accumulate in the cytoplasm of the cells without significant cell death.[20] It is therefore reasonable to assume that these internalized micelles can serve as an intracellular temperature sensor. At present we have only limited information that our micelles can indeed be used as such.

Recently, however, we have proven that the IPN stabilized micelles can be used as probes to measure the local viscosity in cells. Here the idea was that by using fluorescence correlations spectroscopy we can measure the diffusion time of the micelles in cells. The FCS measurements performed at various temperatures show that our micelles can be used under the proper conditions.

In short, HeLa cells were incubated with the temperature sensitive HMA-labeled micelles and their mobility within single HeLa cells was measured for different ambient temperatures. As seen before, due to the presence of a complex mixture of proteins and other small organelles in the cytoplasm, the effective viscosity is larger than that of water and the diffusion time of HMA-labeled micelles is significantly different from that in aqueous solution. The diffusion time is also influenced by the concentration and the size of the micelles. For example, the bigger the micelle, the higher value the diffusion time of micelles in living cell will be. This is confirmed by our measurements, as can be seen from Figure 11.5. From FCS and CLSM studies mentioned above, we learned that the micelle size grows with increasing temperature. The fitting of the autocorrelation curves of FCS routinely reveals multiple diffusion times. Typically two populations with different diffusion times were found. The objects with the shortest relaxation time dominate the spectrum, whereas a minority component was found to have a significantly longer relaxation time. In Figure 11.5 we collected the diffusion times of the micelles in living cell at 20 °C with 37 °C. It was found that the longest diffusion time increased from 5.17 ms to 25.88 ms. This is a remarkable difference and it is seen as a strong indication that our probe does notice the intracellular temperature change (as imposed by the environment).

We also noticed that the intensity of the fluorescent signal is temperature dependent. Before we can use this information, we need a proper calibration of the fluorescent intensity as a function of the temperature, similarly as in the reference solution discussed in Figure 11.2b. Once calibrated, the fluorescence intensity will be a reliable measure of the temperature inside the cells. Work is in progress to prove this.

In summary, the IPN stabilized Pluronic micelle is potentially useful for mea-

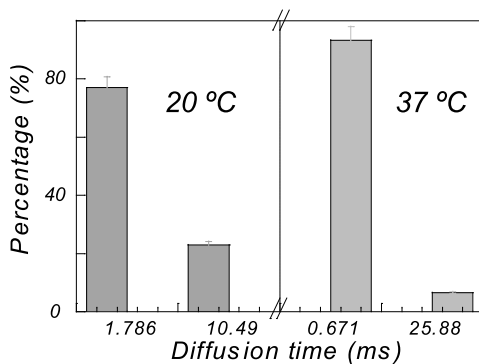


Figure 11.5: FCS measured diffusion time of HMA labeled core cross linked Pluronic P85 micelle in HeLa cell at 20 °C and 37 °C.

suring intracellular temperature and can be used as an indicator for cellular events that induces cellular temperature change.

11.3 Conclusions

Pluronic micelles are stabilized by an interpenetrating network, which keeps them stable for months. When fluorescent molecules are covalently polymerized in the interpenetrating network, the resulting nanoparticles can act as nanometer sized thermal sensors. Within a short temperature range, the emission of the nanoparticles changes dramatically and reversibly as a function of temperature. These stabilized fluorescent micelles can be easily taken up by HeLa cells, where they can be used as intracellular nanosized thermometers.

Bibliography

- [1] C.R. Cantor, P.R. Schimmel, **1980**. *Biophysical Chemistry Part III: The Behavior of Biological Macromolecules*, Freeman, San Francisco, CA.
- [2] S. Duhr, D. Braun, *Proc. Natl. Acad. Sci. U.S.A.* **2006**, *103*, 19678-19682.
- [3] H.F. Hamann, M.O. Boyle, Y.C. Martin, M. Rooks, H.K. Wickramasinghe, *Nature Mater.* **2006**, *5*, 383-387.
- [4] L.R. Hirsch, R.J. Stafford, J.A. Bankson, S.R. Sershen, B. Rivera, R.E. Price, J.D. Hazle, N.J. Halas, J.L. West, *Proc. Natl. Acad. Sci. U.S.A.* **2003**, *100*, 13549-13554.
- [5] N.W.S. Kam, M.O. Connell, J.A. Wisdom, H. Dai, *Proc. Natl. Acad. Sci. U.S.A.* **2005**, *102*, 11600-11605.
- [6] C. Plieth, U.P. Hansen, H. Knight, M.R. Knight, *Plant J.* **1999**, *18*, 491-497.
- [7] D. Kondepudi, I. Prigogine, **1998**. *Modern Thermodynamics*, Wiley, Chichester, West Sussex, UK.
- [8] C. Gota, K. Okabe, T. Funatsu, Y. Harada, S. Uchiyama, *J. Am. Chem. Soc.* **2009**, *131*, 2766-2767
- [9] P. Petrov, M. Bozukov, C.B. Tsvetanov, *J. Mater. Chem.* **2005**, *15*, 1481-1486
- [10] P. Petrov, M. Bozukov, M. Burkhardt, S. Muthukrishnan, A.H.E. Muller, C.B. Tsvetanov, *J. Mater. Chem.* **2006**, *16*, 2192-2199.
- [11] E.V. Batrakova, S. Li, V.Y. Alakhov, D.W. Miller, A.V. Kabanov, *J. Pharmacol. Exp. Ther.* **2003**, *304*, 845-854.

- [12] J.P.A. Custers.; P. Kelemen.; L.J.P. van den Broek, M.A. Cohen Stuart.; J.T.F. Keurentjes, *J. Am. Chem. Soc.* **2005**, *127*, 1594-1595.
- [13] S. Uchiyama, N. Kawai, A.P. de Silva, K. Iwai, *J. Am. Chem. Soc.* **2004**, *126*, 3033-3034
- [14] O. Stoevesandt, K. Köhler, R. Fischer, I.C.D. Johnston, R. Brock, *Nat. Methods* **2005**, *2*, 833-835
- [15] S.J. Briddon, R.J. Middleton, Y. Cordeaux, F.M. Flavin, J.A. Weinstein, M.W. George, B. Kellam, S.J. Hill, *Proc. Natl. Acad. Sci. USA* **2004**, *101*, 4673-4678
- [16] Y. Geng, P. Dalhaimer, S. Cai, R. Tsai, M. Tewari, T. Minko, D.S. Discher, *Nature Mater.* **2007**, *2*, 249-255.
- [17] A. Gabizon, H. Shmeeda, Y. Barenholz, *Clin. Pharmacol.* **2003**, *42*, 419.
- [18] A.L. Klibanov, K. Maruyama, V.P. Torchilin, L. Huang, *FEBS Lett.* **1990**, *268*, 235-237.
- [19] P. Photos, B.M. Discher, L. Bacakova, F.S. Bates, D.E. Discher, *J. Control Release.* **2003**, *90*, 323-334.
- [20] F. Li, A.T.M. Marcelis, F.A.M. Leermakers, M.A. Cohen Stuart, E.J.R. Sudhölter, *submitted* (Chapter 10)

Chapter 12

Summary and general discussion

Amphiphilic block copolymers can, in selective solvents such as water, assemble into various shapes and architectures. Among those, polymer vesicles, polymer micelles and polymer fibers are very popular structures in current nanotechnology. These objects each have their own particular properties and can serve as containers or templates for different nanotechnological applications. Polymer vesicles, for example, can encapsulate both hydrophobic and hydrophilic molecules, and are therefore considered as attractive candidates for drug delivery, nanoreactors and also microtemplates. Polymeric micelles are usually significantly smaller. Their hydrophobic cores are typically used to solubilize hydrophobic drugs or carry biomolecules. Polymer fibers by construction are long continuous entities. Because of this, they easily form gels at relatively low concentrations and may find functions as templates/substrates in biological applications. In some cases they can carry or conduct charges which may trigger their use in electronic devices.

In reality, many applications of these objects require stimuli-responsive properties, and very importantly for biomedical applications, the block copolymer building blocks need to have zero or very low toxicity and preferably biocompatibility. It is a big challenge to assemble functional molecules into stable nanostructures with desired size and shape.

To achieve these goals, (bio)functional polymers chains have to be internalized in the objects. For this purpose two distinct routes are proposed. One of them is self-assembly of functional block copolymers into a defined nanoparticle, which is a direct approach. In this case some preliminary work is required because the

(bio)functional groups have to be chemically incorporated in the block copolymer. Alternatively, more than one type of copolymer can be co-assembled into large objects with fixed stoichiometry, each with their own functionalities. In these co-assembled objects, we combine functionalities of its constituents in a controlled way.

Both approaches are applied in this dissertation and results from both routes are promising. Pluronic polymers are an interesting class of materials that in water self-assemble in association colloids of various sizes and shapes. These polymers are highly temperature sensitive. One member of the Pluronics family forms unilamellar vesicles, namely L121, but these vesicles are extremely hard to work with. This is because they are extremely fragile and thermally unstable. Much work that is reported in this dissertation has resulted from attempts to improve the stability of L121 vesicles. It was found that these vesicles now can also act as a template for the assembly of stimuli-responsive polypeptide block copolymers. These co-assembled vesicles can serve as multifunctional containers for transport of several biomolecules *in vivo*. The assembly rules apply to several other systems as well. This dissertation is divided into three parts, and a short overview for each part is given below.

Part 1: Self assembly

In Chapter 2 it is described how Pluronic L121 vesicles can be stabilized by means of a polymerized network of pentaerythritol tetraacrylate (PETA). The permanent interpenetrating network allows the Pluronic L121 copolymers to reversibly associate with the vesicles. The size of the vesicles can easily be varied from at least 100 nm to 1 μm , depending on the pore size of the extrusion membrane. The stabilized vesicles can retain their sizes for more than one month at room temperature.

In Chapter 3 it was shown that such Pluronic L121 vesicles, stabilized by means of a network of polymerized PETA can become negatively charged upon mixing with polyacrylic acid (PAA). This can be used to immobilize these vesicles onto glass as well as onto mica surfaces in combination with Mg^{2+} ions that are used as bridge between the two negatively charged components, polyelectrolyte and the surface. This permits relatively easy observations with CLSM. It was found that the vesicles can change their shape to tubular vesicles upon addition of another

micelle-forming Pluronic block copolymer. The latter shape transition also occurs for corresponding conditions in the bulk.

Part 2: Co-assembly

In Chapter 4 is described how small unilamellar vesicles spontaneously form in simple mixtures of a lamellae-forming block copolymer $PB_{10}PE_{10}$ and a micelle-forming block copolymer $PB_{10}PE_{18}$. The co-assembled vesicles are rather monodisperse with a core radius down to 30 nm. Furthermore, it was found that under these conditions the polymersomes coexist with mixed spherical micelles. The polydispersity of the vesicles as well as their sizes are well controlled both by the mixing ratio of the components as by the polymer concentrations used.

In Chapter 5, a molecularly detailed self-consistent field theory is used to study the assembly characteristics of binary polymer mixtures in a selective solvent. We mimic the binary mixture of the lamellae-forming copolymer $PB_{10}PE_{10}$ mixed with the micelle-forming $PB_{10}PE_{18}$ species. It is possible to arrive at a mixing ratio where small unilamellar vesicles coexist with many spherical micelles. We argue that the vesicle size can be tuned by the copolymer mixing ratio. For still modest PE_{18}/PE_{10} ratios, one enters a regime where the micelles are the dominant species and these micelles buffer the chemical potential of the copolymers in the system. In such a situation one can store more PE_{18} chains in smaller vesicles than in larger ones. Hence, upon an increase of the amount of $PB_{10}PE_{18}$ in the system, the vesicles evolves towards small sizes. In addition the SCF model explains many other salient properties of these systems. Hence, the SCF analysis gives strong support for the expectation that in binary polymer mixtures it is possible to have thermodynamically stable small unilamellar vesicles.

In Chapter 6, a new type of co-assembled, highly-ordered conjugated nanotape, made from either positively or negatively charged triblock peptide copolymers, and a conjugated zwitterionic polythiophene derivative (PTT) is described. The interaction of these compounds results in a change of the conformation and the electronic structure of the polythiophene. Morphological studies show that the co-assembled nanotapes are longer at a higher concentration and a higher PTT/triblock peptide copolymer ratio.

In Chapter 7, a similar species was prepared from this conjugated zwitterionic polythiophene (PTT) derivative and a low molecular weight gelator. The inter-

action of these compounds results in complex assemblies with very large aspect ratios, wherein the polythiophenes molecules are in an extended, planar conformation. Morphologic studies have shown that the co-assembled nanowires adopt a helical structure that forms well-defined nanowires with lengths up to several μm long. These nanowires can be rather simply and reversibly manipulated by external stimuli, such as pH.

Part 3: Applications

In an attempt to further improve the working window of L121 vesicles, in Chapter 8, Pluronic L121 vesicles were stabilized by both PETA and Pluronic P85 micelles. The double-stabilized Pluronic L121 vesicles are stable to at least 33 °C. We can routinely control the size of these vesicles by extruding them through an appropriately sized filter before the interpenetrating polymer network is formed. Furthermore, we can covalently polymerize fluorescent molecules in the interpenetrating network, and these stabilized fluorescent vesicles can be easily taken up by cells. This system is potentially useful for molecular imaging, biological assays, as biomarker, for cell-labeling, etc.

In Chapter 9, a study on the co-assembly of a genetically designed peptide block copolymer with Pluronic vesicles to form templated protein vesicles is described. Now, several oppositely charged biological polyelectrolytes can interact with the peptide in the vesicle and become incorporated into the protein polymer. The structural features of the protein polymersome are investigated in detail, and the functionalized protein vesicles can be simply internalized in human cells. This method provides an intelligent approach to incorporate multifunctional materials for drug delivery and gene delivery applications.

In Chapter 10, Pluronic micelles are stabilized by an interpenetrating network, which keeps them stable for months. Furthermore, fluorescent molecules are covalently polymerized in the interpenetrating network, and these stabilized fluorescent micelles can be easily taken up by HeLa cells and remain integrated in the cytoplasm. FCS studies of these micelles in living cells indicate that the diffusion properties are significantly different from those of micelles dissolved in aqueous solution. These results may be used to probe the local viscosity in the cell, because there is sufficient evidence that the micelles do not change their size and shape after internalisation.

In Chapter 11, it is shown that similar nanoparticles can act as nanometer-sized thermal sensors. Within a short temperature range, the emission of the nanoparticles changes dramatically and reversibly as a function of temperature. These stabilized fluorescent micelles can be easily taken up by HeLa cells, where they can be used as intracellular nanosized thermometers.

Outlook

Gene medicine has been considered as a next generation therapy to provide cures for common human diseases. By manipulating DNA and RNA on a nanometer scale, one gains the possibility to treat diseases on gene level. However, to use such a therapy properly, a few critical issues must be addressed. Firstly, it is important to direct these molecules to specific cells (such as tumors). Secondly, it is essential to prevent their degradation during delivering. Finally, it is essential to deliver these DNA or RNA sequences across the biological membranes to enter the cytoplasm of cells and from whereon the transport to the nucleus can commence. There is consensus that it is important to compact genes in functionalized nanocontainers, *i.e.* to encapsulate the DNA or RNA fragments in certain targetable vesicles. Meanwhile, to follow this delivery process, it is helpful to integrate an imaging probe along with the therapeutic agents into a targetable vesicle. So far, only few successes have been reported on such a sophisticated novel system.

RNA interference (RNAi), for instance, is a powerful tool for suppressing gene expression and offers the potential to dramatically accelerate *in vivo* drug target validation. It also carries promise for creating novel therapeutic approaches if it can be effectively applied *in vivo*. Very recently, Motomus Shimaoka and his coworkers, highlight the type of targeted systems that may be optimized to provide a robust siRNA (small interference RNA) delivery to the liver, and tumor cells. They modified the liposome surface with hyaluronan and covalently attached an antibody. Subsequently, they lipophilized the liposome and then hydrolyzed in the presence of siRNA. As a result, they ended up with siRNA encapsulated inside anti-body functionalized liposomes. From this we see that, although it is expected to be an efficient therapy, the protocols require many components and multiple assembly steps to package siRNA in a delivery system.

Results described in this dissertation could lead to more general, more flexible, more efficient and relatively straight-forward approaches for novel *in vivo* delivery

systems. The multifunctional protein nano-containers described in this dissertation can be provided with biofunctional molecules (siRNA, DNA, peptides) and with several imaging agents and/or detecting probes (fluorescently labeled peptides with variable excitation and emission wavelength, fluorescently labeled polymers, fluorescently labeled plasmid DNA or siRNA and other types of probes). They may also be provided with several different targeting ligands, carbohydrates, antibodies, etc, which may be covalently linked to the nano-container through various approaches. The latter may be used to enhance the *in vivo* delivery efficiency of these nanomedicines. With containers, properly targeted to specific diseases, organelles or cell-types, it is possible to deliver a variety of molecules (DNA, siRNA and peptides) and possibly cure diseases.

Samenvatting

Amfifiele blokkopolymeren kunnen assembleren in verschillende vormen en architecturen. Vooral polymere vesicles, micellen en vezels zijn tegenwoordig erg populaire structuren in de nanotechnologie. Deze structuren hebben elk hun eigen specifieke eigenschappen en kunnen dienen als containers of sjablonen voor verschillende nanotechnologische toepassingen. Polymere vesicles, bijvoorbeeld, kunnen zowel hydrofobe en hydrofiële moleculen bevatten, en worden daarom beschouwd als aantrekkelijke kandidaten voor de afgifte van medicijnen, nano-reactoren en ook als microtemplates. Micellen zijn over het algemeen een stuk kleiner. Hun hydrofobe kernen worden vaak gebruikt om hydrofobe medicijnen in op te lossen of ze kunnen voorzien worden van biomoleculen. Polymere vezels zijn lange, continue entiteiten. Door deze vorm, vormen ze gemakkelijk gelen bij relatief lage concentraties en kunnen daardoor gebruikt worden als templates en substraten in biologische toepassingen.

In de praktijk is het een grote uitdaging om functionele moleculen te assembleren tot stabiele nanostructuren met de gewenste grootte en vorm. Om dit doel te bereiken, moeten (bio) functionele polymere ketens worden geventueerd in de objecten. Voor dit doel worden twee verschillende routes voorgesteld. Eén hiervan is de zelf-assemblage van functionele blokkopolymeren tot een nanodeeltje; dit is de directe aanpak. In dit geval zijn een aantal voorbereidende werkzaamheden noodzakelijk, omdat de (bio)functionele groepen chemisch moeten worden opgenomen in de blokkopolymeren. Als alternatief kan meer dan één soort copolymeer worden geassembleerd tot grote objecten met een vaste stoichiometrie, elk met hun eigen functies. In de op deze wijze co-geassembleerde objecten, worden de functionaliteiten van de bestanddelen op een gecontroleerde manier gecombineerd.

Beide benaderingen worden toegepast in dit proefschrift en de resultaten van beide routes zijn veelbelovend. Dit proefschrift is verdeeld in drie delen; polymeer zelf- assemblage, polymeer co-assemblage en toepassingen daarvan. Een gedetailleerde beschrijving van elk onderdeel wordt in dit proefschrift gegeven.

Acknowledgements

Over the years it has been my good fortune to encounter many people who have given me much of their time, companionship, patience, professional and personal help. Thank all of you.

First of all, I would like to thank my supervisor, Martien Cohen Stuart. He not only gave me the scientific support and supervision that a graduate student can expect from his professor, but also trusted and encouraged me to switch to a new project which was more suitable to me. Thanks to him, I have never been without a desk, a computer, a friendly ear, and a chance to do my research work in the past years. Without these, I would never have been able to bring this research this far.

Secondly I would like to thank Frans Leermakers, my daily supervisor and promoter. His ideas, enthusiasm and open mind contributed a lot to the bedrock on which this thesis was built. I feel sorry but happy to have taken so much of his time in the past years, especially in those extra working hours and during the weekends, and would like to say "thank you" to his wife and children too. Frans, thank you, for you are always there for me: willing to discuss both professional and personal problems with me and help me solve these problems with kindness and patience. You are more than a supervisor in my heart.

And also thank you Ton Marcelis, my other daily supervisor. I enjoyed the whole process of working together with him. His kindness and flexibility supported me to feel free to work out all those ideas in my mind, including some of those away from our original goal, while his rigorous attitude of scholarship prevented the thesis from a too unconstrained style. Thank you Ton, especially for all those critical remarks you gave me during the paper writing, which no doubt help me a lot to become a real scientist.

Now I would like to thank Ernst Sudhölter, another supervisor and promoter of me. With his position changing to Delft, we did not have as much time as before to discuss the project, but Ernst tried his best to be in Wageningen every one or two months to have a discussion with me about my research, my life and my academic career. Thank you, Ernst, thank you for the time you gave to me and especially for helping me with my job hunting.

Then my thanks goes to all my fellow researchers at the Physical Chemistry and Colloid Science group and the Organic Chemistry group at Wageningen University and co-workers in other groups, universities and institutes. Among them, I would specifically like to say thanks to: Richard Kik for showing me how to work with the extruder, Ioan Paraschiv for the help with the chemical synthesis, Ilja Voets for her help with measuring and implementing the earliest SANS measurements, Josie Zeevat, Anita ter Haar, Mara Winkels, Elly Geurtsen, Aleida Ruisch-Jansen, Ronald de Bruin for the help with personal documents and the ordering of chemical. Milena Rosso-Vasic and Loes Ruizendaal for the fluorometer, Yansen Lauw for looking for job possibilities for me, Marc Lemmers and Slav Semerdijev for their contributions to my project, Ruud Cuypers and Jacob Baggerman for the translation into Dutch and Marat Charlaganov for the Latex thesis template. Tijs Ketelaar, Barend van Lagen, Remco Fokkink, Marcel Giesbers, Adrie Westphal, Jan van Lent, Sylvain Prévost, Ralf Schweins, Menno de Jong, Andres Åslund, Peter Konradsson, Aernout Martens, Frits de Wolf and all those whom I did not mention for providing me with fascinating materials and helping me carrying out rather exciting experiments. A special word of gratitude, finally, to my paranymphs, Kim de Lange and Marc Lemmers.

Also, I would like to thank my thesis reading committee: Herbert Amerongen, Jan van Esch, Wim Hennink and Roeland Nolte. For some of you, my Ph.D. defense might be the first time that we meet, never the less thanks for taking part in this special day for me.

Moving towards more personal acknowledgements, I would like to extend a lot of thanks to all my foreign friends and Chinese fellows: Han Zuilhof, Marijke Zuihof and their sons David and Yan, Carolien van der Kolk, Koos van der Kolk and their son Tom, Yun Yan, Qiang Zhang, Wenfeng Tan, Menglong Yang, Bin Sun, Bo Chen, Lei Zhang, Dan Liang, Lin Cai, Hua He, Yue Wang, Zhenghong Chen, Ningwen Zhang, Ke Lin, Yulin Bai, Zifu Yan, Jinbo Wan, Jifeng Tang, Xingfeng Huang, Xiaomin Tang, Xi Wan, Zhanhu Bai, Xu Chen, Tao Chen,

Kexin Jiang, Jin Shi, Ran Gao, Yuan Li, Junyou Wang for all your support and help during the past years.

I am, of course, indebted to my mother Xianli Wang, my father Qishan Li, my mother-in-law Huiqin Wang, my father-in-law Huairui Zhang, and my sister-in-law Ting Zhang, and particularly, to my dearest wife Yuan Zhang and my son Zhi zhang Li (KuoKuo) for their monumental, unwavering support and encouragement on all fronts. They have truly always been there for me, and without them none of this would have been even possible.

*Wageningen,
October 2009*

Feng Li

List of Publications

THIS DISSERTATION:

- F. Li, T. Ketelaar, A.T.M. Marcelis, F.A.M. Leermakers, M.A. Cohen Stuart, E.J.R. Sudhölter **Stabilization of polymersome vesicles by an interpenetrating polymer network** *Macromolecules* 40, 329-333, (2007). (Chapter2)
- F. Li, T. Ketelaar, M.A. Cohen Stuart, E.J.R. Sudhölter, F.A.M. Leermakers, A.T.M. Marcelis **Gentle immobilization of nonionic polymersomes on solid substrates** *Langmuir* 24, 76-82, (2008). (Chapter3)
- F. Li, A. Martens, A. Åslund, P. Konradsson, F.A. de Wolf, M.A. Cohen Stuart, E.J.R. Sudhölter, A.T.M. Marcelis, F.A.M. Leermakers **Formation of nanotapes by co-assembly of triblock peptide copolymers and polythiophenes in aqueous solution** *Soft Matter* 5, 1668-1673, (2009). (Chapter 6)
- F. Li, L.H.J. de Haan, A.T.M. Marcelis, F.A.M. Leermakers, M.A. Cohen Stuart, E.J.R. Sudhölter **Stabilization of polymersome by core cross linked polymer micelles** *Soft Matter* 10.1039/b903656c, (2009). (Chapter 8)
- F. Li, S. Prévos, R. Schweins, A.T.M. Marcelis, F.A.M. Leermakers, M.A. Cohen Stuart, E.J.R. Sudhölter **Small monodisperse unilamellar vesicles from binary copolymer mixtures** *Soft Matter* 10.1039/b904522h, (2009). (Chapter 4)
- F. Li, M.A. Cohen Stuart, E.J.R. Sudhölter, A.T.M. Marcelis, F.A.M. Leermakers **Field Theoretical Modeling of the Coexistence of Micelles**

and Vesicles in Binary Copolymer Mixtures *Soft Matter* 10.1039/b904525b, (2009). (Chapter 5)

- F. Li, G. Palaniswamy, M. R. de Jong, A. Åslund, P. Konradsson, M.A. Cohen Stuart, E.J.R. Sudhölter, A.T.M. Marcelis, F.A.M. Leermakers **Nanowires formed by the coassembly of a negatively charged low molecular weight gelator and a zwitterionic polythiophene** *Submitted*. (Chapter 7)
- F. Li, F. A. de Wolf, M.A. Cohen Stuart, E.J.R. Sudhölter, A.T.M. Marcelis, F.A.M. Leermakers **Triggered templated assembly of protein polymersomes** *Submitted*. (Chapter 9)
- F. Li, A. Westphal, M.A. Cohen Stuart, E.J.R. Sudhölter, A.T.M. Marcelis, F.A.M. Leermakers **Fluorescent micelle thermometer for intracellular thermometry** *Submitted*. (Chapter 11)
- F. Li, L.H.J. de Haan, M.A. Cohen Stuart, E.J.R. Sudhölter, A.T.M. Marcelis, F.A.M. Leermakers **Mobility of fluorescently labeled polymer micelles in living cells** *Submitted*. (Chapter 10)
- F. Li, M.A. Cohen Stuart, E.J.R. Sudhölter, A.T.M. Marcelis, F.A.M. Leermakers **Confinement of nematic liquid crystal in polymersome in preparation**

OTHER WORK:

- S. VE Prigent, A. G. J. Voragen, F. Li, A. J.W. G. Visser, G. A. van Koningsveld, H. Gruppen **Covalent interactions between amino acid side chains and oxidation products of caffeoylquinic acid (chlorogenic acid)** *J Sci Food Agric* 88, 1748-1754, (2008).

Curriculum Vitae

Feng Li was born in Lin He (Inner Mongolia, China) on October 31, 1979. After finishing his Bachelor in Food Science and Technology at Nanjing Agriculture University in China in 2002, he came to the Netherlands to pursue his Master of Food Technology with the specialty of Food Chemistry at Wageningen University. He got his Master in 2004 and started his Ph.D. research in the group Physical Chemistry and Colloid Science at Wageningen University in the same year. In 2005 he took part in a joined project of Organic Chemistry group and Physical Chemistry and Colloid Science group at Wageningen University.